

INTEGRATION OF REMOTELY-SENSED/GEOPHYSICAL DATA
WITH
GROUND-TRUTH STRUCTURE:
EVIDENCE FOR FAULT SYSTEMS
IN PART OF
CAYUGA COUNTY

NYSERDA AGREEMENT # 6123-ERTER-ER-00

February 1, 2011

DRAFT

Submitted by:
Dr. Robert Jacobi
Norse Energy USA
3556 Lake Shore Road, Suite 700
Buffalo, New York 14219
(716) 218 4234
Email: Rjacobi@norseenergy.com

Submitted to:
Dr. John Martin, NYSERDA Senior Project Manager (retired)
NYS Energy Research and Development Authority
17 Columbia Circle
Albany, NY 12203-6399

NOTICE

This report was prepared by Dr. Robert Jacobi in the course of performing work contracted for and sponsored by the New York State Energy Research and Development Authority (hereafter "NYSERDA"). The opinions expressed in this report do not necessarily reflect those of NYSERDA or the State of New York, and reference to any specific product, service, process, or method does not constitute an implied or expressed recommendation or endorsement of it. Further, NYSERDA, the State of New York, and the contractor make no warranties or representations, expressed or implied, as to the fitness for particular purpose or merchantability of any product, apparatus, or service, or the usefulness, completeness, or accuracy of any processes, methods, or other information contained, described, disclosed, or referred to in this report. NYSERDA, the State of New York, and the contractor make no representation that the use of any product, apparatus, process, method, or other information will not infringe privately owned rights and will assume no liability for any loss, injury, or damage resulting from, or occurring in connection with, the use of information contained, described, disclosed, or referred to in this report.

ABSTRACT

Eight characteristics of about 1650 fractures were measured in the study area that encompasses Skaneateles and Otisco lakes, central New York State. The predominant fracture set in the study area strikes NNW; other prominent fracture sets strike EW, ENE, N, NNE, NW and WNW, in descending order of fracture abundances. Two localities were discovered that exhibit faults: one is the Tully Formation Borodino Reef locality that has northerly striking normal faults in outcrop with calcite slickenside surfaces. The second fault locality exhibits both dextral ENE-striking faults and NNW, west dipping thrusts. Other evidence for faults in the Borodino Reef area are anomalous Tully elevations, N-striking FIDs, and N-trending topographic and aeromagnetic lineaments. In total, these coincident features suggest that a northerly trending fault system is located in the Borodino Reef region that extends down to basement, and the reef was probably localized along the upthrown block side of the fault. Dolomite and quartz fills in the fractures of the reef point to hydrothermal circulation in this region in Acadian and/or Alleghanian times.

Steep aeromagnetic gradients are coincident with the Owasco Lake valley, the Otisco Lake valley, and are near the Skaneateles Lake valley and the Bear Swamp Creek valley. Such gradients and coincidence with topography suggest that faults in the Precambrian extend up through the Paleozoic cover. Anomalous elevations of the Tully support the fault hypothesis. Two distinctive ENE-trending broad valleys, which are coincident with ENE-trending aeromagnetic gradients, and several ENE-striking FIDs, probably mark basement-rooted fault systems that may be reactivated Iapetan-opening fault systems.

ACKNOWLEDGMENTS

This report included a strong field component; I am especially pleased to acknowledge the field personnel with whom I worked on this project; they are all fine geologists, even under sometimes trying field conditions. Field personnel included Josh Stroup and several field assistants. This report is an integration of all the personnel's contributions. I also wish to acknowledge Dr. John Martin for his continued support and his viewpoints that added considerably to discussions concerning this research.

TABLE OF CONTENTS

	page
SUMMARY	
INTRODUCTION	1
SELECTED PREVIOUS RESEARCH	1
RESULTS	6
FRACTURES	6
<u>Fracture Orientations and Fracture Frequency</u>	6
<u>Fracture Abutting Relationships: Fracture History</u>	8
<u>Introduction.</u>	8
<u>Present Study Area Results.</u>	10
FAULTS OBSERVED AND INFERRED FROM OUTCROPS	11
HIGH RESOLUTION AEROMAGNETICS AND FAULTS	12
DEM LINEAMENTS AND FAULTS	14
CONCLUSIONS	16
REFERENCES	18
FIGURES	24
TABLES	71

LIST OF GRAPHICAL MATERIALS

	<u>page</u>
Figure 1a. Location of the focus area in central New York State.	24
Figure 1b. Location of the focus area in central New York State with respect to Bouguer gravity.	25
Figure 1c. Location of the focus area in central New York State with respect to aeromagnetic anomalies.	26
Figure 1d. Enlargement of regional aeromagnetics and gravity with respect to location of the focus area in central New York State.	27
Figure 2a. Field Area and lineament test area on a DEM (digital elevation model) background.	28
Figure 2b. Generalized geology of field area and adjoining region overlaid on a DEM (digital elevation model) background.	29
Figure 2c. Generalized stratigraphic column of field area and adjoining region	30
Figure 3. Modified rose diagrams of fractures and faults in the Skaneateles study area.	31
Figure 4. Modified rose diagrams for inset #4 in Figure 3.	32
Figure 5. Modified rose diagrams for inset #5 in Figure 3.	33
Figure 6. Modified rose diagrams for inset #6 in Figure 3.	34
Figure 7. Modified rose diagrams for inset #7 in Figure 3.	35
Figure 8. Modified rose diagrams for inset #8 in Figure 3.	36
Figure 9. Modified rose diagrams for inset #9 in Figure 3.	37
Figure 10a. Explanation for modified rose diagram.	38
Figure 10b. Specific abutting relationships displayed in the lower semicircles of a modified rose diagram	39
Figure 11a. Histogram of fracture orientations for various bin sizes.	41
Figure 11b. Defined ranges for various fracture sets, based on the histograms in Figure 10a and abutting relationships.	42
Figure 12. Fracture frequency distribution for various major fracture sets.	43
Figure 13. Examples of structures in the Skaneateles region.	
Figure 13a shows locations of the photos.	44
Figure 13b. Typical orthogonal fractures in the thickly bedded Tully Formation on the southwestern side of Skaneateles Lake.	44
Figure 13c. Fractures in the Devonian Genesee Group in Fillmore Glen, about 5 km	

south of the central study area.	45
Figure 13d. Dipping beds (350 ⁰ , 30 ⁰ W) on the flank of the Borodino reef in the Tully Formation.	46
Figure 13e. Breccia and ferroan dolomite fill in the Borodino Reef.	46
Figure 13f. Breccia and ferroan dolomite fill in interstices and in planar fractures in the Borodino Reef.	47
Figure 13g. ENE-striking fractures with calcite vein fills at the Borodino Reef in the Tully Formation.	47
Figure 13h. Fracture intersection and interaction at Staghorn Point in the Genesee Group.	48
Figure 13i. Fracture intensification in the Genesee Group at Fillmore Glen.	48
Figure 13j. Fracture intensification domain of NNW-striking fractures in the Genesee Group in Fillmore Glen.	49
Figure 13k. Fracture intensification in the Genesee Group at Fillmore Glen.	49
Figure 13l. Enlargement of Figure 13j.	50
Figure 13m. Larger view of the vertical outcrop in the Genesee Group at Fillmore Glen.	50
Figure 13n. Faults at Borodino Reef (Tully Formation).	51
Figure 14. Fracture set history in the Chenango County area, based on abutting relationships	52
Figure 15a. Kriged surface of Tully Formation and possible faults.	53
Figure 15b. Kriged surface of Tully Formation and alternative possible faults.	54
Figure 16a. Reduced-to-pole aeromagnetics in central New York State.	55
Figure 16b. DEM from figures 2 and 3 superimposed on reduced-to-pole aeromagnetics in the study area from Figure 16a.	56
Figure 17. Topographic lineaments.	57
Figure 18. Buffered NW-trending topographic lineaments on the DEM base.	58
Figure 19. Buffered NW-trending EarthSat (1997) lineaments on the DEM base.	59
Figure 20. Buffered NNW-trending topographic lineaments on the DEM base.	60
Figure 21. Buffered NNW-trending EarthSat (1997) lineaments on the DEM base.	61
Figure 22. Buffered N-trending topographic lineaments on the DEM base	62
Figure 23. Buffered ENE-trending topographic lineaments on the DEM base.	63
Figure 24. Buffered ENE-trending EarthSat (1997) lineaments on the DEM base	64
Figure 25. Buffered Type IIa ENE-trending topographic lineaments on the DEM base.	65
Figure 26. Buffered Type IIa ENE-trending EarthSat (1997) lineaments on the DEM base.	66
Figure 27. Buffered Type IIb E-trending topographic lineaments on the DEM base.	67
Figure 28. Buffered Type IIb E-trending EarthSat (1997) lineaments on the DEM base.	68

Figure 29. Buffered topographic lineaments of all trends on the DEM base.	69
Figure 30. Relationships among the total area of various lineament trends (with buffer), the percent of sites in the lineament buffer that exhibit fractures striking collinearly with the lineament tend, and contrast values of 1 and 0.	70

SUMMARY

The objective of this research was to establish whether faults systems characterized the Skaneateles and Otisco lakes study area of central New York State. Fault systems can mark reservoirs in the Ordovician Trenton/Black River and in fracture plays such as the Auburn field in the faulted Ordovician Queenston Formation. Major faults were suspected in the focus area by the grant proposer, based Landsat lineaments (EarthSat, 1997) that are coincident with gravity and aeromagnetic gradients. The present proposed research was to integrate surface fracture/faults studies with lineament studies and the single available east-west 2D seismic line to determine if major NNW- to NW-striking faults exist in the focus area.

The east-west seismic line was procured, but the proper shot point coordinates had been lost; thus, the only EW 2D seismic line in the region was thus not accessible. Nevertheless, a fracture field study that was conducted in 2002 and 2005 revealed faults in outcrop and fracture intensification domains that elsewhere have been related to faulting. A DEM lineament study was also accomplished in the study area in 2005 (Stroup et al., 2006). Groundtruthed lineaments are useful both as a method of extending the fracture domains that typify the lineament away from the field sites in the lineament, and as a crude measure of the structural fabric in the region. This report is a summary of those investigations and indicates that faults do occur in the focus area, even at the surface.

Eight characteristics of about 1650 fractures were measured in the study area that encompasses Skaneateles and Otisco lakes, central New York State. The predominant fracture set in the study area strikes NNW; other prominent fracture sets strike EW, ENE, N, NNE, NW and WNW, in descending order of fracture abundances. Two localities were discovered with faults: one is the Devonian Tully Formation Borodino Reef locality that has northerly-striking normal faults in outcrop with calcite slickenside surfaces. Other evidence for faults in the Borodino Reef area are anomalous Tully elevations, N-striking FIDs, and N-trending topographic and aeromagnetic lineaments. In total, these coincident features suggest that a northerly trending fault system is located in the Borodino Reef region that extends down to basement, and reef growth was probably localized along the upthrown block side of the fault. Dolomite and quartz fills in the fractures of the reef point to hydrothermal circulation in this region in Acadian and/or Alleghanian times. The second fault locality exhibits both dextral ENE-striking faults and NNW, west dipping thrusts. ENE-trending topographic and EarthSat (1997) lineaments pass through the site with the ENE-striking fault, and are therefore thought to represent the fault and associated fractures. Similarly, a lineament passes close to the thrust, and is thought to be groundtruthed by the thrust.

Steep aeromagnetic gradients are coincident with the Owasco Lake valley to the west, with the Otisco Lake valley to the east, and are near the Skaneateles Lake valley and the Bear Swamp Creek valley. Such gradients and coincidence with topography suggest that faults in the Precambrian extend up through the Paleozoic cover. Support for the fault hypothesis comes from the elevations of the Tully, which have anomalous elevations along Skaneateles Lake, suggesting a fault along the lake. An ENE-trending broad valley west of Skaneateles Lake, “Dutch Hollow Brook” valley, is coincident with a major ENE-trending aeromagnetic gradient, and an ENE-trending valley farther east between Skaneateles and Otisco lakes (“Woodland” valley) is approximately on strike with the aeromagnetic gradient. This eastern valley lineament is confirmed by several ENE-striking FIDs. These ENE-trending coincident FIDs, topographic lineaments, and EarthSat (1997) lineaments suggest fault systems that are basement rooted, but extend up through the section. Such faults may well be reactivated Iapetan-opening fault such as those that localized the Trenton/Black River gas fields to the southwest. In total, although an EW brokered seismic line across the northern end of the lakes was not able to be processed satisfactorily, the field work, geopotential fields, and associated lineaments strongly suggest that NNW, N, and ENE-striking faults chop the region into blocks.

INTRODUCTION

The original objective of the proposed research was to establish whether faults systems characterized the Skaneateles and Otisco lakes study area of central New York State (Figures 1 and 2). Major faults were suspected in the focus area by the grant proposer (Jacobi), based on a significant NW-trending gravity low coincident with bordering lineaments from Landsat data (EarthSat, 1997) and aeromagnetic data (Jacobi, 2002). Additionally, north of the study area Rickard (1973) proposed a northerly-striking Trenton-aged graben, based on two well bores. This structure could be reinterpreted to strike NNW, on strike with the NNW lineament and gravity trends. The present proposed research was to integrate surface fracture/faults studies with lineament studies and the single available EW 2D seismic line to determine if major NNW- to NW-striking faults exist in the focus area.

The EW seismic line was procured, but when reprocessed, it became apparent that incorrect shot point coordinates had been assigned to this line, because it was located on top of another line that is oriented NS. The seismic broker was contacted and they attempted to secure the proper coordinates for several years, but finally the conclusion was reached that the original data were lost in a flood, and the improper (?) coordinates were all that remained. The only EW 2D seismic line in the region was thus not accessible. A fracture field study was conducted in 2002 and 2005, which revealed exposed faults and fracture intensification domains that can be related to faulting. A DEM lineament study was also accomplished in the study area in 2005 (Stroup et al., 2006). Groundtruthed lineaments are useful both as a method of extending the fracture domains that typify the lineament away from the field sites in the lineament, and as a crude measure of the structural fabric in the region. This report is a summary of those investigations and indicates that faults do occur in the focus area, even at the surface.

SELECTED PREVIOUS RESEARCH

The northern part of the study area was mapped in detail between 1926 and 1932 by Smith (1935). He found that the Upper Devonian Skaneateles Formation of the Hamilton Group is the lowest bedrock unit in the northern part of the study area, and that the Ithaca Formation (flags) of the Genesee Group is the uppermost unit in the southern part of the study area. The Tully limestone and the overlying Genesee black shale (basal member of the Genesee Group) are prominent markers in the southern part of the study area (Figure 2b). The type locality of the

Marcellus black shale (basal unit in the Hamilton Group) is about 6 km north of the field area near Marcellus, NY. Smith (1935) reported a few faults in the Skaneateles quadrangle, including one thrust in the Malley Onondaga quarry (about 1 km south-southeast of the Marcellus village center). This thrust fault strikes about EW, dips north between 18° and 20° , has down-dip slickensides, and has perhaps 2.6 m of stratigraphic throw, although Smith (1935) points out this throw is based on tenuous correlations of cherty layers in the Onondaga, and other geologists have estimated less throw. Folds described by Smith (1935) in the Skaneateles quadrangle strike about east-west, and so are probably related to the “Main Phase” of the Alleghanian orogeny (e.g., Engelder, 1985), which south of this area is characterized by approximately E-striking macroscopic folds (Wedel, 1932). A thrust ramp and flat is exposed in the Hamilton shales on the west shore of Skaneateles Lake between 4.8 and 6.4 km south of the north end of the lake. The thrust ramps steeply to the S, and a “flat” along gently southerly-dipping bedding extends south from the ramp. Fault breccia occurs along the fault. Smith (1935) considered this to be an ice-welded shove effect, based on the clean breccia in the fault zone, the fault zone breccia that appears to grade into a till breccia at the southern exposure, and the transport direction that is to the southeast.

Heckel (1973) described in detail the Tully limestone across its E-W outcrop belt in central NYS. He measured and described about ten Tully localities in the study area, including the Borodino reef. Based on the locations of three quarries and a new road cut in the Borodino reef, as well as the facies variations in the reef, Heckel (1973) believed that the reef is narrow (on the order of 23 [75 ft] to 30 m [100 ft] wide) and elongate (305+ m [1000+ ft] long) along a NNW trend. Heckel (1973) observed minor normal faults in the reef complex which he thought were similar to high angle faults elsewhere in the Skaneateles region commented on by Smith (1935), but Heckel (1973) believed the Borodino faults were a syndepositional loading phenomena resulting from localized subsidence of the higher density reef material. Heckel (1973) also considered observed dip of beds on the flank of the upper reef section to be syndepositional, i.e., the dip is original and reflects the flanks of the reef that dip away from the topographically high core. Heckel (1935) reported that “ferroan dolomite spar” (p.109) filled reef vugs and a network of polygonal fractures. Although Heckel (1973) proposed a northerly-striking faulted syndepositional anticline and yoked basin in Tully time to the east of the study area, no regional faults were proposed for the study area. Heckel (1973) did propose, however, regional facies boundaries that passed through the study area, including 1) in the uppermost Hamilton a northerly-trending boundary along the eastern shore of Skaneateles Lake with marine shale on the east and non-deposition on

the west, 2) in the lower Tully similar northerly-trending boundaries located between Skaneateles Lake and Owasco Lake that are characterized in the Cuyler Bed by laminated muddy siltstone east of the facies boundary and non-deposition west of the boundary and in the Vesper Bed sandy limestone east of the facies boundary and non-deposition west of the boundary. The Vesper Bed also significantly thins from east to west near the Borodino reef, and changes from muddy siltstone to sandy limestone. Furthermore, Heckel's (1973) cross-section shows that near Moravia, NY, about 5 km south of the southwest corner of the field area, most units of the Tully thicken significantly to the west from Fillmore Glen to the west side of the valley, a distance of about 2-3 km. This thickening is coincident with major NNW-trending Landsat lineaments (EarthSat, 1997) and geopotential lineaments (Jacobi, 2002), and suggests a growth fault in Tully-time with down-on-the-west motion.

Brett and Baird (1996) summarized their detailed work in the Middle Devonian Upper Hamilton Group stratigraphy in western and central NYS, from Skaneateles Lake westward. They found significant thickness and facies variations from the Skaneateles region west into the center of a depositional trough located in the region of Cayuga and Seneca lakes ("Central Finger Lakes Trough"). Jacobi (2002) suggested that this trough was (partly?) controlled by syndepositional faulting along Jacobi's (2002) proposed fault systems that are coincident with the margins of the trough. Brett and Baird (1996) proposed that erosion during sea level rises in Ludlowville Formation time along the margin of Central Finger Lakes Trough at the present east shore of Skaneateles Lake, coupled with sediment cutoff, resulted in a submarine scarp several meters high. The scarp was located between the eastern and western shores of Skaneateles Lake. This model is similar to the incised shore face model that calls upon wave action to create a scarp, the location of which Smith and Jacobi (1999, 2001) suggested was influenced by minor faulting, but Brett and Baird (1996) and Martin et al. (2008) did not indicate that faults and fault block activity had any influence in their model. It should be noted that syndepositional faults at the time of deposition (e.g., Ludlowville Formation time) might not have reached upsection to the depositional/non-depositional paleosurface itself; rather, deeper faulting could result in subtle drape folds in the unconsolidated/poorly consolidated sediments over the faulted units at depth, thus hiding the fault effect at, for example, the Ludlowville Formation scarp. In contrast, Smith (1935) suggested that the scarps were channel walls (his Figure 23), in which case the discussion above concerning ramps between the Skaneateles shores is moot.

Grasso's (1986) cross-section of the Devonian Marcellus shows an 8-fold increase in thickness on the west side of Skaneateles Lake, compared outcrops on the east side. This abrupt thickening is consistent with a growth fault operating in Marcellus time along Skaneateles Lake, with down-on-the-west motion. The location and proposed throw of this fault system is also consistent with the paleoslopes and scarps proposed for the younger Hamilton Group by Brett and Baird (1996, see above). As discussed for the Ludlowville Formation above, it should be noted that such syndepositional faults at the time of deposition (e.g., Hamilton Group time) might not have reached upsection to the depositional/non-depositional paleosurface itself.

The closest stratigraphic and depositional environment study of lower part of the Middle Devonian Marcellus Formation (the Union Springs-Cherry Valley interval) was carried out at Marcellus, NY (about 5 km north of the study area) by Griffing and van Straeten (1991) who examined the interval across central and eastern NYS. At Marcellus they found orthocone nautiloids in the Cherry Valley that are unidirectionally oriented toward the southeast, orthogonal to the regional isopachs of the Union Springs-Cherry Valley interval. Their detailed study showed that the westward thinning Union Springs-Cherry Valley interval has led to incorrect thicknesses assigned to the Cherry Valley limestone, since thin carbonate concretions and layers of the "Chestnut Street Beds" have been included in the Cherry Valley in west central NYS where the Chestnut Street Beds lie directly below the Cherry Valley (as at Marcellus, NY), whereas farther east the Chestnut Street Beds are distinctly separated from the Cherry Valley by thickening black and gray shale and siltstone units .

Prior to this project, no detailed structural study or lineament study was undertaken in the study area, and to the limits of the author's knowledge, no comprehensive structural data have been previously published in the study area. Engelder and Geiser (1980) measured fractures at 4 localities in the study area: three in the Skaneateles Lake area and one in the Otisco area. They found N-striking (Set 1a) cross-strike fractures that rotate to a more NNE-strike immediately to the east of the study area, and NNW-striking (Set 1b) cross-strike fractures that gradually rotate to NW-striking west of the study area. Engelder and Geiser (1980) discovered Set II fractures ("strike-parallel") trend WNW in the study area. Since Engelder and Geiser (1980) did not provide a locality map for Set II fractures (those fractures that are orientation-invariant fracture across NYS at 60°; Engelder and Geiser, 1980), it is not clear whether Engelder and Geiser (1980) found Set III fractures in the study area. Engelder and Geiser believed that Set I fractures

were the oldest, and resulted from an Alleghanian stress field (for reviews of the fracture sets, see Jacobi, 1996, 2007).

Lash et al. (2004) measured fractures in Fillmore Glen (about 5 km south of the southwest corner of the field area), where they found ENE and cross-strike (NNW-striking) fractures in both the Genesee black shale and the overlying gray shale of the Sherburne Member of the Ithaca Formation. They found variable fracture frequencies in the black shale, from as high as about 10 fractures/m to as low as about 0.1 fractures/m. Lash et al. (2004) showed that the ENE-striking fracture set decreases in fracture frequency upsection from the base of the Genesee black shale into the overlying gray shale. They found that the NNW-striking fractures at the top of the black shale exhibit the highest fracture frequency they had observed anywhere in the Devonian section of New York State. They believed both fracture sets were hydrocarbon-driven, and that the ENE-striking set began developing in late Acadian (Early Carboniferous) in this region, whereas the NNW-striking fractures began developing later in this region. However, both sets continued developing into the Alleghanian.

Engelder et al. (2009) found ENE-striking fractures in the Marcellus shale at Marcellus (about 5 km north of the study area), and Jacobi (2009, 2010) found at the same general locality that the Onondaga limestone carries northerly ($\sim 350^{\circ}$) striking fractures that abut some of the ENE-striking fractures (70°). A third prominent set strikes 10° and dips 67° E. Spacing on the 350° set is about 1.5 m, and on the 70° is about 2.5 m. In the overlying Marcellus black shale at the same general locality, fractures that strike about $65-70^{\circ}$ are master to a less prominent set that strikes about 345° . Spacing of the 65° set varies from 6 cm to 30 cm to 100 cm, and spacing of the 345° set varies from about 0.5 to 2 m. About 15 km west of the study area near Cayuga Lake Engelder et al. (2009) found ENE and NNW striking fractures in the Upper Devonian Levanna and Skaneateles formations.

High resolution seismic reflection data has been collected in the Finger Lakes, including Skaneateles and Owasco lakes (e.g., Mullins et al., 1991; Mullins and Halfman, 2001; Lyons et al., 2005). These high resolution studies only imaged the Holocene and recent sediments covering bedrock. However, Lyons et al (2005) noted that a steep south-facing slope on the bedrock surface in Skaneateles Lake was approximately on strike with a prominent topographic lineament to the west, and suggested the slope might reflect faulting.

Bouguer gravity and aeromagnetic anomalies were integrated with EarthSat (1997) lineaments from Landsat images to propose numerous faults across the Appalachian Basin of New York State (Jacobi, 2002). This integration suggested that NNW/NW and ENE/NE-striking major fault systems cross the study area (Figure 1a). For example, a prominent NW-striking gravity gradient, coincident aeromagnetic gradient and Landsat (EarthSat, 1997) lineaments are located along Skaneateles Lake, and extend NW and SE beyond the lake where these and similar lineaments SE of Otisco Lake are intersected (and “offset”) by ENE/NE trends (Figure 1d). The northwestern margin of the major NE trending gravity low west of the Scranton Gravity high (Figure 1d) is also intersected by, and “offset” by, the NNW/NW-trending bundles (Figure 1d). Harper and Laughrey (1987) suggested that the major gravity low is related to structures associated with Iapetan opening (the Rome Trough extension). Jacobi et al. (2004 2006 2007) and Jacobi (2010) suggested that during Iapetan rifting of Laurentia this major NNW/NW trending gravity/magnetic/lineament bundle may be a transfer/accommodation zone between offset rift segments, as outlined by the northwestern ragged margin of the gravity low, and that the transfer zone location was guided by still older structures.

RESULTS

FRACTURES

Fracture Orientations and Fracture Frequency

Eight characteristics of about 1650 fractures were measured in the field area at 125 sites generally using the abbreviated method of Jacobi and Zhao (1996 a, b), although a few scanline data sets were also collected. The measured characteristics included such features as fracture orientation, spacing, apparent height, apparent length, character (e.g., planar), abutting relationships (both vertical and horizontal), sediment type and bedding characteristics (see Jacobi, 2007, for detailed explanation of data collection). The orientation and abutting relationships are shown in modified rose diagrams for the various sites in figures 3-9, and the explanation for the modified rose diagrams is shown in Figure 10. Rose diagrams are judged to be a satisfactory method to display fractures in these generally flat lying rocks because most of the fractures have very high dips—on the order of 85⁰ and higher.

The fractures orientations were grouped in sets, based primarily upon the distribution of fracture orientation (Figure 11), and to a lesser extent, abutting characteristics and other characteristics (e.g., planar vs. curvy). Figure 11 shows histograms for the fracture frequency for different bin sizes (different ranges for the fracture orientations). It is clear from the plots in Figure 11 that for this data set bin sizes of 3 to 6 degrees yield the same modes, whereas bin sizes of 9 and 10 degrees begin to smooth the histogram to the point that mode separation becomes difficult. The predominant fracture set in the study area strikes NNW (the primary mode in Figure 11a); other prominent fracture sets strike EW, ENE, N, NNE, NW and WNW, in descending abundances (Figure 11a). The only orientation not represented with any significant abundance in the area is NE. Figure 11b delimits the ranges of the fracture sets, and displays the mean and SD for each fracture set. The NNW fracture set can be equated to Engelder and Geiser's (1980) Set Ib and in the region of the study area they defined Set Ia as striking N. About 15 km east of Otisco Lake they found set 1a fractures striking NNE. The E-striking fractures are equivalent to Engelder and Geiser's (1980) Set II, and the ENE-striking fractures correspond to Engelder and Geiser's (1980) Set III (now J1).

The distribution of fracture frequencies of the various major fracture sets at outcrops where six or more fractures were measured are shown in Figure 12. All fracture sets have their primary population in the 0-4 fracture/m range. A significant secondary mode and population for ENE-, E-W-, and NNW-striking fractures occur between 4 and 8.5 fractures/m. Another population ranges between 9 and 15 fractures/m with a mode at 10-10.5 fractures/m for NNW, 11 to 13 fractures/m for ENE, 12.5 to 14.5 fractures/m for NS and 12.5 to 13 fractures/m for NW. NS-, ENE- and EW-striking fractures have another mode at 16.5 to 17 fractures/m. Even accounting for the change in bin size in Figure 12b, NNW-, NS- and ENE- striking fractures have another population and mode between 20 and 30+ fractures/m. Some of these modes and populations may shift with more data points, but the general conclusion will remain valid (based on other detailed studies in NYS (e.g., Jacobi 2007b), that all fractures sets have a primary mode in the 0-4 fractures/m range, and most have secondary modes in intermediate values, and a few have modes in high fracture frequencies. Only NE-striking fractures do not have significant modes in the higher fracture frequencies. As expected, the thick rigid member of the Tully generally carries low fracture frequencies (Figure 13) compared to the fracture frequency of similarly –oriented fractures in the thinner interbedded siltstone and shales, and especially in the gas-generated fractures near the bases of the black shales. Examples of higher fracture frequencies are shown Figure 13.

These intermediate to high fracture frequencies have been ascribed to gas generation where observed near the base of black shale units (e.g., Lash et al., 2004), to “gas chimneys” in and above black shales (e.g., Engelder and Lash, 2008), to an effect related to faulting (a fracture intensification domain [FID], e.g., Jacobi and Fountain, 1996; Jacobi, 2007a), and in some outcrops the high fracture frequencies are clearly short-length fringe cracks as detailed by Younes and Engelder (1999) and Jacobi (2007a). Elsewhere in New York State, especially in interbedded sandstones, siltstones and shales, the secondary modes > 4 fractures/m have been shown to occur where other evidence indicates faults either in the fractured section, or down section from the fractured section (e.g., Jacobi and Fountain, 1996; Jacobi, 2007a). Jacobi et al. (2008, 2009) demonstrated that even in the black shale sections, anomalously high fracture frequencies (significantly above the upsection fracture frequency decay curve) correspond spatially to faults that were independently proposed based on stratigraphic offsets and/or seismic reflection data. Thus, the high fracture frequencies > 4 should not be regarded as necessarily related only to a gas-driven phenomenon—a zone with anomalously high fracture frequencies could be gas-driven superimposed on (and localized/controlled by) active fault stresses, or could reflect fault stresses alone. Such an example may occur at Fillmore Glen, where N-striking FIDs in black shale (Figure 13i and Lash et al., 2004) could be gas-generated, but the orientation and tight spacing may also indicate an influence by northerly-striking faults, consistent with the stratigraphic/depositional data that suggest Devonian syndepositional faulting in the region (see introduction) and gravity/aeromagnetic data that also suggest a northerly-basement fault system (as well as a NNW-trending fault system) in the region.

Fracture Abutting Relationships: Fracture History

Introduction. Engelder and Geiser (1980) were not able to definitively determine the fracture development history, primarily because they lacked definitive and consistent abutting relationship data, although they proposed an extremely complicated scenario in which Set 1a fractures developed first during the Alleghanian Orogeny, followed by Set 2 fractures, in turn followed by Set 1b fractures that developed in response to a residual strain that had been induced before Set 1a fractures developed. Since that time literally hundreds of publications have made significant advances in the complicated history of fracturing in NYS (see reviews by Jacobi and Fountain, 1996; Jacobi, 2007a; Engelder et al., 2009). Part of the issue is that some sets apparently episodically developed through time. The ENE-striking set of fractures (Set 3, now J1) were thought to be neotectonic along the Niagara Escarpment in NYS by Gross and Engelder (1991),

although ENE-striking fractures in FIDs in Allegany County to the south were the oldest fractures observed (e.g., Jacobi et al., 1990, Jacobi and Fountain, 1996). Gross et al. (1992) revised their estimate of the age of ENE-striking, vein-filled fractures along the Niagara Escarpment to be Acadian. In the Finger Lakes region, Engelder et al. (2001) suggested the same (Acadian) age, based on slip of ENE-striking fractures along Alleghanian cross-strike fractures. The Jacobi UB Rock Fracture Group (UBRFG; e.g., Jacobi and Fountain, 2001, Jacobi et al. 2002; Jacobi, 2007a) also found in some areas of the Seneca and Cayuga lakes region that the ENE-striking fractures predated the cross strike fractures, especially in FIDs. They suggested that the early ENE-striking fractures were related to early fault motion in the underlying units, faults which are observed on seismic reflection profiles. The UBRFG did not, however, suggest that the ENE-fractures were Acadian—they could be early Alleghanian, since in many areas the ENE and cross-strike fracture sets intersected or had mutually abutting relationships that suggest the fracture systems had continued to develop through the Alleghanian. East of the study area in Chenango County, Jacobi (2007b) found that ENE-striking fractures were commonly oldest, followed cross-strike (Set I) fractures which strike NNE in Chenango County, in turn followed by WNW-striking fractures (Figure 14). As shown in Figure 14, in a few outcrops the reverse timing relationship between ENE and the cross-striking fractures was found.

More recently, Lash et al. (2004), Lash and Engelder (2009), and Engelder et al. (2009) have proposed that the ENE-striking fracture set developed during early Alleghanian collision as Africa slid by present-day North America, and that the cross-strike set developed when Africa later rotated and collided more nearly head-on with North America. In this scenario the ENE-striking fractures should have ceased developing in the early Alleghanian, but the fact that ENE-striking fractures can be observed abutting the cross strike fractures has led Lash and Engelder (2009) to suggest that the ENE-striking fractures that abut cross-strike fractures began development in the Alleghanian, but never grew their full length (to meet the present master cross-strike fractures) until recent uplift, making the ENE-striking set both older and younger than the cross-strike fractures.

In the general Skaneateles region (including Fillmore Glen, about 5 km south of the central field area), Lash et al. (2004) found that the cross strike and ENE-striking fracture sets are “mutually cross-cutting” (p. 144), which they believed was consistent with a deeper burial in this region compared to western NYS where the cross-strike fracture are master to (and therefore predate) the ENE-striking set. In this burial model the basin in this region had subsided sufficiently to promote

initial generation of the ENE-striking fractures before the cross-strike fractures developed in later Alleghanian time. Some of the ENE-striking fractures “fully” developed before cross-strike fractures develop (leading to the early ENE-striking masters), and may have continued to develop through the Alleghanian and possibly into recent times, as proposed for western New York (Lash and Engelder, 2009). These later ENE fractures would abut the cross-strike fractures. This repeated generation of ENE and NNW fractures can also be viewed in terms of local fault stresses superimposed on the gas generation and far field stresses. In that case, especially in terms of FIDs, one might expect to find both “early” and “late” FIDs if a fault system history can also when the cross strike fractures also developed.

Present Study Area Results. In the present study area, based on fracture intersections in sites shown in Figures 3-9 and summary Table 1, the cross strike (NNW- striking) and Set 3 (J1) ENE-striking fractures exhibit mutually abutting relationships. Of 33 sites with intersections between the two sets, 18 intersections have NNW as the master (and 15 have ENE as the master fracture, Table 1). By assigning values of 1 for the older fracture set at the intersection, and 2 for the younger set, one can calculate the SD of the relative timing for each fracture set; 1 SD for NNW is 0.51 and for ENE is 0.56, meaning that there is no predictable order between the two sets as to which came first, although at slightly more sites the NNW set was the master. This nearly equal distribution is consistent with Lash et al.’s (2004) observation, but not with the data from farther east in Chenango County (Jacobi, 2007), where the ENE-striking fractures are the clear dominate master. This eastward progression is consistent with Lash et al.’s (2004) suggestion that greater (and earlier) subsidence occurred farther east, resulting in more time to develop the ENE fractures before the onset of the Alleghanian Phase that resulted in the cross-strike fractures.

Other fracture set intersections are equally non-definitive in the Skaneateles area. Of 22 sites with intersections between NNW and NS fractures, NS is master at 12 sites and NNW is master at 7 sites, and at 3 sites the fractures mutually intersect. Although the SD values for these intersections are also high, the significantly higher number of NS masters mat indicate that the NS set began developing before the NNW set. A similar scenario was proposed for early NS fractures in the Seneca and Cayuga Lake region (e.g., Jacobi 2007a). There the early NS fractures are associated with FIDs and are on strike with faults proposed on the basis of stratigraphy and structure contours (Jacobi, 2007a). At only three sites in the present field area are NNW and NNE fracture intersections found, and in all three sites NNW came first. Only one site exhibited both NS- and NNE-striking fractures, and the NNE set was master. Three sites displayed both ENE and WNW

fractures, and at all three ENE predates WNW. At five sites, apparent stress rotation about a vertical axis can be inferred from closely-oriented abutting relationships between closely oriented fracture sets. Two suggested counterclockwise rotation and three suggested clockwise (Table 1). Such conflicting rotations have been documented elsewhere as well (e.g., Jacobi et al., 2002), in contrast to the early work of Zhao and Jacobi's (1997) and Younes and Engelder (1999), who suggested clockwise rotation should be the norm in the eastern part of the curvature of the Pennsylvanian Salient. Jacobi et al. (2002) suggested that local stress field perturbations resulting from faults might account for the local conflicts, and that timing issues (e.g., not all ENE fractures are the same age) might also lead to conflicting inferred rotations.

FAULTS OBSERVED AND INFERRED FROM OUTCROPS

A few faults were observed in the study area, all with minimal stratigraphic offset. These include normal faults at Borodino Reef of the Tully Formation (Figure 13n). Several faults with slickenfibers cross the outcrop, all with very minor stratigraphic throw. The faults strike north (8° , 50° W and 6° , 61° W), and slickenfibers and slickenlines plunge obliquely with a range from 243° , 30° to 278° , 58° . These faults are thus both normal faults (down-to-the-west) and oblique slip with a left lateral component. Other faults include a NNW-striking thrust (eastward directed) on the east side of Skaneateles Lake (Figure 4) and an ENE-striking right lateral fault in the same area (Figure 4). Fracture intensification domains (FID) have been ascribed to fault related activity (either in the immediate section, or down section from the FID) (e.g., Jacobi and Fountain, 1996). One NNW-striking (340°) FID was observed in the Genesee Group at Fillmore Glen (about 5 km south of the central study area) that has recognizable throw on each fracture (Figure 13k, l, m).

Faults can also be inferred from elevations of the Tully Formation at the starred locations in Figure 15 (with elevations annotated); these elevations clearly indicate that faults have dislocated the Tully, but the actual fault trends and locations that could account for the anomalous elevations are nearly limitless. Figure 15a and b shows two possible scenarios, but these are only some of the possibilities. The consistent elevations of about 1300 ft along the eastern side of Skaneateles Lake suggest that in this area the strike is about NNW/NW (Figure 15a, b). This strike is anomalous compared to regional Appalachian basin strikes in the Skaneateles quadrangle (Smith, 1935), and may indicate a transfer zone between the more normally (easterly) striking zones farther west and east. Such a transfer zone would be localized along Skaneateles Lake, where

other elements also suggest a fault system, such as the as the aeromagnetic anomalies along Skaneateles Lake (see discussion below and Figure 16) and the stratigraphic relationships suggesting a sharp depositional slope to the west of the eastern shore of Skaneateles Lake (e.g., Brett and Baird, 1996, and Martin et al., 2008).

Two sites should be considered more fully before using their elevations. Heckel (1973) estimated that the Borodino reef (for location see “B” on Figure 15) was built up about 15 ft (4.5 m) above the surrounding sediments (in present thicknesses, not original uncompressed thicknesses). Thus, the elevation of the Tully here may be 15 ft (4.5 m) higher than the surrounding non-reefal Tully (and those 4.5 m should not be used in calculating faulting). However, the two closest Tully sites also have comparable elevations, and in fact the 1380 ft elevation of the Tully site to the south of Borodino Reef indicates that either the Borodino reef site is too low relative to the 1380 site, or the 1380 site too high, given a regional dip of about 25 to 30 ft/mile (7.6 m to 9.1 m/mile) to the south (Smith, 1935). The elevation of the Borodino field site is accepted as a legitimate Tully elevation, and a fault placed between the Borodino field site and the field site to the south. The fault has a northerly-strike, as do the faults in the Borodino outcrop.

The second site to be considered has a highly anomalous elevation near the southern tip of Skaneateles Lake (Figure 15). Although this very small limestone outcrop was ascribed to the Tully in the field, it may be more probable that it is actually the Portland Point Limestone of the Moscow Formation (as mapped by Smith, 1935). In that case the faults separating the southwest outcrop in both alternative fault models are not necessary for at least this outcrop.

In Figure 15a, most of the faults have a northerly strike, based on the faults at the Borodino Reef, and the faults are assumed to have minor stratigraphic throw. In Figure 15b, the primary fault extends along Skaneateles Lake, with minor faults trending either ENE (as shown, based on fracture trends), or EW (not shown), based on the Alleghanian faults exposed elsewhere in the region.

HIGH RESOLUTION AEROMAGNETICS AND FAULTS

High resolution reduced-to-pole aeromagnetics (JP Fagan, pers. commun, 2005) are shown in Figure 16 for part of central New York State. Steep, large-amplitude, linear gradients in aeromagnetics in the northern Appalachian Basin are coincident with fault systems at the surface

in other parts of NYS (e.g., Jacobi, 2002). In Figure 16b, lineaments along the trends of selected major aeromagnetic gradients are highlighted; these lineament trends include NNW, NNE, NS, and ENE. The lineaments were picked before the DEM was superimposed to guard against biasing the locations of the aeromagnetic gradient lineaments. It is therefore impressive that NNW-trending aeromagnetic lineaments A and C are coincident with Owasco and Otisco lake valleys (respectively), and NNW-aeromagnetic anomaly B is collinear with Skaneateles Lake (Figure 16b). Aeromagnetic anomaly B is also within 2 km, and collinear with, the prominent NNW-trending valley of Bear Swamp Creek (Figure 16b). The NNW-trending portion of Skaneateles Lake is coincident with a small negative aeromagnetic anomaly with amplitudes on the order of 100 nT (Figure 16). Such a small amplitude anomaly could result from the absence of sedimentary rocks (with low magnetic susceptibilities) in the valley compared to the surrounding hills, but similar valleys (e.g. Otisco) with similar rock units do not show such an anomaly. Thus, it is probable that the small aeromagnetic anomaly is sourced deeper than the Paleozoic sedimentary section (i.e., it also is sourced in the Precambrian basement). To the east in Chenango County and the west in the Seneca/Cayuga lake region, Jacobi (2007a, b) showed that most of the reactivated faults that penetrate the entire sedimentary section have very high dips, and that they are associated with FIDs that are less resistant to erosion, especially glacial action. Thus, it is not surprising that faults in the Precambrian, inferred from linear steep aeromagnetic gradients, coincide with valleys, indicating that these faults, or related fracture systems, also extend to the surface. In particular, aeromagnetic lineament B and the small amplitude anomaly along Skaneateles Lake support the fault proposed along the lake based on the elevation of the Tully and the stratigraphic relationships discussed in the introduction. Another NNW-trending lineament that is coincident with topographic relief is aeromagnetic lineament D (compare lineament location to small topographic relief trends in the DEM, for better viewing, see DEM in figures 2 and 3).

Northerly-trending aeromagnetic gradients are also prominent in the study area, including anomalies G and H (Figure 16b). Aeromagnetic anomaly G is within 1 km of the northerly striking fault observed in the Borodino Reef and the fault proposed on the basis of Tully elevations (Figure 15). It is thus probable that the small faults in the Borodino Reef and the Tully elevation changes reflect (probably reactivated) faults in a fault system that extends to basement. Aeromagnetic anomaly H is collinear with, and less than 3 km from, the northerly trending portion of Tully Valley (east of Otisco Lake, Figure 16b), and therefore the northerly striking

portion of the Tully Valley also most likely follows FIDs/faults in the sedimentary section that are associated with basement faults.

ENE-trending aeromagnetic anomalies E and F abut northerly trending aeromagnetic anomalies west of the study area. This relationship might suggest that the northerly-trending faults here predate the abutting ENE-striking fault systems or that the ENE- striking fault systems are older and were offset along the northerly trending faults. This abutting relationship is similar to that observed in the Finger Lakes region farther west (Jacobi 2007a), where ENE-striking Iapetan-opening faults abut (and transfer along) northerly-striking assumed reactivated intra-Grenvillian faults. Such a situation may occur here, in which case the broad ENEs-trending valley along aeromagnetic anomaly F represents a (reactivated) Iapetan opening FID/fault system.

DEM LINEAMENTS

Topographic lineaments were identified from the DEM shown in Figure 17; only those longer than 0.5 km were included in the figure. Quality assurance/quality control was effected by having both operators (Jacobi and Stroup) indentify lineaments in the same orange boxed area (Figure 17) in the same allotted time, each at two different scales 1:50,000 and 1:250,000. As detailed in Table 2, 78% of Stroup's lineaments matched Jacobi's lineaments. The average difference of angles between the lineaments picked by Jacobi and those by Stroup was 4.3° , and the SD was 5.1° . The average difference in length between the lineaments picked by Jacobi and those by Stroup was more significant: 611 m. This lager difference was driven by lineaments in the major valleys, in which Stroup identified single lineaments and Jacobi segmented the lineaments. In the study Stroup identified the lineaments.

Verification of the lineaments was accomplished by the weights of evidence in which buffers are placed around the topographic lineament (Figures 18 to 29), and then the buffered lineament areas are tested to determine the number (area) of 50 m buffered field sites that intersect or fall within the lineament buffer. The field sites considered are those that have fractures oriented parallel to the lineament. Larger positive contrast values indicate larger spatial overlaps among lineaments and field site buffers (essentially that field sites verify the lineament). (See Cruz et al., 2005, and Jacobi (2007a, b for explanation of this methodology). Table 3 presents the weights-of-evidence calculations, and Table 3m summarizes which topographic and EarthSat (1997) lineaments have significant positive contrast values. Table 3m shows that only the NW-trending

topographic and EarthSat (1997) lineaments (Figures 18 and 19) are consistently groundtruthed by field sites with appropriately oriented fractures. Other relatively strongly groundtruthed lineaments trend NE and ENE. Weakly confirmed trends include NS, NNW, and EW. Figure 30 displays the relationships among the total area of various lineament trends (with buffers), the percent of sites in the lineament buffer that exhibit fractures striking collinearly with the lineament trend, and contrast values of 1 and 0. For the study area, only Iib (EW) with all fracture frequencies, ENE with all fracture frequencies, and NW with FID fracture frequencies (> 4 fractures/m) have: 1) contrast values over 1, have significant lineament areas, and have a high percent of sites in the lineament buffer with the appropriate fracture strikes.

The groundtruthed NW-trending lineaments for both topography and Landsat (EarthSat, 1997) are primarily along the shores of Skaneateles Lake (Figures 18 and 19) where NW-striking fractures with all fracture frequencies occur, including high fracture frequencies (FIDs, red in Figures 18 and 19). Note that the bear Swamp creek NW-trending anomaly that is nearly coincident with an aeromagnetic anomaly does not have any sites that could be used to groundtruth the lineament.

NNW-trending topographic lineaments (Figure 20) were weakly verified by weights of evidence if 500 m buffers were placed around the sites (Table 3m). The lineaments that were groundtruthed by NNW-striking fractures (with frequencies ranging from less than 2 fractures/m to greater than 4 fractures/m) were lineaments along Skaneateles Lake and Otisco Lake (Figure 20). However, NNW-trending EarthSat (1997) lineaments (Figure 21) were not verified by the weights of evidence (Table 3). In the northern part of the study area, a NNW topographic and EarthSat lineament are within 1 km of a NNW-striking, west-dipping thrust. N-trending topographic lineaments (Figure 22) were also weakly verified by weights of evidence if 500 m buffers were placed around the sites (Table 3m). The lineaments that were groundtruthed by N-striking fractures (with frequencies ranging from less than 2 fractures/m to greater than 4 fractures/m) were lineaments that pass through the Borodino Reef area ("B" on Figure 22) and other short lineaments including clusters near the south end of Skaneateles Lake and near the western shore of Skaneateles Lake. N-trending EarthSat (1997) lineaments were not verified by the weights of evidence (Table 3).

ENE-trending topographic and EarthSat (1997) lineaments (Figures 23 and 24) were strongly verified by the weights of evidence (Table 3). Many of the topographic anomalies are short, and

may therefore reflect fracture systems rather than FID/fault systems (as proposed by Jacobi et al. 2002b), but the few that are verified by sites with FIDs striking ENE may reflect faults. Furthermore, one of the ENE-trending topographic lineaments is only 2.5 km long, but is coincident with a right lateral fault (Figure 23). The broad ENE-trending valley (“Woodland low”) in the northern part of the study area is a longer lineament, and it also is verified by several ENE striking FIDs (Figure 23). This lineament is on strike with an aeromagnetic gradient (“F” in Figure 16b) which indicates that this fracture/fault/lineament zone may be an ENE extension of an ENE-striking fault system that extends to basement. Significantly, Triana drilled a deep test about 4 km north of the valley, and since they always targeted deep structure, it is possible that these ENE-striking fault systems are related to reactivated Iapetan-opening faults. The ENE-trending aeromagnetic anomaly “F” (Figure 16b) is also coincident with a broad ENE trending valley west of Skaneateles Lake (the broad valley of Dutch Hollow Brook). These coincident features suggest that faults and/or associated fractures in basement extend to the surface. These ENE-trending lineaments and associated FIDs/aeromagnetic gradients may reflect reactivated Iapetan-opening fault such as those that localized the Trenton/Black River gas fields to the southwest (e.g., Jacobi et al., 2003, 2004 a, b)

Relatively few E-striking lineaments were indentified either from topography (Figure 27) or from Landsat images (EarthSat, 1997). Weights of evidence weakly confirmed the lineaments. The only EW EarthSat (1997) lineament was confirmed by an E-striking FID in the broad valley in the north of the study area (Figure 24).

CONCLUSIONS

Eight characteristics of about 1650 fractures were measured in the study area that encompasses Skaneateles and Otisco lakes, central New York State. The predominant fracture set in the study area strikes NNW; other prominent fracture sets strike EW, ENE, N, NNE, NW and WNW, in descending order of fracture abundances. Two localities were discovered with faults: one is the Tully Formation Borodino Reef locality that has northerly striking normal faults in outcrop with calcite slickenfiber surfaces. Other evidence for faults in the Borodino Reef area are anomalous Tully elevations, N-striking FIDs, and N-trending topographic and aeromagnetic lineaments. In total, these coincident features suggest that a northerly trending fault system is located in the Borodino Reef region that extends down to basement, and the reef was probably localized along

the upthrown block side of the fault. Dolomite and quartz fills in the fractures of the reef point to hydrothermal circulation in this region in Acadian and/or Alleghanian times. The second fault locality exhibits both dextral ENE-striking faults and NNW, west dipping thrusts. ENE-trending topographic and EarthSat (1997) lineaments pass through the site with the ENE-striking fault, and are therefore thought to represent the fault and associated fractures. Similarly, a lineament passes close to the thrust, and is thought to be groundtruthed by the thrust.

Steep aeromagnetic gradients are coincident with the Owasco Lake valley to the west, with the Otisco Lake valley to the east, and are near the Skaneateles Lake valley and the Bear Swamp Creek valley. Such gradients and coincidence with topography suggest that faults in the Precambrian extend up through the Paleozoic cover. Support for the fault hypothesis comes from the elevations of the Tully, which have anomalous elevations along Skaneateles Lake, suggesting a fault along the lake. An ENE-trending broad valley west of Skaneateles Lake, “Dutch Hollow Brook” valley, is coincident with a major ENE-trending aeromagnetic gradient, and an ENE-trending valley farther east between Skaneateles and Otisco lakes (“Woodland” valley) is approximately on strike with the aeromagnetic gradient. This eastern valley lineament is confirmed by several ENE-striking FIDs. These ENE-trending coincident FIDs, topographic lineaments, and EarthSat (1997) lineaments suggest fault systems that are basement rooted, but extend up through the section. Such faults may well be reactivated Iapetan-opening fault such as those that localized the Trenton/Black River gas fields to the southwest. In total, although an EW brokered seismic line across the northern end of the lakes was not able to be processed satisfactorily, the field work, geopotential fields, and associated lineaments strongly suggest that NNW, N, and ENE-striking faults chop the region into blocks.

REFERENCES

- Brett, C. E., and Baird, G. C., 1996, Middle Devonian sedimentary cycles and sequences in the northern Appalachian Basin, *in* Witzke, B. J., Ludvigson, G. A., and Day, J., (eds.), Paleozoic Sequence Stratigraphy: Views from the North American Craton: Geological Society of America Special Paper 306, p. 213-241.
- Cruz, Cheri, Jacobi, Robert D., Everett, John R., and Staskowski, Ronald J., 2005, ASTER and Landsat lineaments in central NYS: Image processing and groundtruthing for fractures: Geological Society of America, Abstracts with Programs, Geological Society of America, Abstracts with Programs, v. 37, n. 1, p. 58.
- Engelder, T., 1985, Loading paths to joint propagation during a tectonic cycle: an example from the Appalachian Plateau, *J. of Structural Geology*, 7, 459-476.
- Engelder, T. and Geiser, P., 1980, On the use of regional joint sets as trajectories of paleostress fields during the development of the Appalachian plateau, New York, *J. Geophys. Res.*, 85, 6319-6341.
- Engelder T., and Lash, G.G., 2008, Marcellus shale play's vast resource potential creating stir in Appalachia: *American Oil and Gas Reporter*, v. 51, n. 6, p. 76-87.
- Engelder, T., Haith, B.F., and Younes, A., 2001, Horizontal slip along Alleghanian joints of the Appalachian plateau: evidence showing that mild penetrative strain does little to change the pristine appearance of early joints: *Tectonophysics*, v. 336, p. 31-41.
- Engelder, T., Lash, G.G., and Uzcategui, R., 2009, Joint sets that enhance production from Middle and Upper Devonian gas shales of the Appalachian Basin: *American Association of Petroleum Geologists Bulletin* v. 93, p. 857-889.
- Fisher, D.W., Isachsen, Y.W., and Rickard, L.V., 1970. Geologic map of New York: New York State Museum and Science Service, Map and Chart Series 15, 5 sheets.
- Grasso, T. X., 1986, Redefinition, stratigraphy, and depositional environments of the Mottville Member (Hamilton Group) in central and eastern New York, *in* Dynamic Stratigraphy and Depositional Environments of the Hamilton Group (Middle Devonian) in New York State, Part I, C. E. Brett, (Ed): New York State Museum (Albany, NY), Bull. 457, p. 5-31.
- Griffing, David H., and Ver Straeten, Charles A., 1991, Stratigraphy and depositional environments of the lower part of the Marcellus Formation (Middle Devonian) in eastern New York State, *in* Field Trip Guidebook, James R. Ebert (ed): New York Geological Association, 63rd Annual Meeting (Oneonta, NY), p.205-249.

- Gross, M., and Engelder, T., 1991, A case for neotectonic joints along the Niagara Escarpment: *Tectonics*, v. 10, p. 631-641
- Gross, M., Engelder, T., and Poulson, S., 1992, Veins in the Lockport Dolomite: Evidence for an Acadian fluid circulation system: *Geology*, v. 20, p. 971-974.
- Harper, John A., and Laughrey, Christopher D., 1987, *Geology of the oil and gas fields of southwestern Pennsylvania: Bureau of Topographic and Geologic Survey (Harrisburg)*, 166 p.
- Jacobi, Robert D., 2002, Basement faults and seismicity in the Appalachian Basin of New York State, *in Neotectonics and Seismicity in the Eastern Great Lakes Basin*, R. H. Fakundiny, R. D. Jacobi, and C. F. M. Lewis (eds.): *Tectonophysics*, v. 353, p.75-113.
- Jacobi, Robert D., 2007a, Final Technical Report (May 31, 2000-May 15, 2007): Innovative Methodology for Detection of Fracture-Controlled Sweet Spots in the Northern Appalachian Basin: Department of Energy/NETL, Morgantown, WV, 453 pp.
- Jacobi, Robert D., 2007b, Natural gas exploration in Chenango County, New York State: Economic development of stacked reservoirs: NYSERDA (Albany NY) Final report, 62 pp, 94 figures, and 30 tables.
- Jacobi, Robert D., 2009/2010, Northern Appalachian Basin faults, fractures and tectonics and their effects on the Utica, Genesee and Marcellus black shales: Joint AAPG / University at Buffalo field course notes, 42 p. plus powerpoint presentations.
- Jacobi, Robert D., and Fountain, John C., 2001, The implications of fracture intensification domains (FIDs) for fluid flow: Part I, recognition and characteristics of FIDs and their relation to faults, in Session 5 of Conference Proceedings, B. H. Kueper, K. S. Novakowski, and D. A. Reynolds (eds.): Queens University (website and CD), 4p
- Jacobi, R. D., and Zhao, M., 1996a, Digital imaging and analyses of fractures: Evidence for Appalachian style tectonic in the Appalachian Plateau of western New York: *Geol. Soc. Am., Abstracts with Programs*, v. 28, n. 3, p. 67.
- Jacobi, Robert and Zhao, Meng, 1996b, Rapid and rigorous outcrop fracture trace mapping and analyses, *In Contaminant Hydrogeology in Fractured Bedrock (J. Fountain, Ed.)*: *Geol. Soc. Am. (Northeast Section, Buffalo meeting) short course notes*, p. 1-19.
- Jacobi, R. D., Fountain, J.C., Gill, G., Hunt, E. D., 1990, Evidence for the continuation of the Clarendon-Linden Fault System into central Allegany County, New York: *Geol. Soc. Am., Abstracts with Programs*, v.22, n.2, p.25-26.

- Jacobi, Robert and Fountain, John, 1996, Determination of the Seismic Potential of the Clarendon-Linden Fault System in Allegany County, Final Report: Presented 6/10/96 to NYSERDA, 2106 pp. & 31 oversized maps.
- Jacobi, R. D., Fountain, J., and Loewenstein, S., 2002, Demonstration of an exploration technique integrating EarthSat's Landsat lineaments, soil gas anomalies, and fracture intensification domains for the determination of subsurface structure in the Bass Island Trend, New York State, Final Report: presented to NYSERDA (Albany NY) on 7/22/02, 188 p.
- Jacobi, Robert D., Fountain, John C., Lugert, Courtney M., Wehn, Karen S., Nelson, Travis, Budney, Lucas, and Zybala, Jon G., 2002a, Fracture Intensification Domains, fracture flow, and Trenton-Black River faults in the Finger Lakes region, NYS: Geol. Soc. Am., Northeastern Section Annual Meeting (Springfield, MA) Abstracts, v. 34, n. 1, p. A-11.
- Jacobi, Robert D., Eastler, Thomas E., and Xu, Jiandong, 2002b, Methodology for remote characterization of fracture systems in enemy bedrock underground facilities, *in* The Environmental Legacy of Military Operations, Russell Harmon and J. Ehlen (eds.): Geol. Soc. Am. Engineering Geology Division, v. 14, p. 27-60.
- Jacobi, Robert D., Fountain, John, Lugert, Courtney, Nelson, Travis, Smith, Gerald, Mroz, Thomas, and Martin, John, 2003, Identifying Trenton/Black River targets in the northern Appalachian Basin (NYS): Demonstration of integrated exploration tools: American Assoc. Petrol. Geol. Annual Meeting program, v. 12, p. A44
- Jacobi, Robert D., Loewenstein, Stuart, Smith, Gerald, Fountain, John, Lugert, Courtney, Mroz, Tom, and Martin, John, 2004a, Fault Systems and the Trenton/Black River Play in New York State: AAPG Eastern Section Meeting Abstracts, <http://www.searchanddiscovery.com/documents/abstracts/2004eastern/jacobi01.htm> Accessed February 10, 2005.
- Jacobi, Robert D., Loewenstein, Stuart, Smith, Gerald, Fountain, John, Lugert, Courtney, and Martin, John, 2004b, Iapetan Opening/Rome Trough-Related Faults and Their Reactivation History in New York State: AAPG Eastern Section Meeting Abstracts, <http://www.searchanddiscovery.com/documents/abstracts/2004eastern/jacobi02.htm> Accessed January 3, 2005.
- Jacobi, Robert D. Loewenstein, Stuart, and Smith, Gerald, 2006, Seismic Evidence for Iapetan Fault Control of the Arcuate Map Pattern of the Pennsylvania Salient: Geological Society of America, Abstracts with Programs, v. 41, n. 2, p. 84.

- Jacobi, Robert D., Loewenstein, Stuart, Smith, Gerald, Martin, John, and Mroz, Thomas, 2007, The Pennsylvania salient: seismic and other evidence for an Iapetan arcuate rift influence on the arcuate map pattern: Geological Society of America 2007 national convention. http://gsa.confex.com/gsa/2007AM/finalprogram/abstract_130259.htm
Accessed May 22, 2008
- Jacobi, Robert, Agle, Paul, Smith, Gerald, Lugert, Courtney, Seever, Jodi, Cross, Gareth, and Loewenstein, 2008a, Faulting and fracture heterogeneity in black shales of the Appalachian Basin of New York State: Geological Society of America, Abstracts with Programs, v. 40, n.6 (2008 Joint Annual Meeting, Houston, TX), p. 233.
- Jacobi, Robert, Agle, Paul, Smith, Gerald, Lugert, Courtney, Seever, Jodi, Cross, Gareth, and Loewenstein, 2008b, Faulting and fracture heterogeneity in black shales of the Appalachian Basin of New York State: Geological Society of America, Abstracts with Programs, v. 40, n.6 (2008 Joint Annual Meeting, Houston, TX), p. 233.
- Jacobi, Robert, Agle, Paul, Fisher, Jodi, Loewenstein, Stu, Smith, Gerald J., 2009, Structural anomalies in black shales of the Northern Appalachian Basin in New York State: AAPG National Convention, Denver CO:
http://aapg09.mapyourshow.com/2_1/sessions/session.cfm?ScheduledSessionID=1499&CFID=16152370&CFTOKEN=3b543333e4ce88c0-36743E0A-BC23-81A0-83A1E92588CB683E (accessed 4/24/10).
- Jacobi, Robert, 2010, Geophysical and geological evidence for arcuate Iapetan opening rift faults in the Pennsylvania Salient and New York recess: implications for the ragged Laurentian margin: NYSEERDA (Albany NY) Final Draft Report, 42 pp.
- Lash, G.G., Loewy, S., and Engelder, T., 2004, Preferential jointing of Upper Devonian black shale, Appalachian Plateau, USA: Evidence supporting hydrocarbon generation as a joint-driving mechanism: in Cosgrove, J. W., and Engelder, T., eds., The initiation, propagation, and arrest of joints and other fractures: Geological Society of London Special Publications, v. 231, p. 129-151.
- Lash, G.G., and Engelder, T., 2009, Tracking the burial and tectonic history of Devonian shale of the Appalachian Basin by analysis of joint intersection style: Geological Society of America Bulletin, v. 121, p. 265–277.
- Lyons, R. P. Scholz, C. A. Mullins, H. T., 2005, Seismic stratigraphy of Skaneateles Lake: a high-resolution history of lake level, paleoclimate, and natural hazards in central New York: Northeastern Geology and Environmental Sciences: v. 27; p. 302-316.

- Martin, Jaclyn, Bartholomew, Alexander, Brett, Carlton, and Baird, Gordon, 2008, Biofacies analysis along a Middle Devonian paleogradient: water depth as a primary control on biofacies formation in the Staghorn Point coral biostrome: Geol. Soc. America, Abstracts with Programs (43rd Annual Meeting).
http://gsa.confex.com/gsa/2008NE/finalprogram/abstract_135260.htm, accessed Jan 8, 2011
- Mullins, Henry T. and Halfman, John D.: 2001, High-Resolution Seismic Reflection Evidence for Middle Holocene Environmental Change, Owasco Lake, New York: Quaternary Research
 v. 55 , p. 322-331. doi:10.1006/qres.2001.2232
- Mullins, Henry ., Wellner, Robert W., Petruccione, John L., Hinchey, Edward J., and Wanzer, Steven, 1991, Subsurface geology of the Finger Lakes Region, *in* Field Trip Guidebook, James R. Ebert (ed): New York Geological Association, 63rd Annual Meeting (Oneonta, NY), p.1-54.
- Nyahay, R., Leone, J., Smith, L.B., Martin, J.P., and Jarvie, D.J., 2007, Update on regional assessment of gas potential in the Devonian Marcellus and Utica Shales of New York (abs.), 2007 Eastern Section, American Association of Petroleum Geologists Annual Meeting Program with Abstracts (September 16-18, 2007, Lexington, Kentucky), p. 46.
- Smith, Burnett. 1935, Geology and mineral resources of the Skaneateles quadrangle: New York State Mus. Bull., n. 300, 120 pp.
- Smith, G. J. and Jacobi, R. D., 1998, Fault induced transgressive incised shoreface model for the Canadaway Group, Catskill Delta Complex: Journal of Sedimentary Research, v. 68, n. 4, p.668-683
- Smith, G.J., and Jacobi, R. D., 2001, Tectonic and eustatic signals in the sequence stratigraphy of the Upper Devonian Canadaway Group, New York State: American Association of Petroleum Geologists Bulletin, v. 85, no. 2, p. 325-357.
- Stroup, Joshua T., Jacobi, Robert D., and Nelson, Travis, 2006, Fracture Intensification Domains, Lineaments and Faults in the Skaneateles Lake Region of the Alleghanian Plateau of New York State: AAPG Eastern Section Meeting Abstracts (Buffalo, NY),
<http://www.searchanddiscovery.com/documents/2006/06091eastern/abstracts/stroup.htm>, Accessed January 29, 2007
- Wedel, A. A., 1932, Geologic Structure of the Devonian Strata of South-Central New York: New York State Museum Bulletin, v. 294, 73 p.

Younes, A., and Engelder, T., 1999, Fringe cracks: Key structures for the interpretation of progressive Alleghanian deformation of the Appalachian Plateau: Geological Society of America Bulletin, v. 111, p. 219-239.

Zhao, M. and Jacobi, R. D., 1997, Formation of the regional cross-fold joints in the Appalachian Plateau: J. Struc. Geol., v. 19, n. 6, p. 817-834.



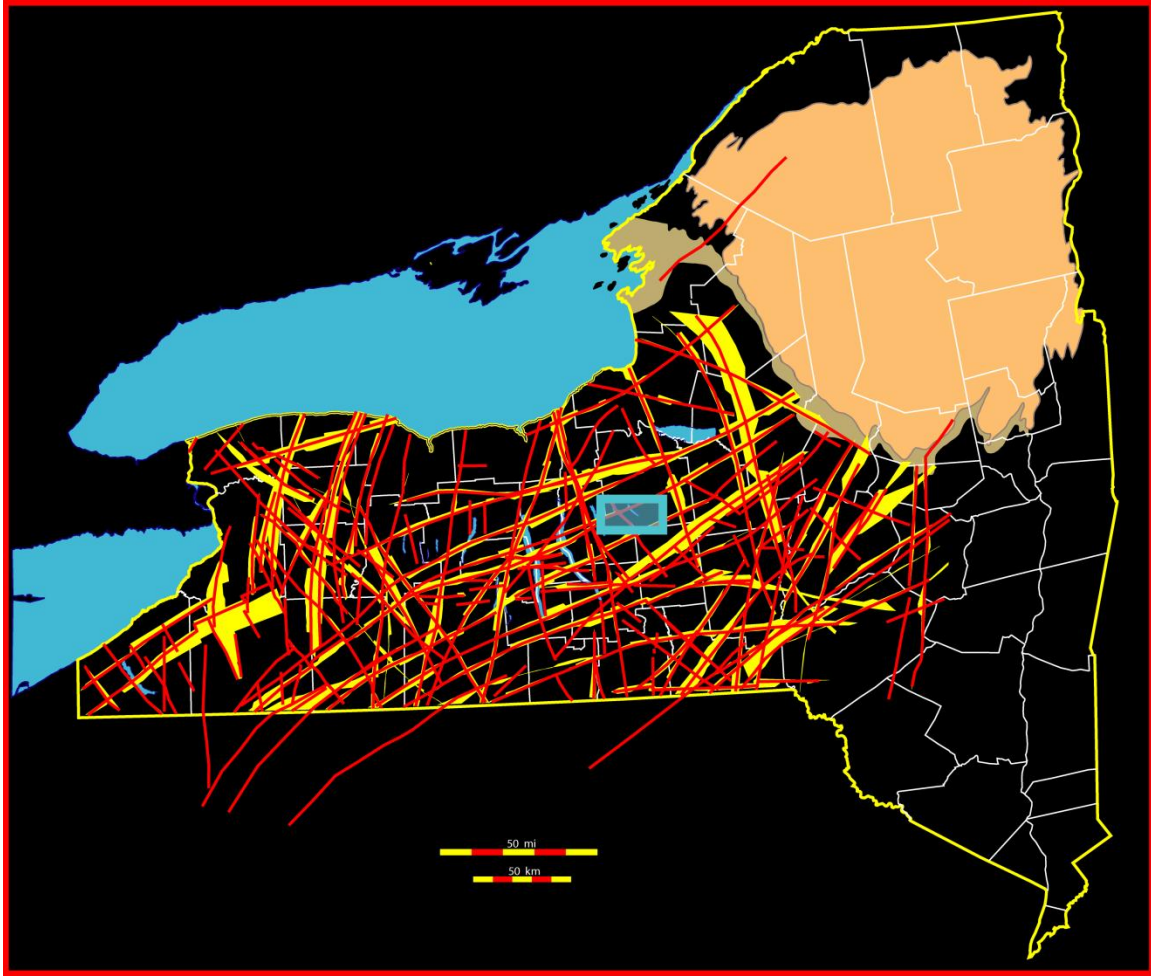


Figure 1a. Location of the focus area in central New York State (blue box). Red lines indicate proposed fault trends, and the yellow bands indicate the extent of proposed fault systems (from Jacobi, 2002).

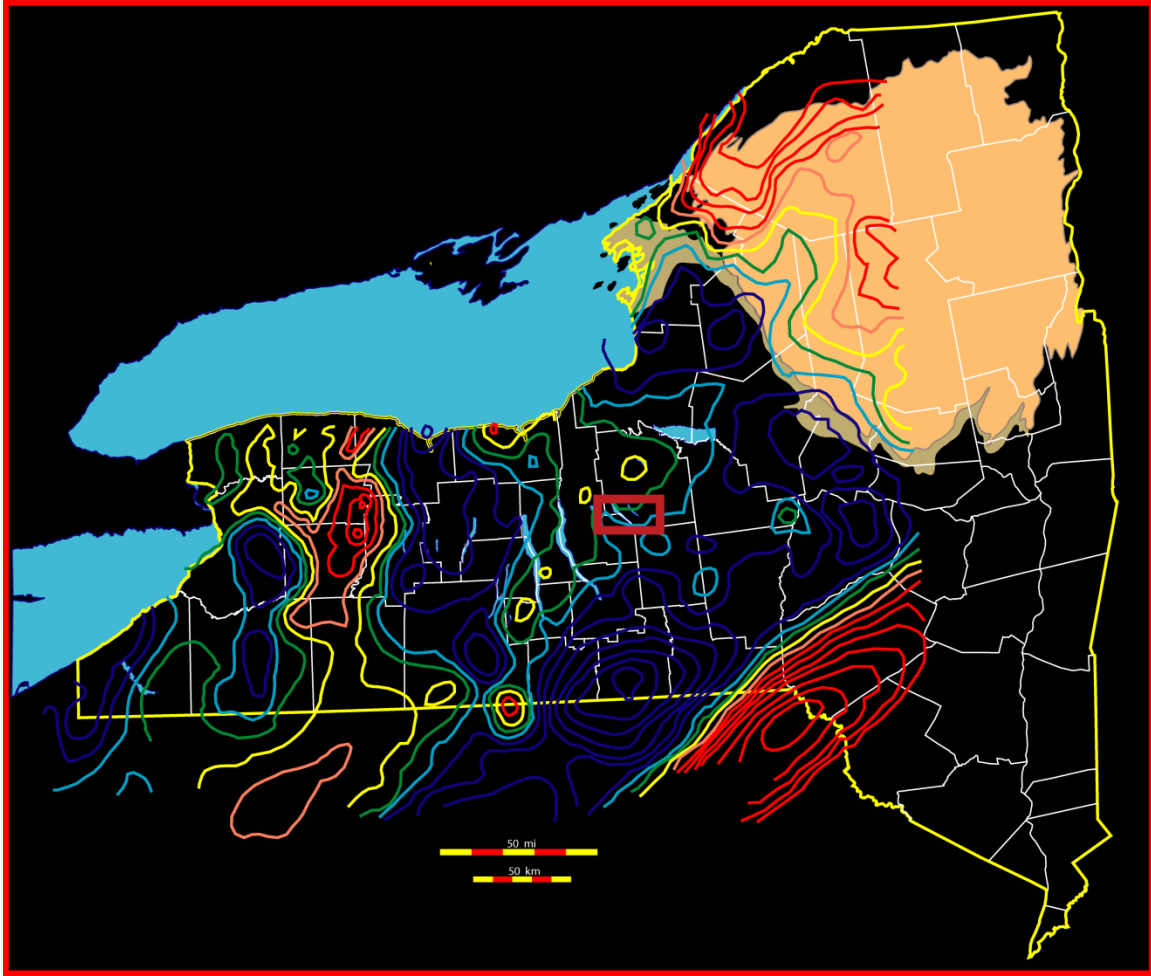


Figure 1b. Location of the focus area in central New York State (red box) with respect to Bouguer gravity. Gravity contour interval equals XX mgal; red indicates high Bouguer gravity values, blue indicates low gravity values (from Jacobi, 2002).

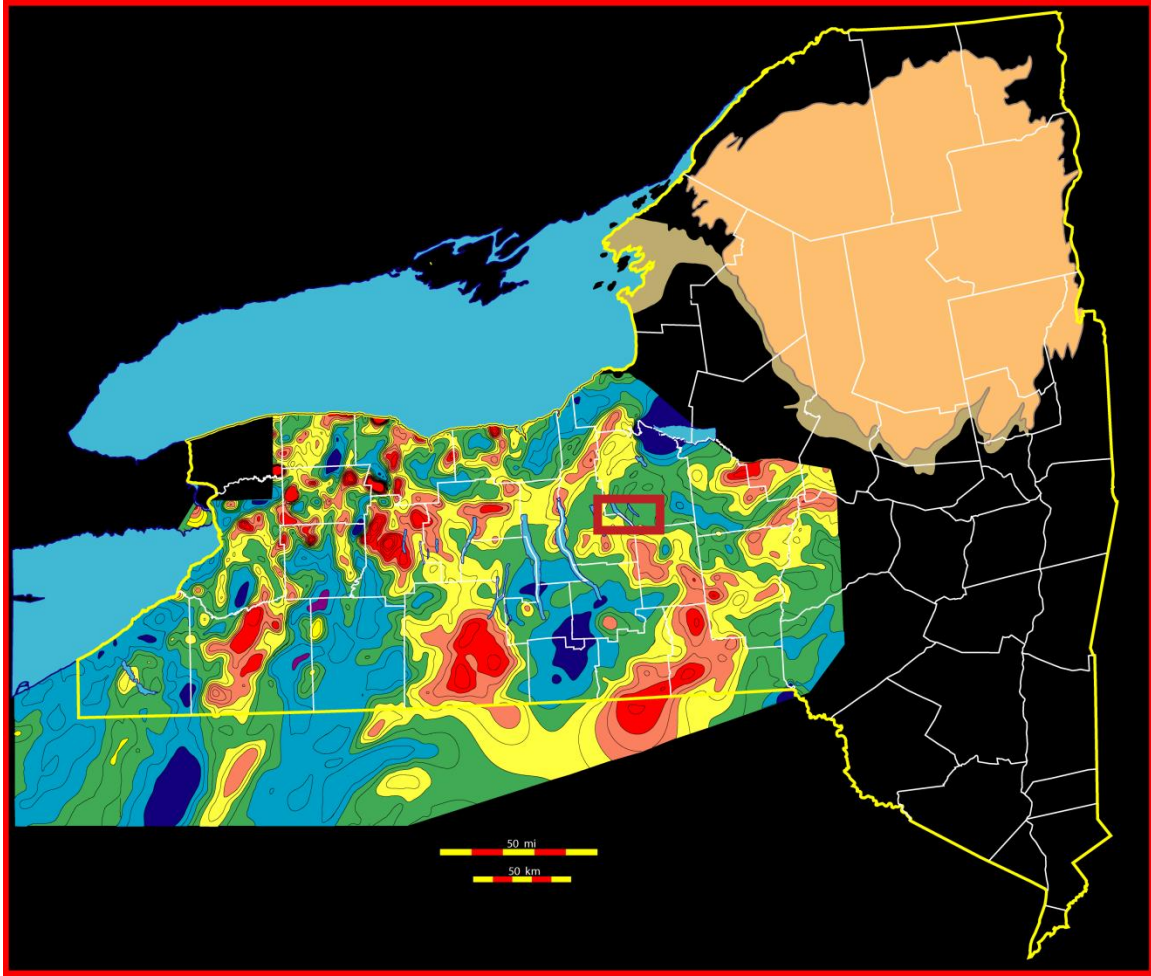


Figure 1c. Location of the focus area in central New York State (red box) with respect to aeromagnetic anomalies. Aeromagnetic anomaly contour interval equals 50 nT; red indicates high aeromagnetic anomaly values, blue indicates low aeromagnetic anomaly values (from Jacobi, 2002).

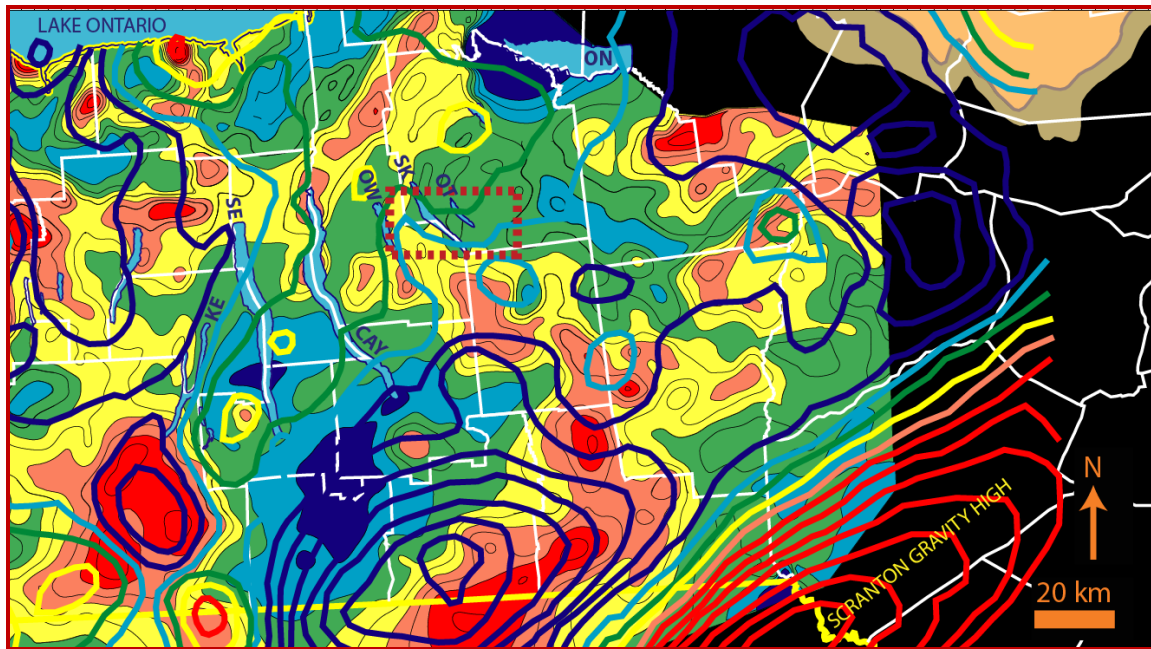


Figure 1d. Enlargement of regional aeromagnetics and gravity with respect to location of the focus area in central New York State (dashed red box). Aeromagnetic anomalies are solid colors, and the contour interval equals 50 nT. Bouguer gravity indicated by bold colored lines and gravity contour interval equals 5 mgal. For both aeromagnetics and gravity, red indicates high values and blue indicates low values. KE = Keuka Lake, CAY = Cayuga Lake, ON = Oneida Lake, OT = Otisco Lake, OW = Owasco Lake, SK = Skaneateles Lake. (After Jacobi, 2002).

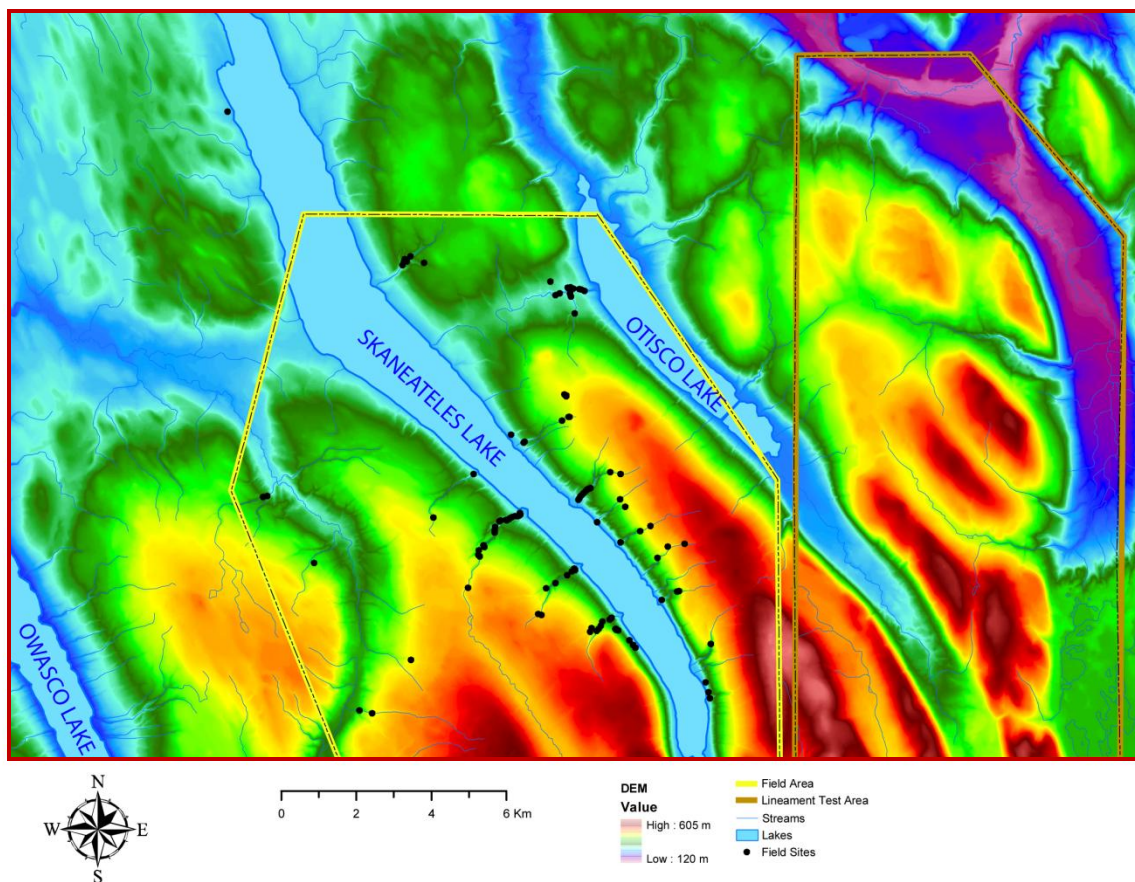


Figure 2a. Field Area and lineament test area on a DEM (digital elevation model) background. Field area outlined in yellow, lineament test area outlined in orange. Field sites indicated by black dots.

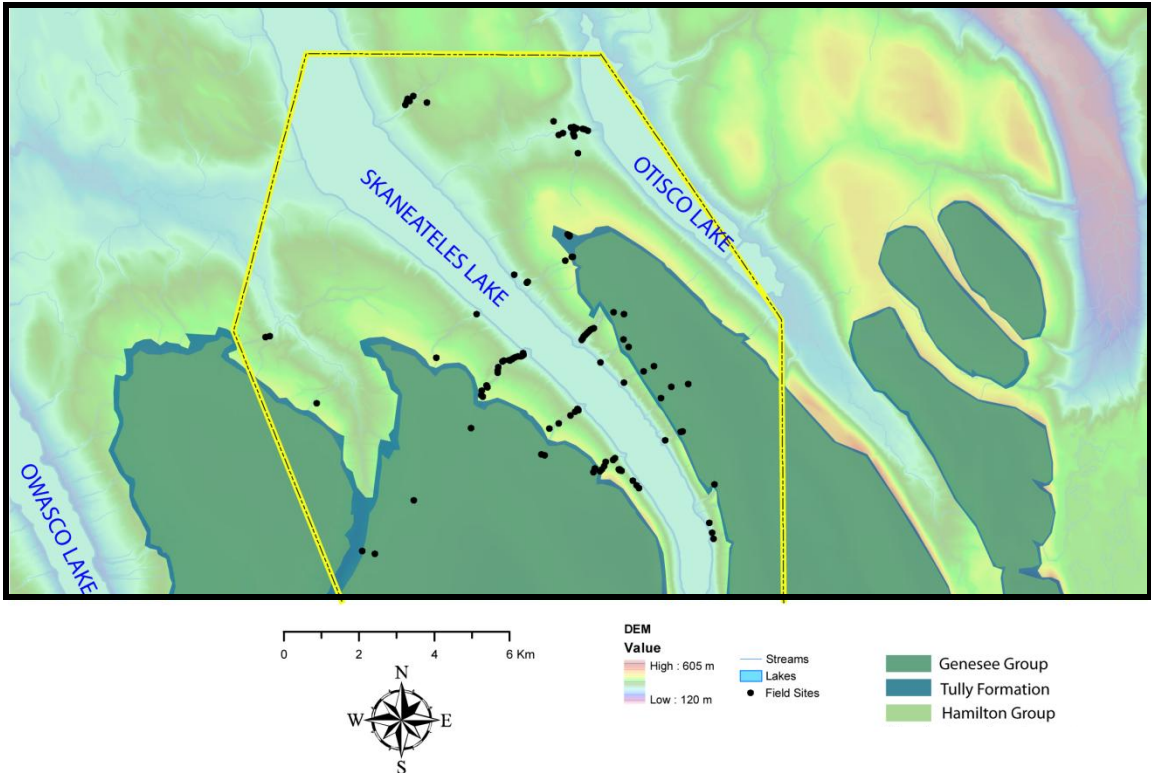


Figure 2b. Generalized geology of field area and adjoining region overlaid on a DEM (digital elevation model) background. Field area outlined in yellow. Field sites indicated by black dots. Geology after Fisher et al. (1970).


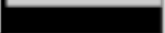





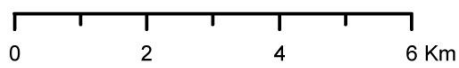
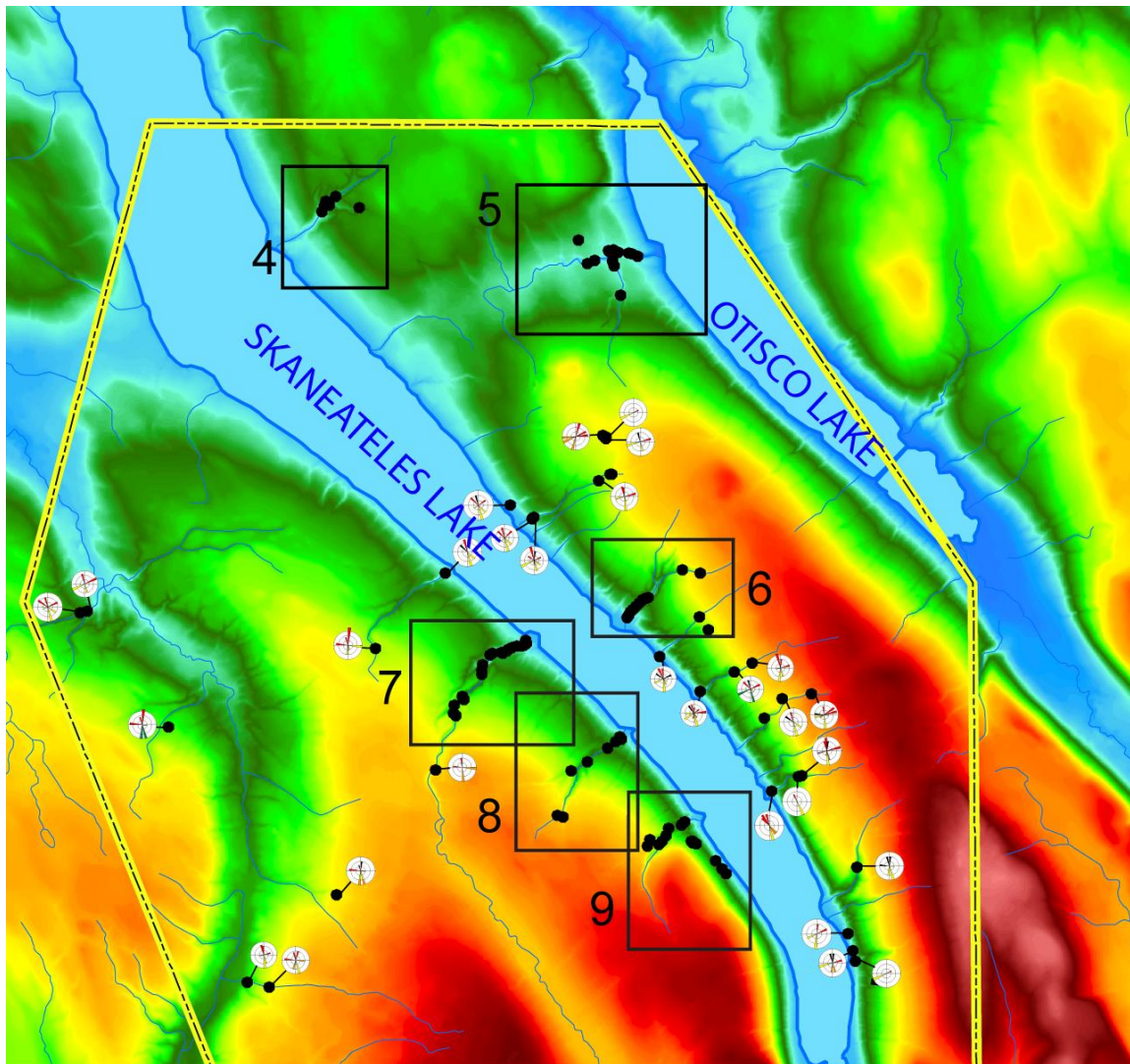
Period		Group	Unit	Lithology
Devonian	Upper	Genesee		
	Middle		Genesee Shale	
			Tully Limestone	
		Hamilton		
		Marcellus Shale		
	TriStates		Onondaga Lst	
			Oriskany Sst	

Figure 2c. Generalized stratigraphic column of field area and adjoining region. Circles with tics indicate potential hydrocarbon reservoirs in central New York State. After Nyahay et al. (2007)



DEM

Value

High : 605 m

Low : 120 m

- Field Area
- Lineament Test Area
- Streams
- Lakes
- Field Sites

Figure 3. Modified rose diagrams of fractures and faults in the Skaneateles study area. Explanation of rose diagrams shown in Figure 10. Labeled boxes indicate enlarged insets in the following figures, and the associated label indicates figure number.

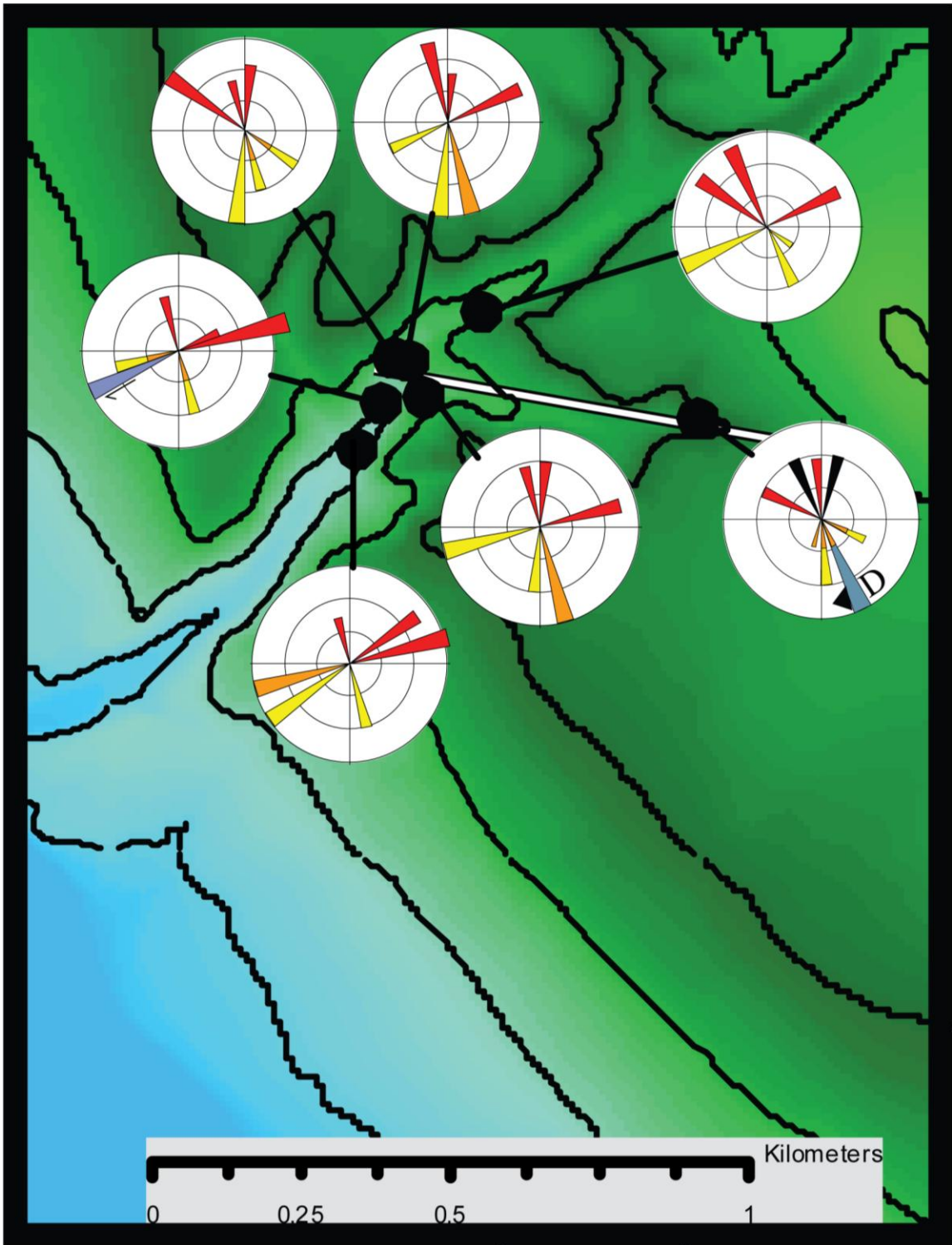


Figure 4. Modified rose diagrams for inset #4 in Figure 3. Explanation of rose diagrams shown in Figure 10. From Stroup et al. (2006).

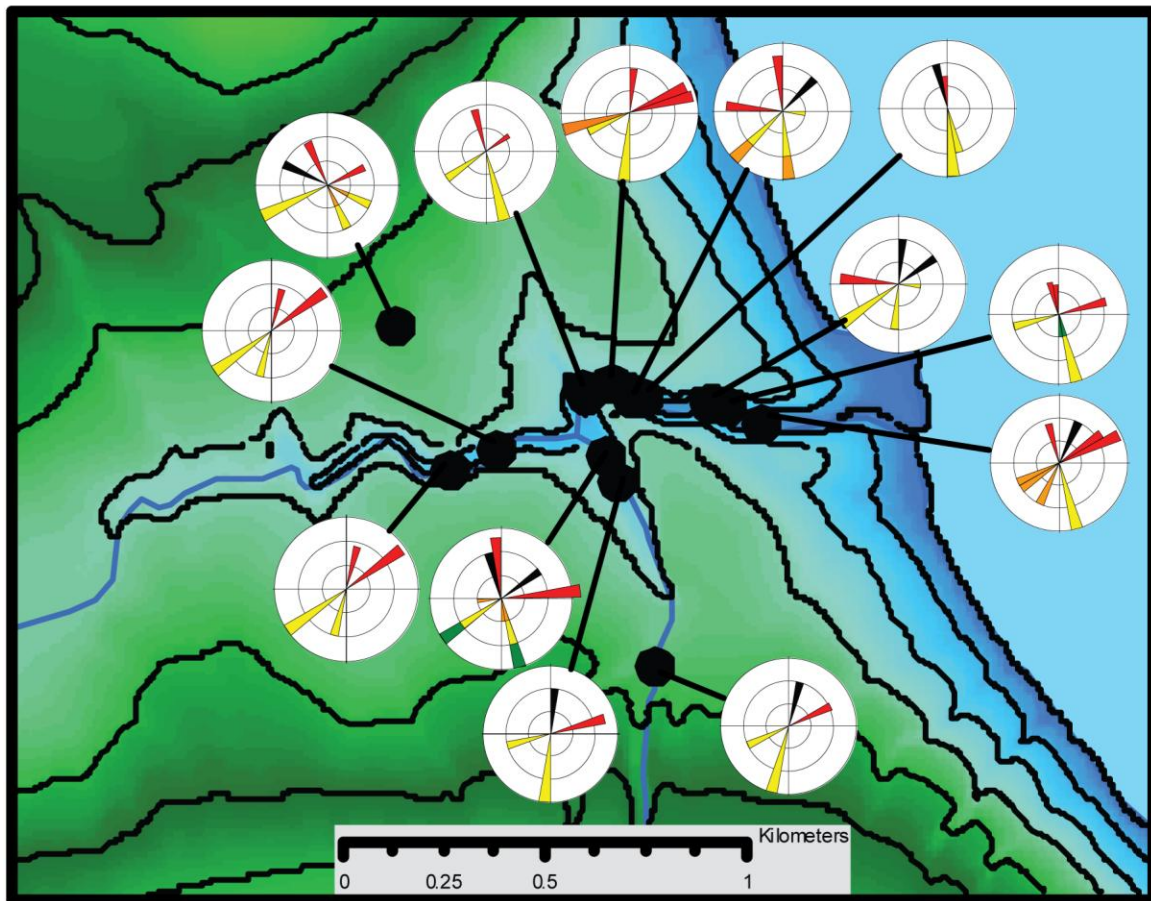


Figure 5. Modified rose diagrams for inset #5 in Figure 3. Explanation of rose diagrams shown in Figure 10. From Stroup et al. (2006).

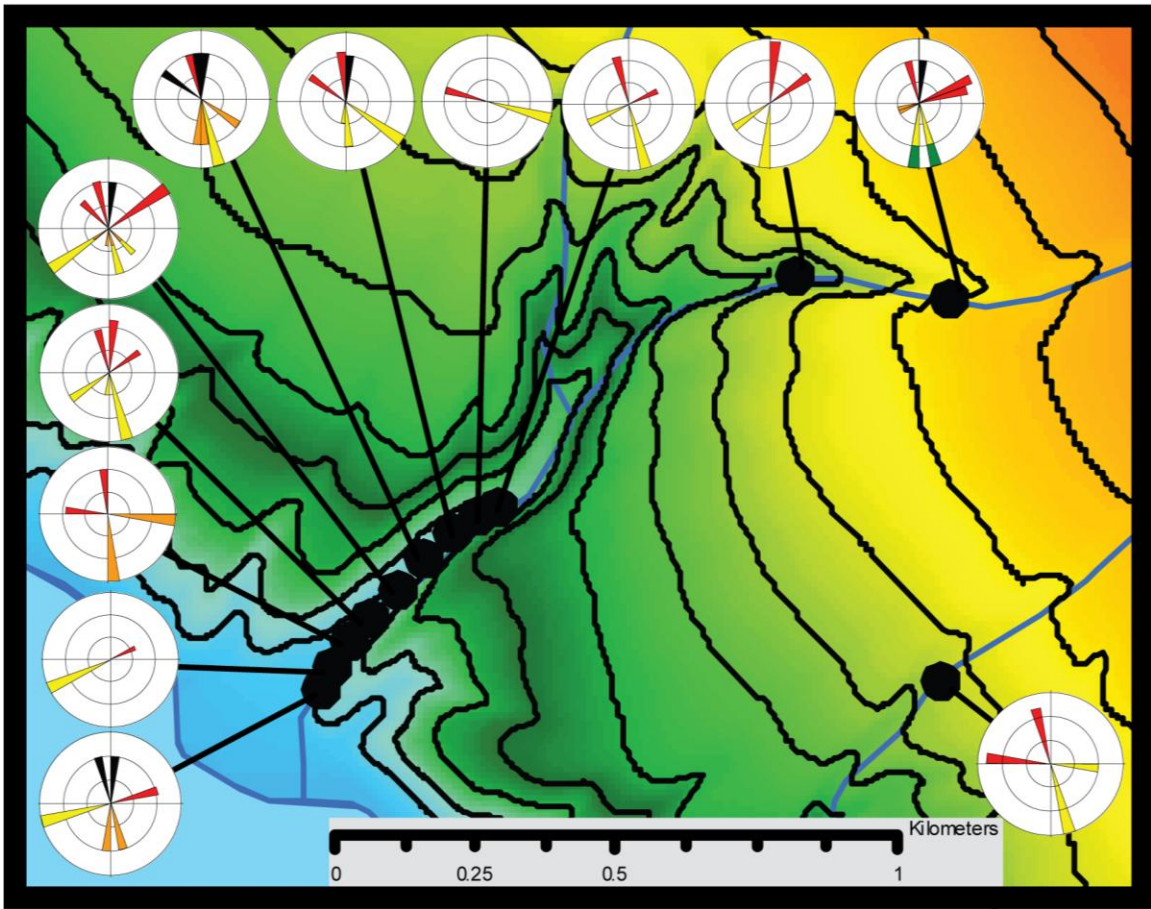


Figure 6. Modified rose diagrams for inset #6 in Figure 3. Explanation of rose diagrams shown in Figure 10. From Stroup et al. (2006).

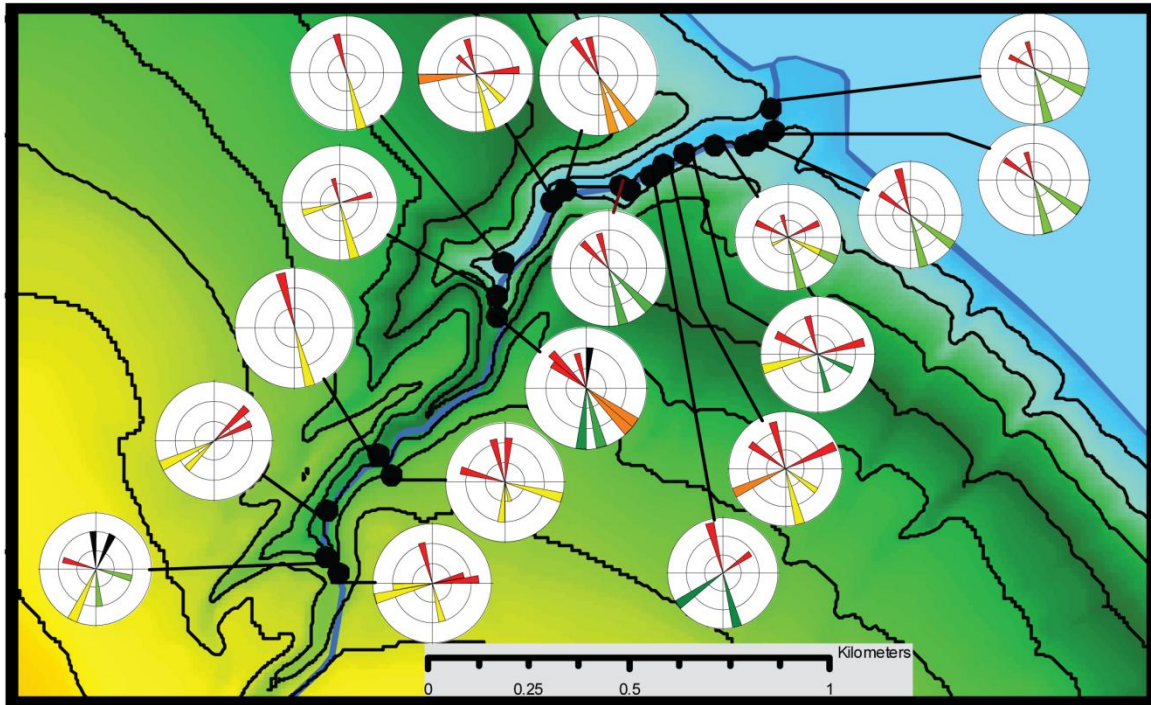


Figure 7. Modified rose diagrams for inset #7 in Figure 3. Explanation of rose diagrams shown in Figure 10. From Stroup et al. (2006).

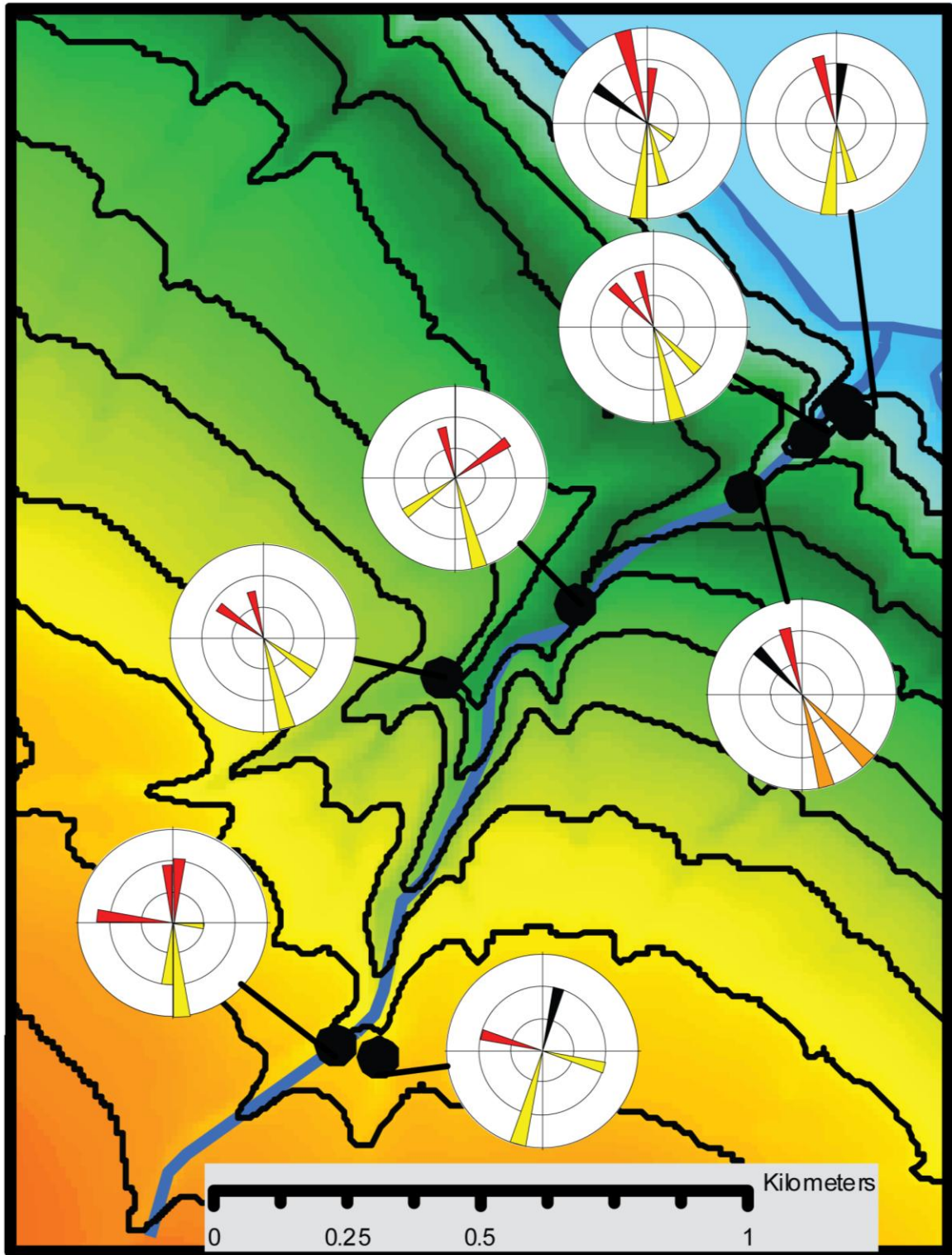


Figure 8. Modified rose diagrams for inset #8 in Figure 3. Explanation of rose diagrams shown in Figure 10. From Stroup et al. (2006).

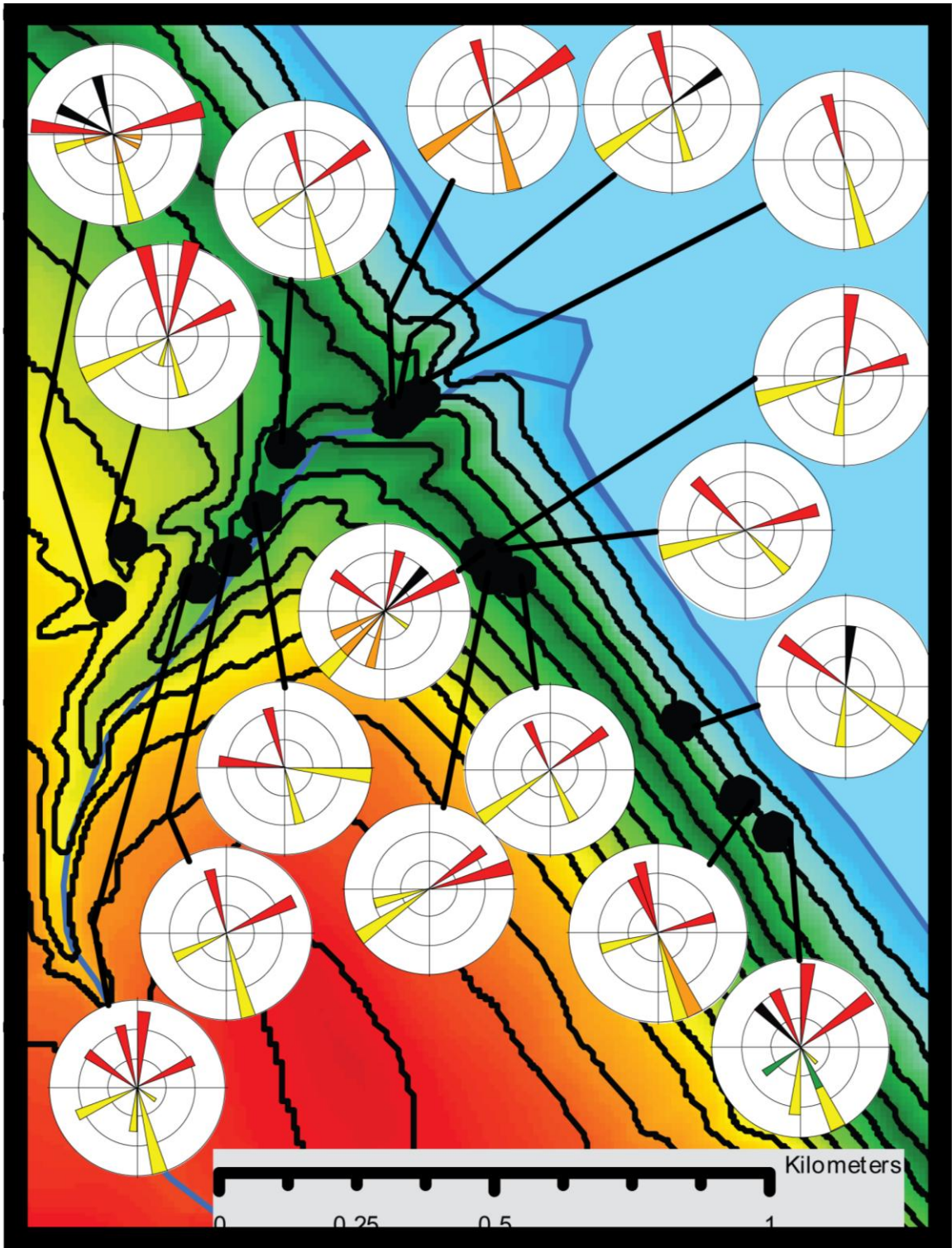


Figure 9. Modified rose diagrams for inset #9 in Figure 3. Explanation of rose diagrams shown in Figure 10. From Stroup et al. (2006).

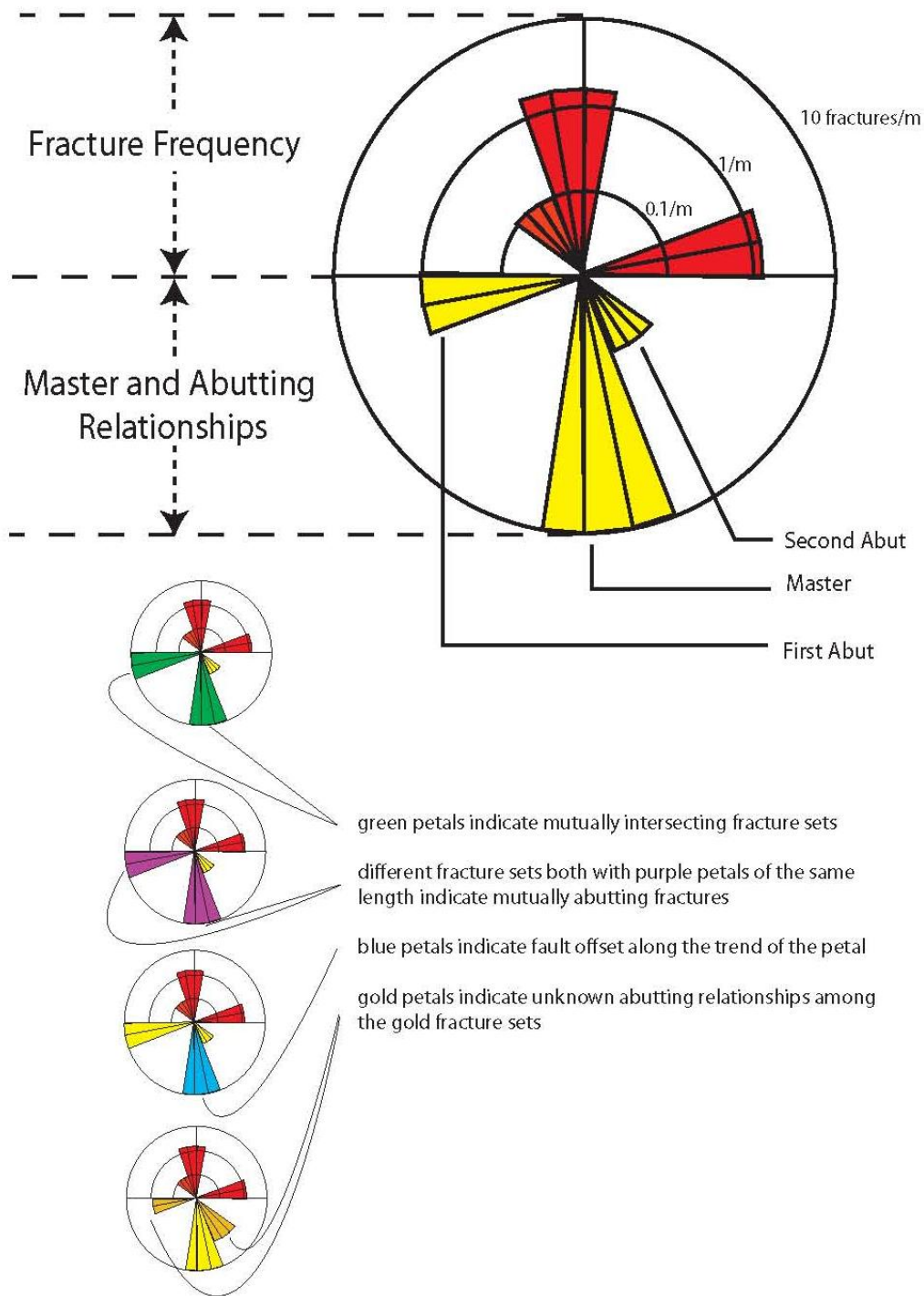
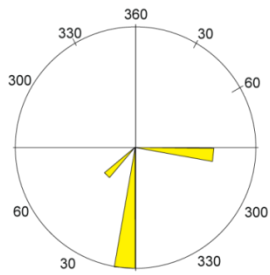
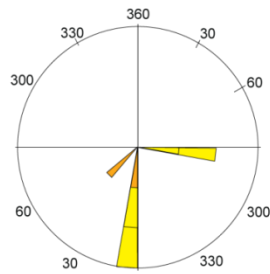


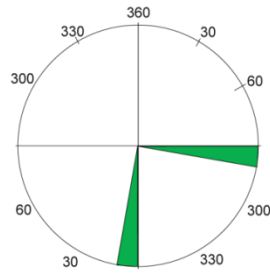
Figure 10a. Explanation for modified rose diagram. In the upper semi circle, the fracture frequency for each fracture set is displayed, and the number of petals indicates the range of fracture orientations in that fracture set. In the lower semi circle, the abutting relationships among the fracture sets are displayed as show (from Jacobi, 2007).



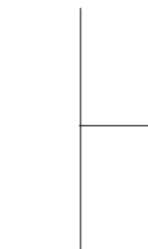
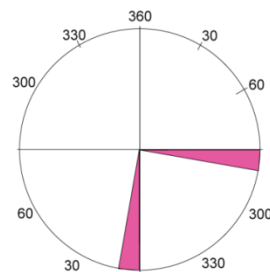
NS master to EW,
EW master to N45E,
NS master to N45E



NS master to EW,
EW master to N45E,
NS/N45E relationship unknown



NS intersects EW



NS and EW mutually abutting

(Figure 10b continued on following page)

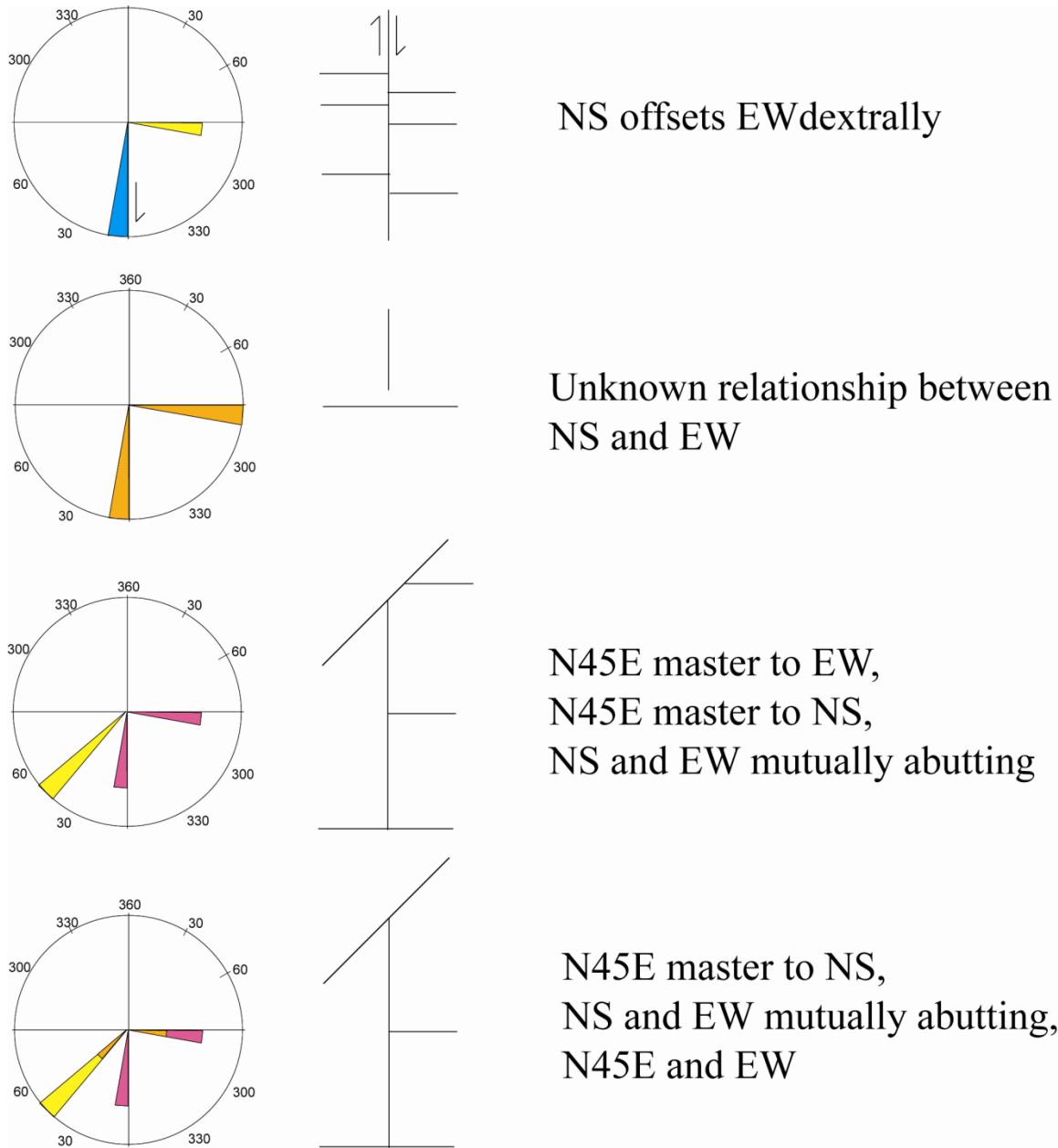


Figure 10b. Specific abutting relationships displayed in the lower semicircles of a modified rose diagram

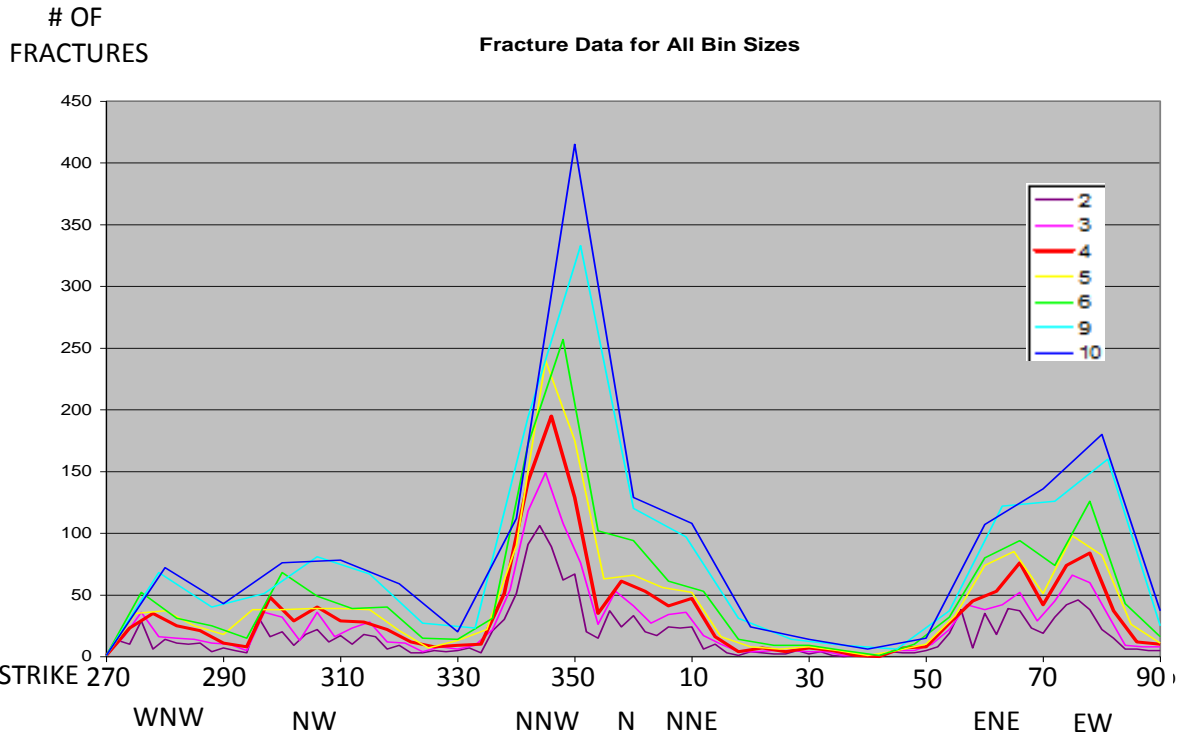


Figure 11a. Histogram of fracture orientations for various bin sizes. The range of strike orientations (in degrees) for bins in each histogram is indicated in key on right.

Mode IIb E-W	mean stdev	278 5.5	range (+/-) 1 standard deviation (+/-) 2 standard deviation range used for analysis	87 81.5 76.0 69	293 298.5 304.0 293
mode IIa ENE	mean stdev	76 3.8	range (+/-) 1 standard deviation (+/-) 2 standard deviation range used for analysis	70 66.2 62.4 54	86 89.8 93.6 82
ENE	mean stdev	61 5.3	range (+/-) 1 standard deviation (+/-) 2 standard deviation range used for analysis	50 44.7 39.4 27.5	70 75.3 80.6 56.25
Mode Ib NNE	mean stdev	8 3.4	range (+/-) 1 standard deviation (+/-) 2 standard deviation range used for analysis	3 356.6 353.2 11.25	18 21.4 24.8 42
N-S	mean stdev	358 4.3	range (+/-) 1 standard deviation (+/-) 2 standard deviation range used for analysis	351 346.7 342.4 344	6 10.3 14.6 12
Mode Ia NNW	mean stdev	344 4.5	range (+/-) 1 standard deviation (+/-) 2 standard deviation range used for analysis	331 326.5 322.0 326.25	354 358.5 363.0 352.5
NW	mean stdev	306 9	range (+/-) 1 standard deviation (+/-) 2 standard deviation range used for analysis	290 281.0 272.0 282	326 335.0 344.0 329

Figure 11b. Defined ranges for various fracture sets, based on the histograms in Figure 10a and abutting relationships.

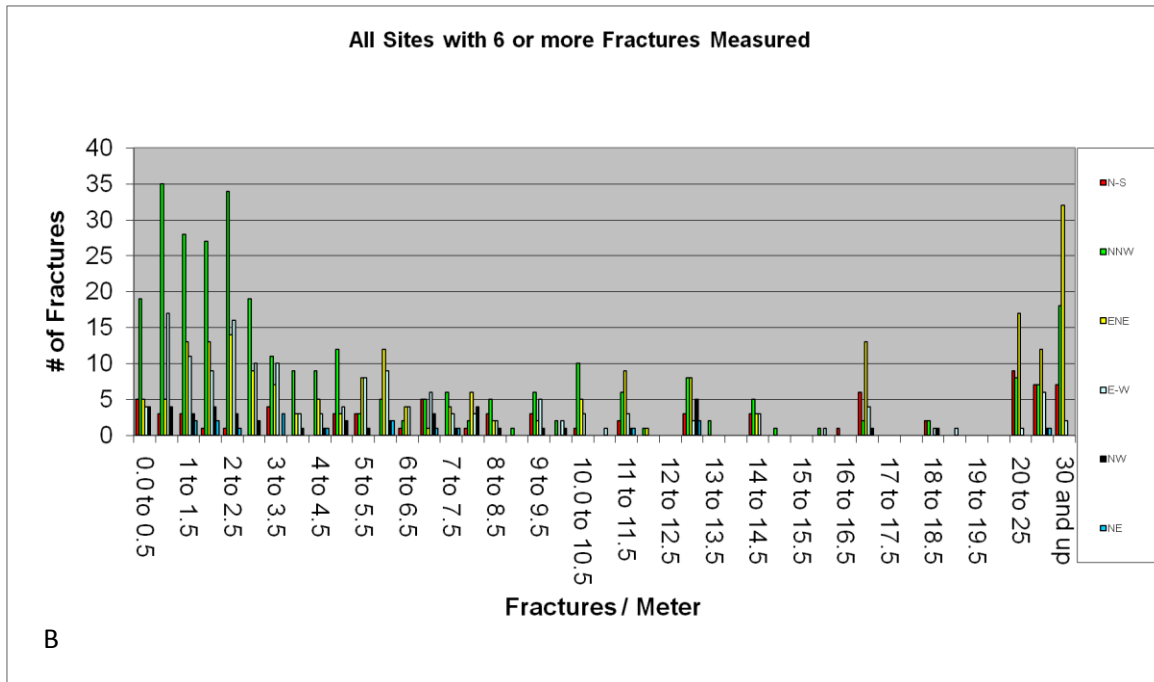
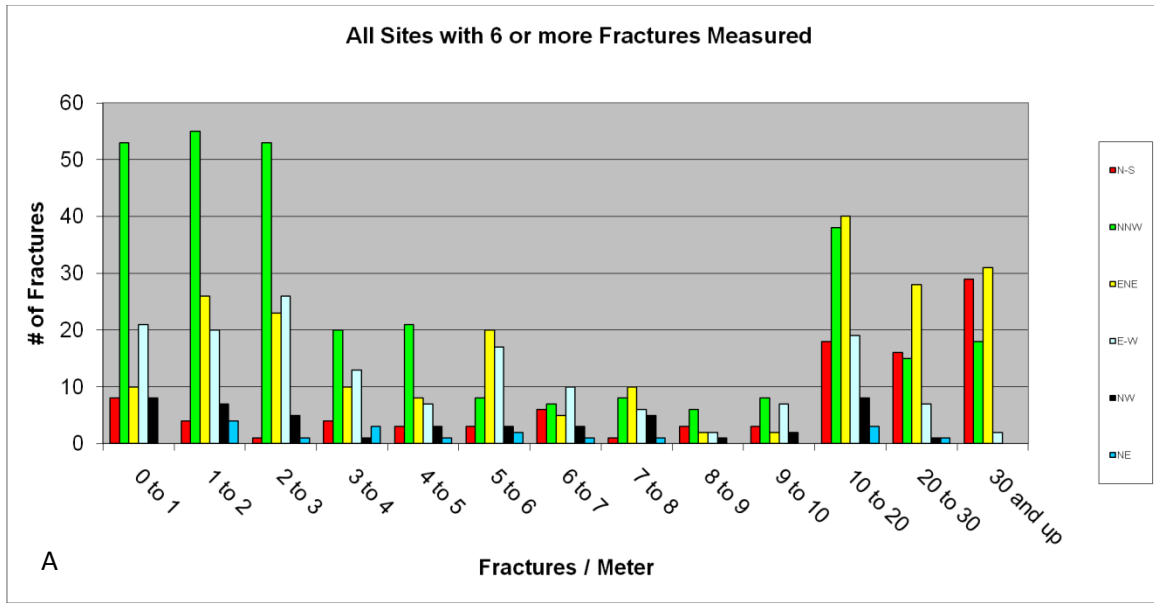


Figure 12. Fracture frequency distribution for various major fracture sets. Figure 12a has a bin size of 1 fracture/m between 0 and 10 fractures/m and a bin size of 10 fractures/m above 10 fractures/m. Figure 12b has a bin size of 0.5 fractures/m between 0 and 20 fractures/m and a bin size of 10 fractures/m above 20 fractures/m.

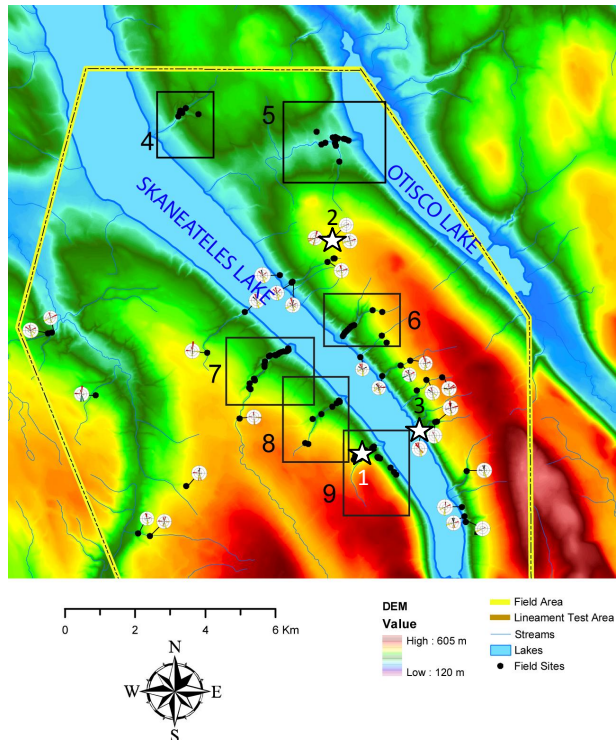


Figure 13. Example of structures in the Skaneateles region. Figure 13a (above) shows locations of the photos below (labeled stars).

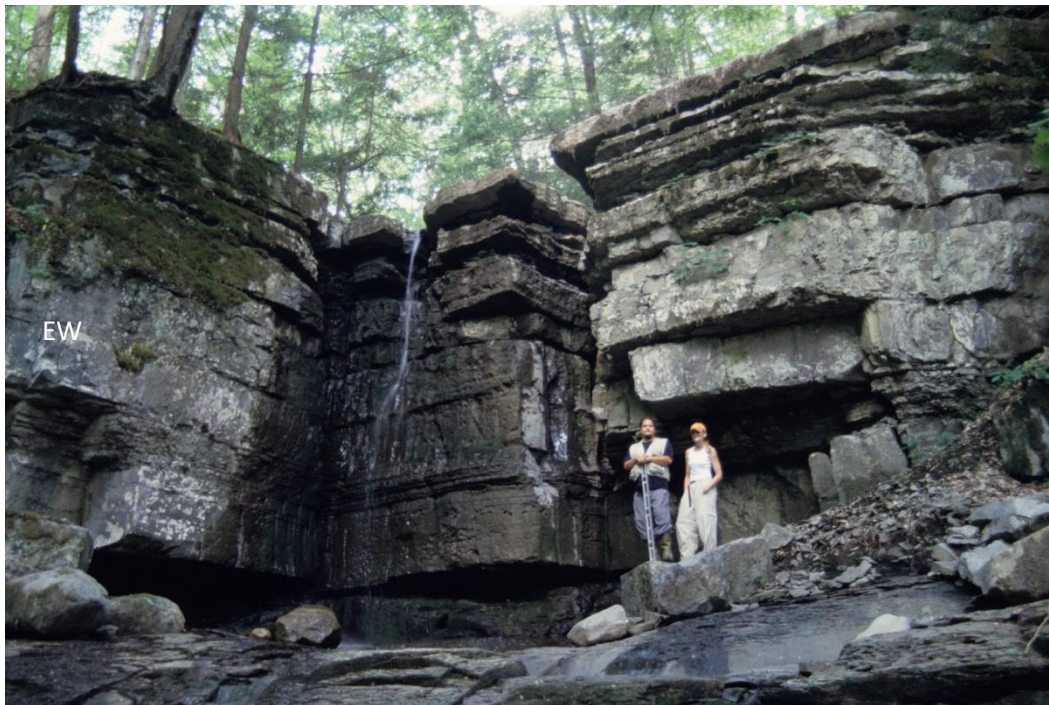


Figure 13b. Typical orthogonal fractures in the thickly bedded Tully Formation on the southwestern side of Skaneateles Lake. The two orthogonal fracture sets strike 350° and EW, as indicated on the photo. (Locality 1 on photograph location map, Figure 13a). Stroup (on left) and field assistant. Photo by Jacobi.



Figure 13c. Fractures in the Devonian Genesee Group in Fillmore Glen, about 5 km south of the central study area. The long fractures strike 340° ; the shorter fractures which strike 60° both abut and intersect the NNW-striking fractures. Photo by Jacobi.



Figure 13d. Dipping beds (350° , 30° W) on the flank of the Borodino reef in the Tully Formation. Heckel (1973) believed these bedding dips were original, marking the flank of the reef. Northwest is to the left. (Locality 2 on photograph location map, Figure 13a). Photo by Jacobi.



Figure 13e. Breccia and ferroan dolomite fill in the Borodino Reef. Heckel (1973) suggested the breccia was syndepositional. (Locality 2 on photograph location map, Figure 13a). Photo by Jacobi.



Figure 13f. Breccia and ferroan dolomite fill in interstices and in planar fractures in the Borodino Reef. (Locality 2 on photograph location map, Figure 13a). Photo by Jacobi.



Figure 13g. ENE-striking fractures with calcite vein fills at the Borodino Reef in the Tully Formation. (Fractures range in strike from $N76^{\circ}E$ to $N60^{\circ}E$). (Locality 2 on photograph location map, Figure 13a). Photo by Jacobi.



Figure 13h. Fracture intersection and interaction at Staghorn Point in the Genesee Group. The master (older) fracture strikes 343° and the younger curving intersection fractures trend about 326° . Photo looking down on outcrop. (Locality 3 on photograph location map, Figure 13a). Photo by Jacobi.



Figure 13i. Fracture intensification in black shale of the Genesee Group at site 84, Fillmore Glen (about 5 km south of the central study area). The master (older) and dominant fractures strikes north, whereas the abutting, less prevalent fractures strike NNW (340°). Stroup and 120 cm rule for scale. (Locality 3 on photograph location map, Figure 13a). Photo by Jacobi.



Figure 13j. Fracture intensification domain of NNW-striking fractures in the Genesee Group in Fillmore Glen (about 5 km south of the central study area. Engelder and Lash (2008) have suggested that fracture intensifications such as these mark gas chimneys. Photo by Jacobi.



Figure 13k. Fracture intensification in the Genesee Group at Fillmore Glen (about 5 km south of the central study area). The dominant fractures strike strike NNW (340°). Photo looking at cliff. Ruler is 15 cm long. A small amount of offset occurs on each fracture, as seen in Figure 13l. Photo by Jacobi.



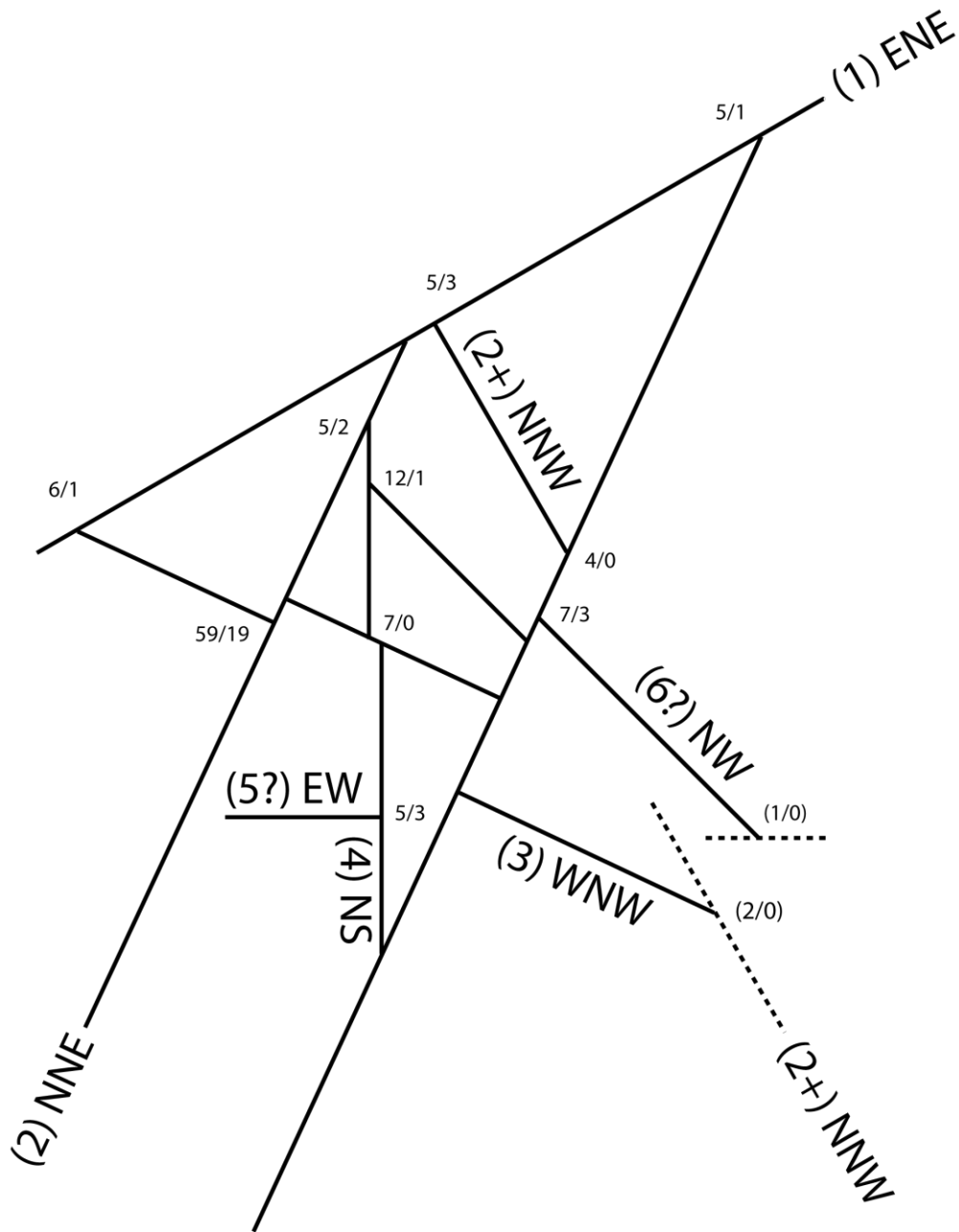
Figure 13l. Enlargement of Figure 13j. Note the small offsets on the fractures (down to the right) marked especially by the coarser beds (for example at the arrow). Photo by Jacobi.



Figure 13m. Larger view of the vertical outcrop in the Genesee Group at Fillmore Glen (about 5 km south of the central study area) shown in Figures 13k and l. The dominant fractures/faults strike NNW (340°). Ruler is 15 cm long and in same position as in the preceding two figures. Photo by Jacobi.



Figure 13n. Faults at Borodino Reef (Tully Formation). This is an enlargement of Figure 13d. Several faults with slickenfibers (such as the fault in red paint at the arrow) cross the outcrop, all with very minor stratigraphic throw. The faults strike north (8° , 50°W and 6° , 61°W). Slickenfibers and slickenlines plunge obliquely with a range from 243° , 30° to 278° , 58° . These faults are thus both normal faults (down-to-the-west) and oblique slip with a left lateral component. Photo by Jacobi.



RDJ 2007

Figure 14. Fracture set history in the Chenango County area, based on abutting relationships. Large numbers in parentheses indicate the order of fracturing (1 = oldest), and a + symbol indicates that the fracture is merely younger than the stage indicated, but the lack of abutting relationships precludes determining its order with respect to later events. The small number ratios indicate the number of fracture intersections that support the drawn abutting relationship (numerator) and the number of abutting relationships that do not support the drawn abutting relationship (denominator). From Jacobi (2007).

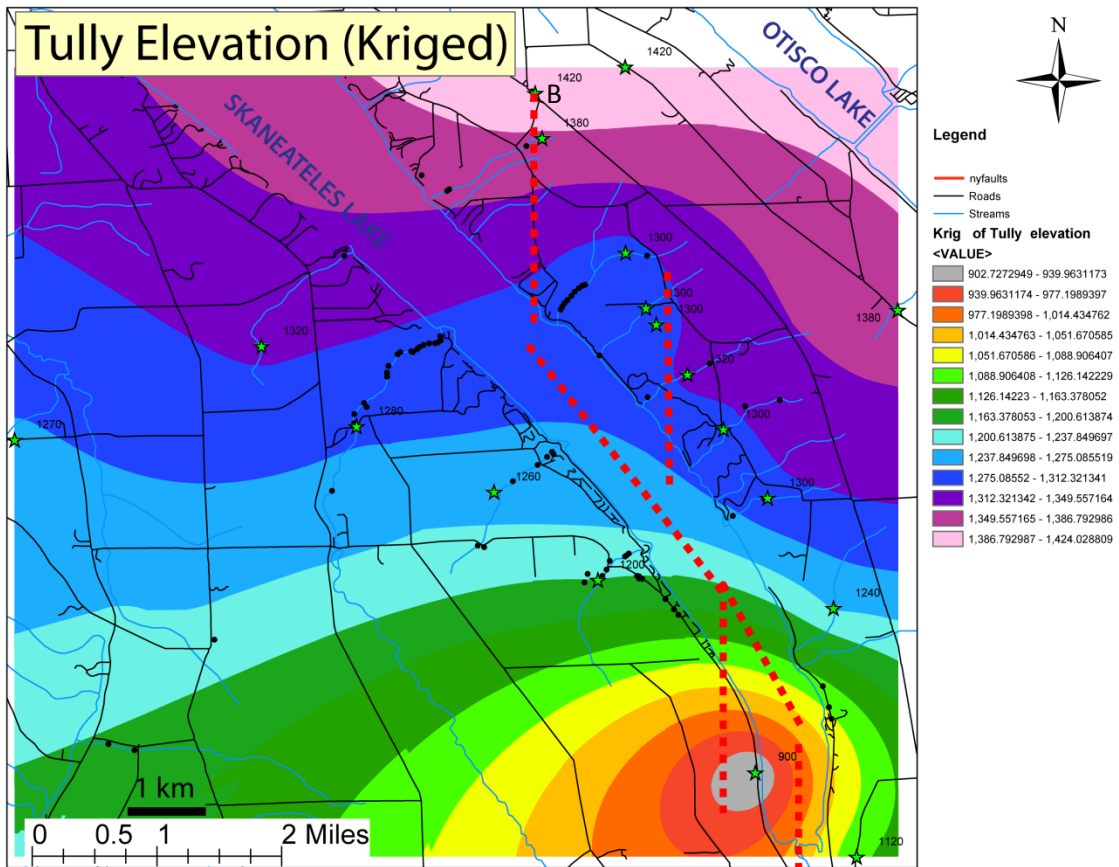


Figure 15a. Kriged surface of Tully Formation and possible faults. The elevation discontinuities indicate faults between elevation data points. This figure portrays northerly striking faults (dashed red lines).

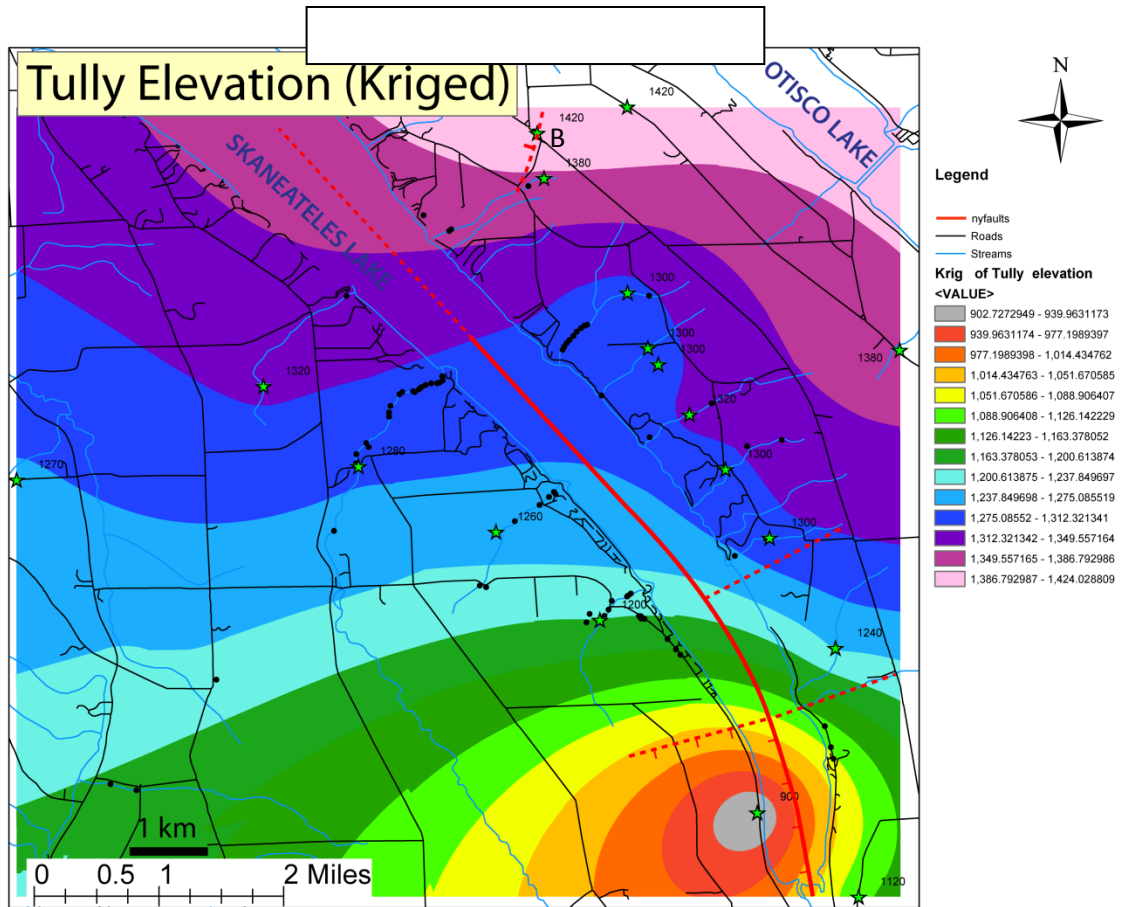


Figure 15b. Kriged surface of Tully Formation and alternative possible faults. The elevation discontinuities indicate faults between elevation data points. This figure portrays northerly striking faults and ENE-striking faults. The solid red line indicates that a fault most likely exists in this region (and is in both alternatives (Figure 15a and b). The bull's eye pattern in the southeast corner of the map reflects one limestone locality that well may be limestone of the Portland Point Member of the Moscow Formation, not the Tully. In that case the bull's eye and consequent fault are not necessary. B = Borodino Reef locality.

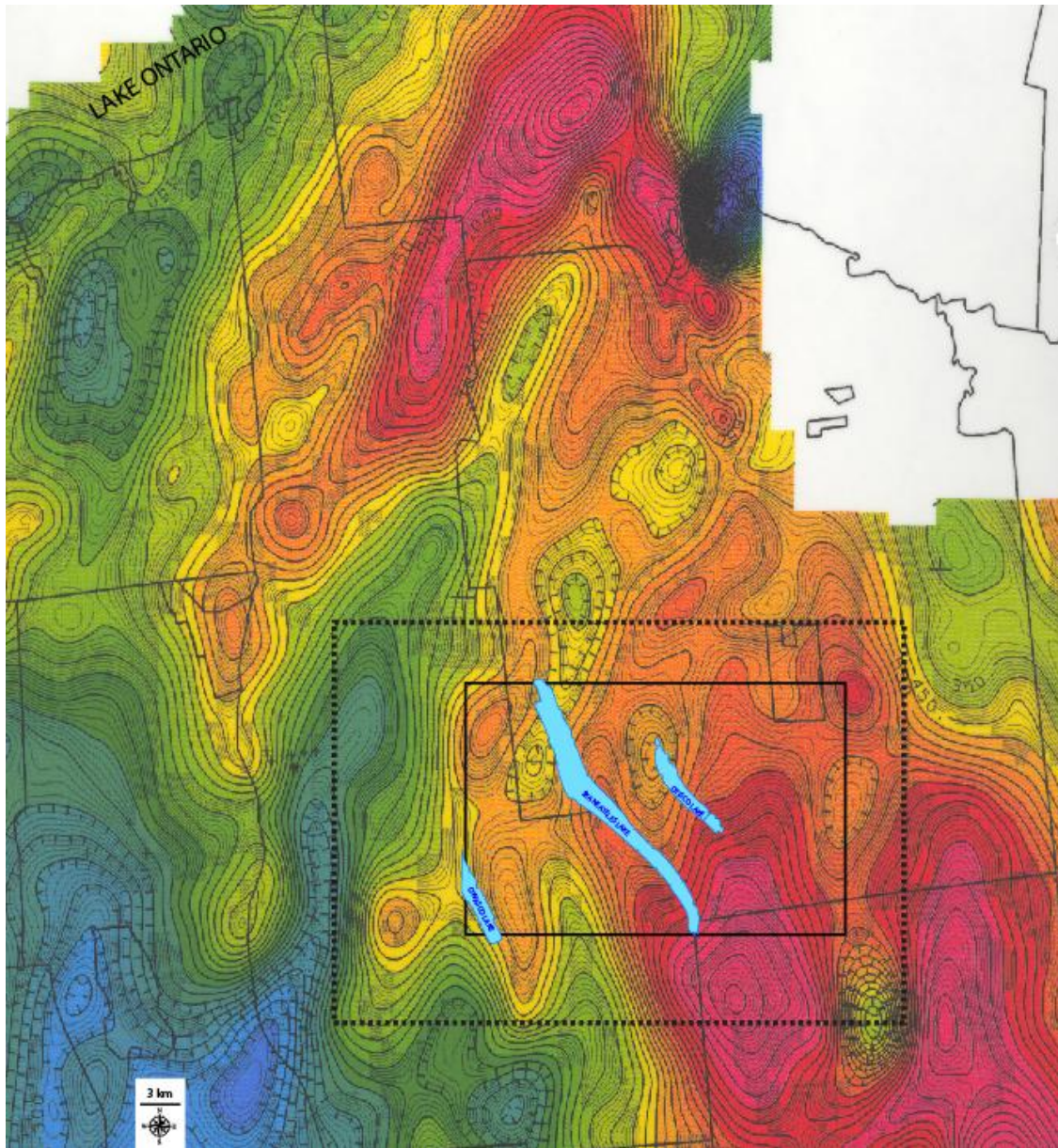


Figure 16a. Reduced-to-pole aeromagnetics in central New York State. County boundaries and lakes of interest shown for reference. Dashed line box indicates extent of Figure 16b. Solid line box indicates extent of DEM in Figure 16b. Thick contour lines indicate 50 nT, red is high, blue is low. Aeromagnetics from JP Fagan, Centennial Geoscience (pers. commun. 2005).

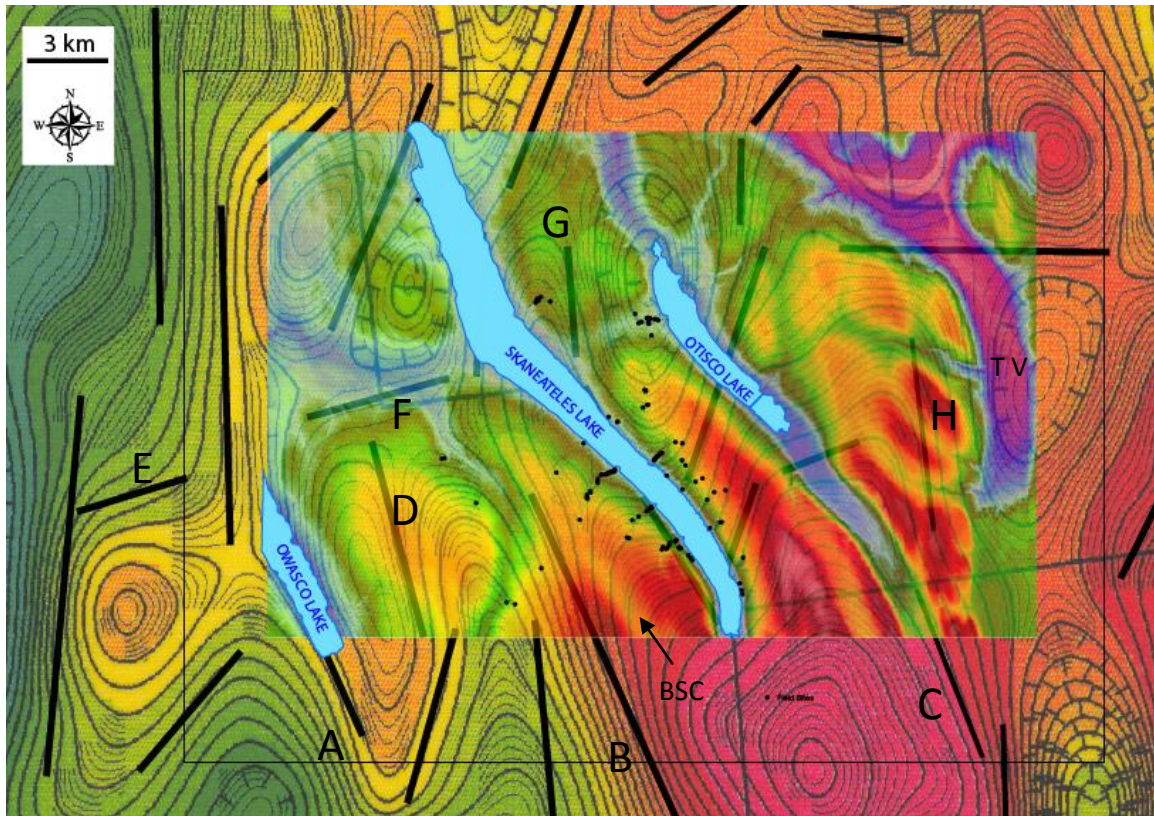


Figure 16b. DEM from figures 2 and 3 superimposed on reduced-to-pole aeromagnetics in the study area from figure 16a. Lakes of interest are shown for reference locations. Small dots indicate field site locations (Figures 2 and 3). Thick black straight lines indicate lineaments of steep gradients in the aeromagnetics. Labeled lineaments discussed in the text. Thick contour lines in the aeromagnetics indicate 50 nT, red is high, blue is low. BSC = Bear Swamp Creek; TV = Tully Valley. Gradient "F" coincides with broad ENE-trending valley of Dutch Hollow Brook. Aeromagnetics from JP Fagan (pers. commun. 2005).

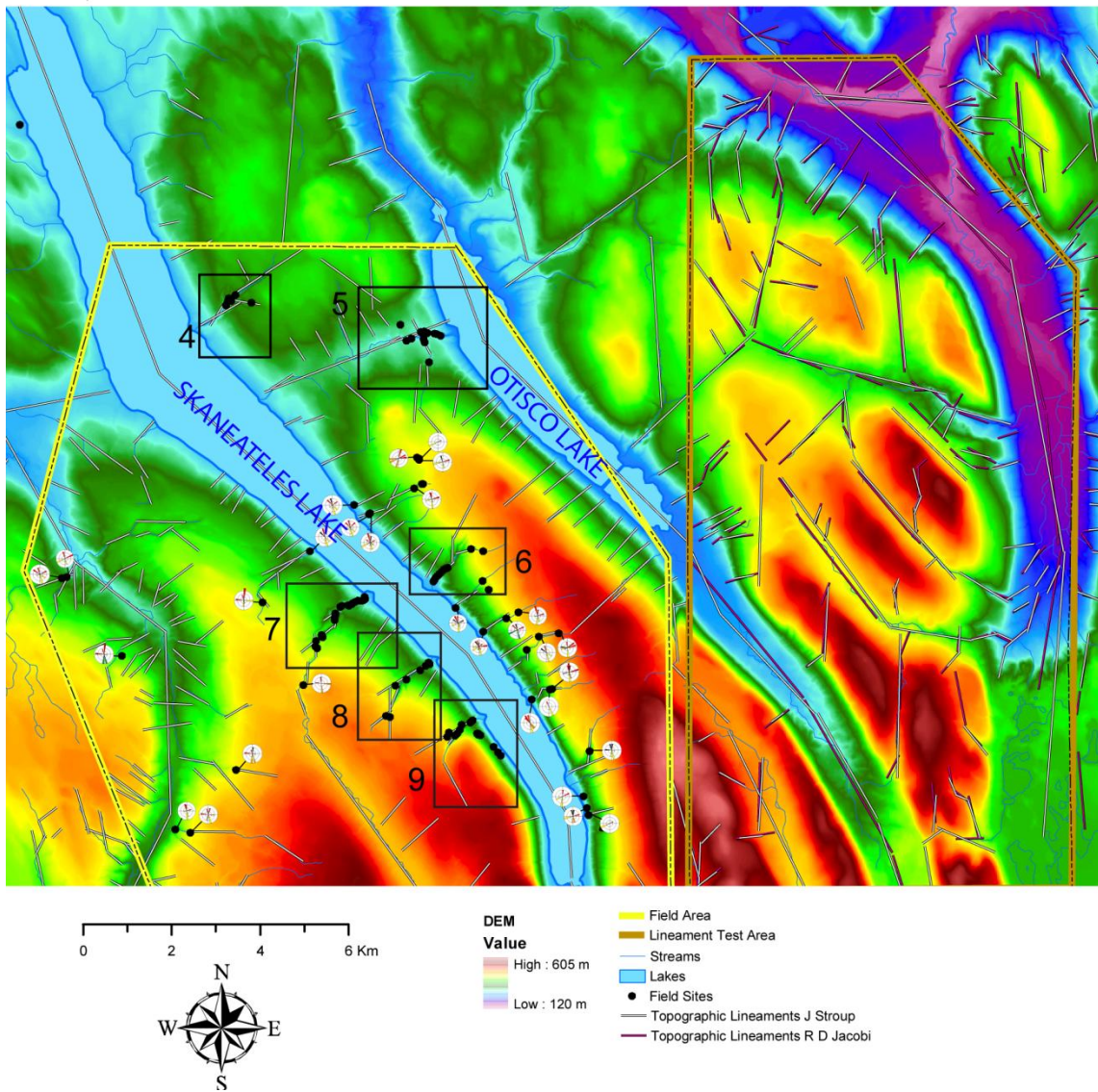


Figure 17. Topographic lineaments. In the orange boxed area, both Jacobi and Stroup picked topographic lineaments for operator comparison in the same allotted time. 78% of Stroup's lineaments matched Jacobi's lineaments (for more detailed results, see Table 2). In the yellow boxed area (the study area) Stroup identified the lineaments in white and black outline.

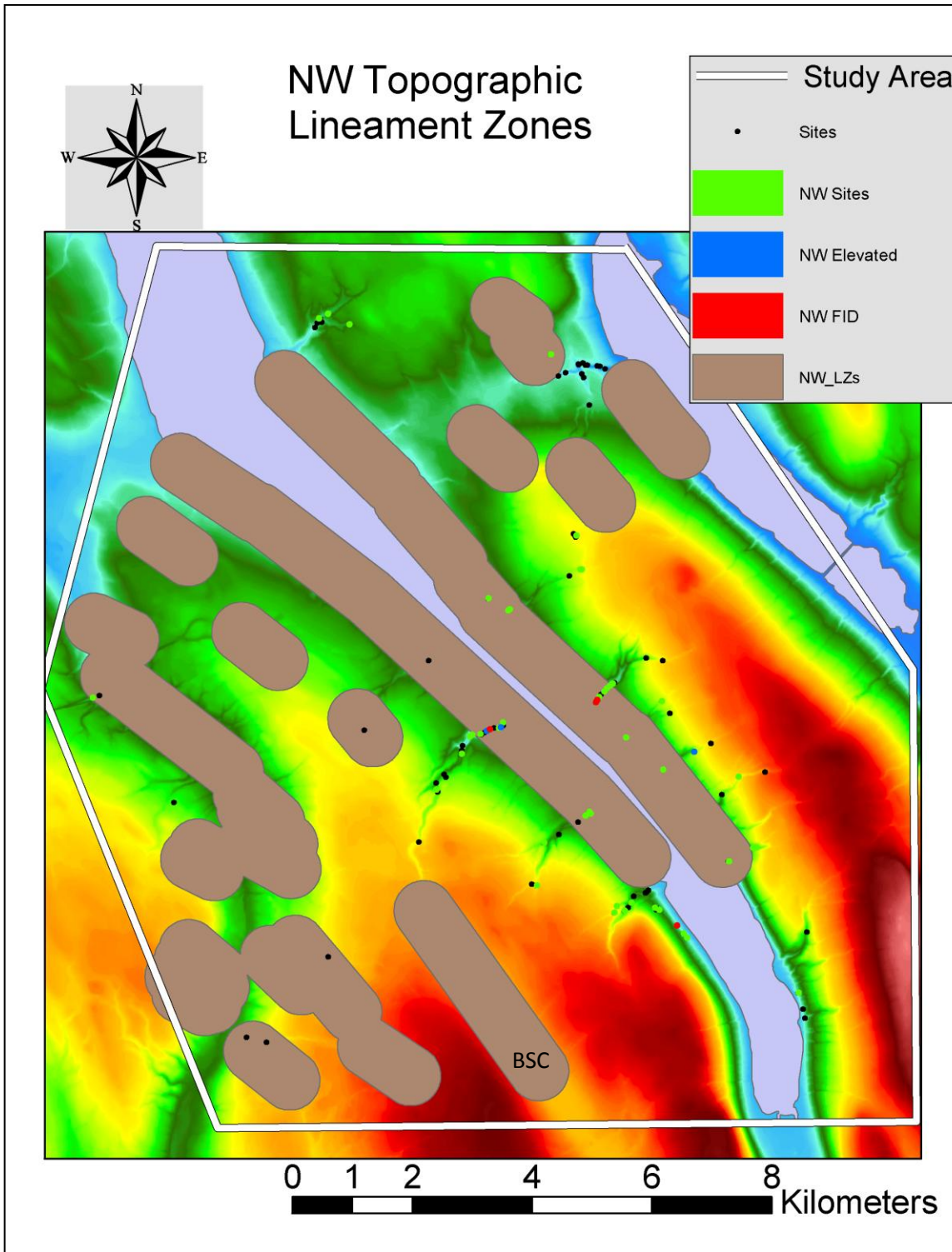


Figure 18. Buffered NW-trending topographic lineaments on the DEM base. Buffer is 0.5 km. Colored field sites indicate those that exhibit fractures with strikes collinear with the lineament trend. Sites with elevated fracture frequencies (2-4 fractures/m) shown in blue, and those sites with above 4 fractures/m shown in red. BSC = Bear Swamp Creek.

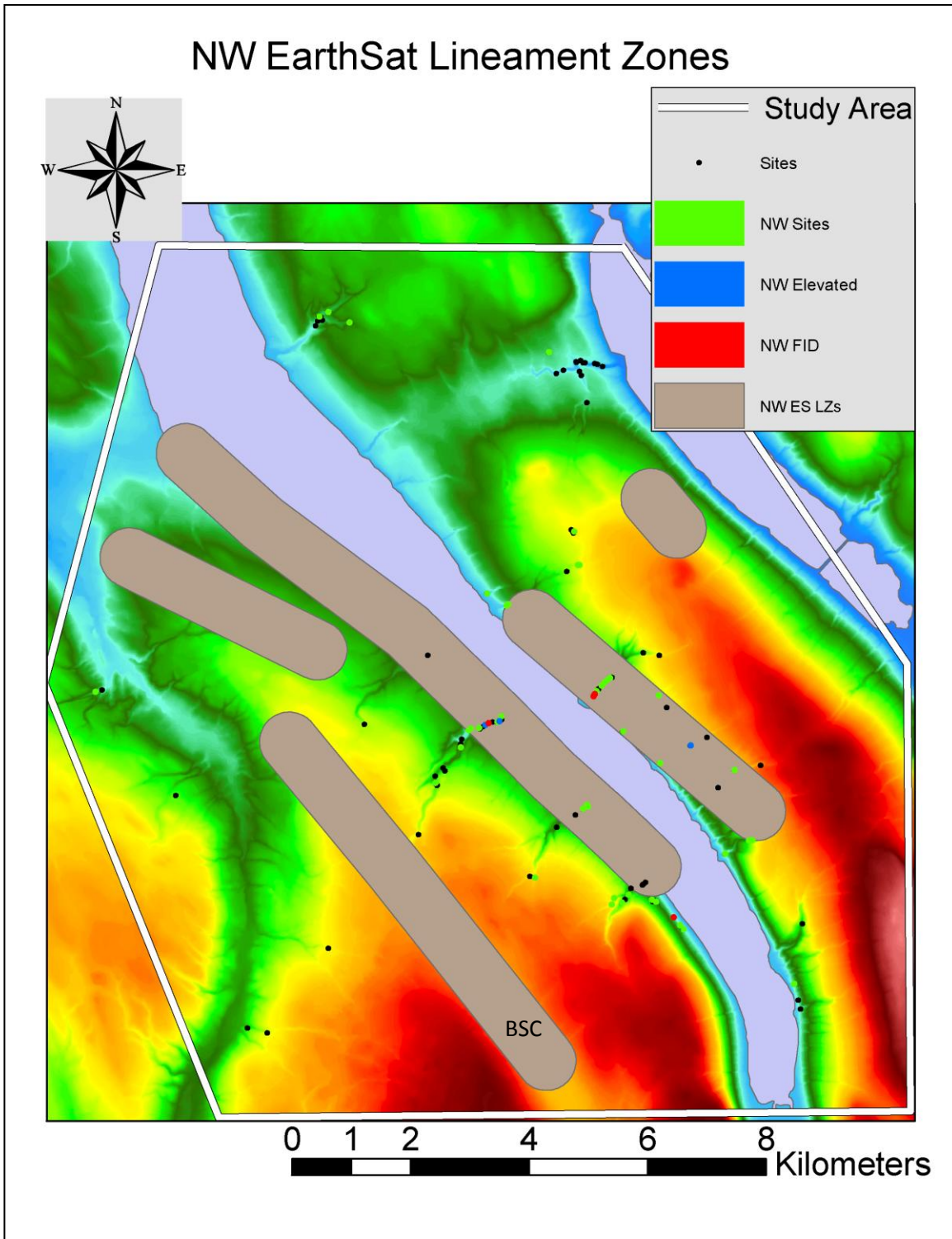


Figure 19. Buffered NW-trending EarthSat (1997) lineaments on the DEM base. Buffer is 0.5 km. Colored field sites indicate those that exhibit fractures with strikes collinear with the lineament trend. Sites with elevated fracture frequencies (2-4 fractures/m) shown in blue, and those sites with above 4 fractures/m shown in red. BSC = Bear Swamp Creek.

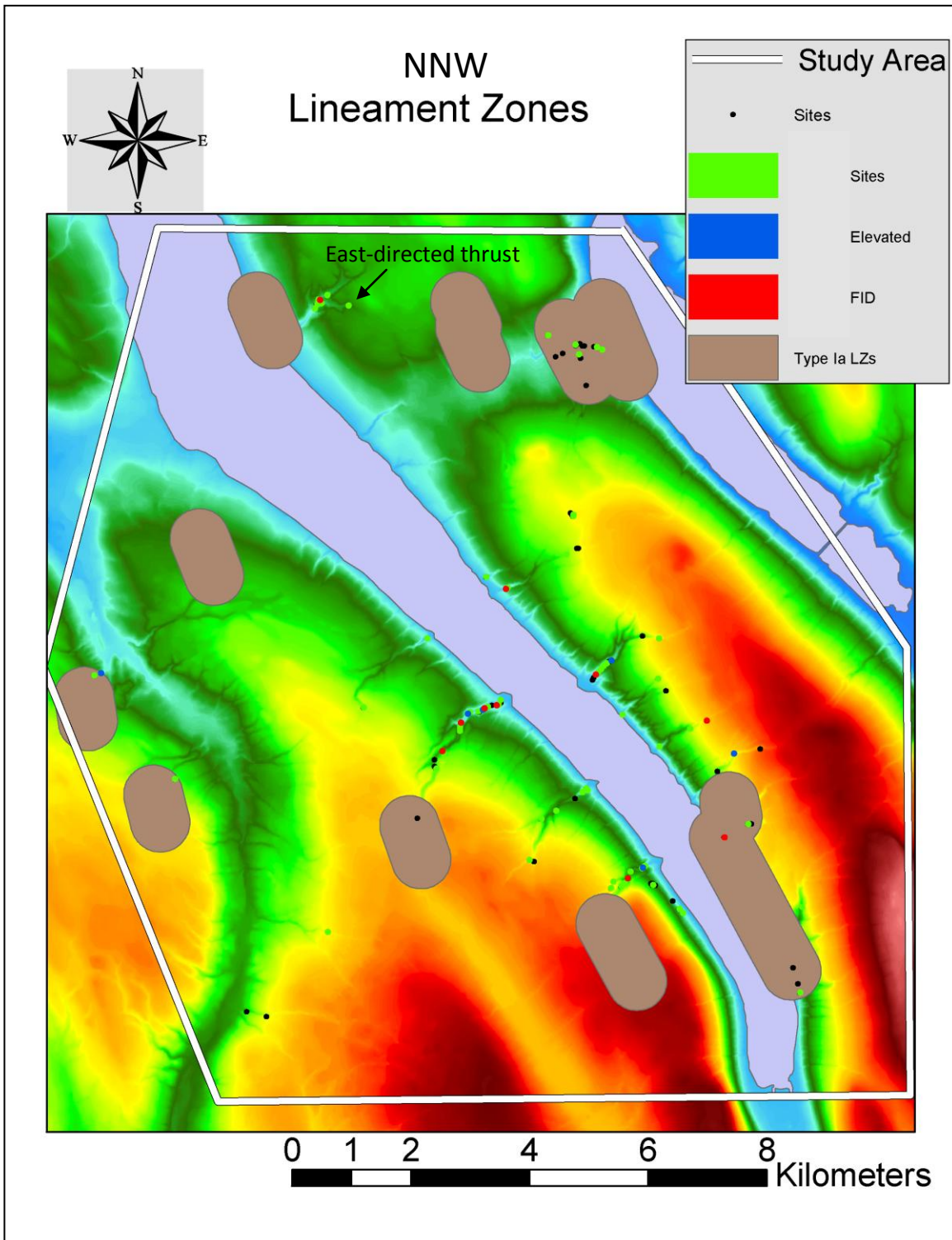


Figure 20. Buffered NNW-trending topographic lineaments on the DEM base. Buffer is 0.5 km. Colored field sites indicate those that exhibit fractures with strikes collinear with the lineament trend. Sites with elevated fracture frequencies (2-4 fractures/m) shown in blue, and those sites with above 4 fractures/m shown in red. The east-directed thrust strike NNW.

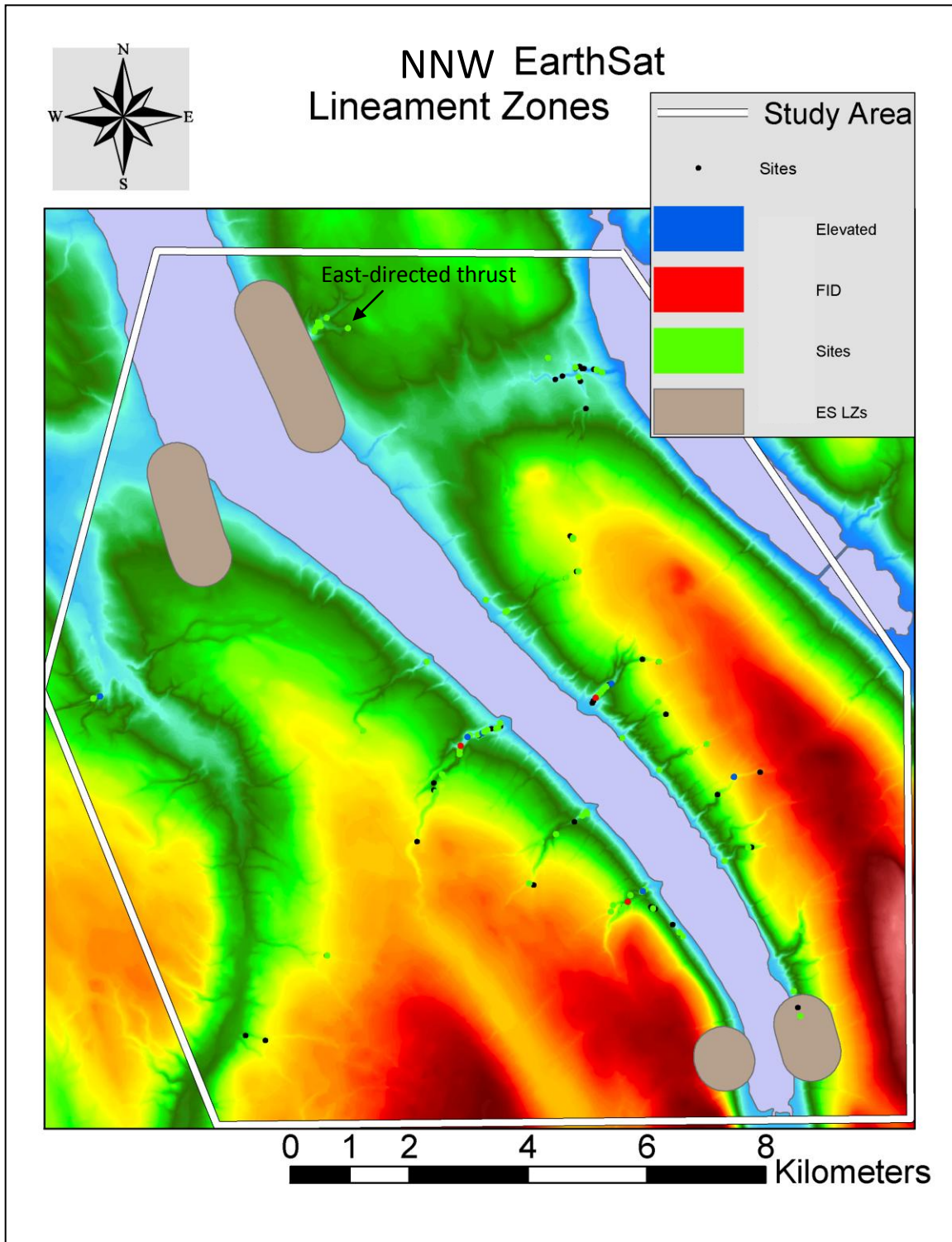


Figure 21. Buffered NNW-trending EarthSat (1997) lineaments on the DEM base. Buffer is 0.5 km. Colored field sites indicate those that exhibit fractures with strikes collinear with the lineament trend. Sites with elevated fracture frequencies (2-4 fractures/m) shown in blue, and those sites with above 4 fractures/m shown in red. The east-directed thrust strike NNW.

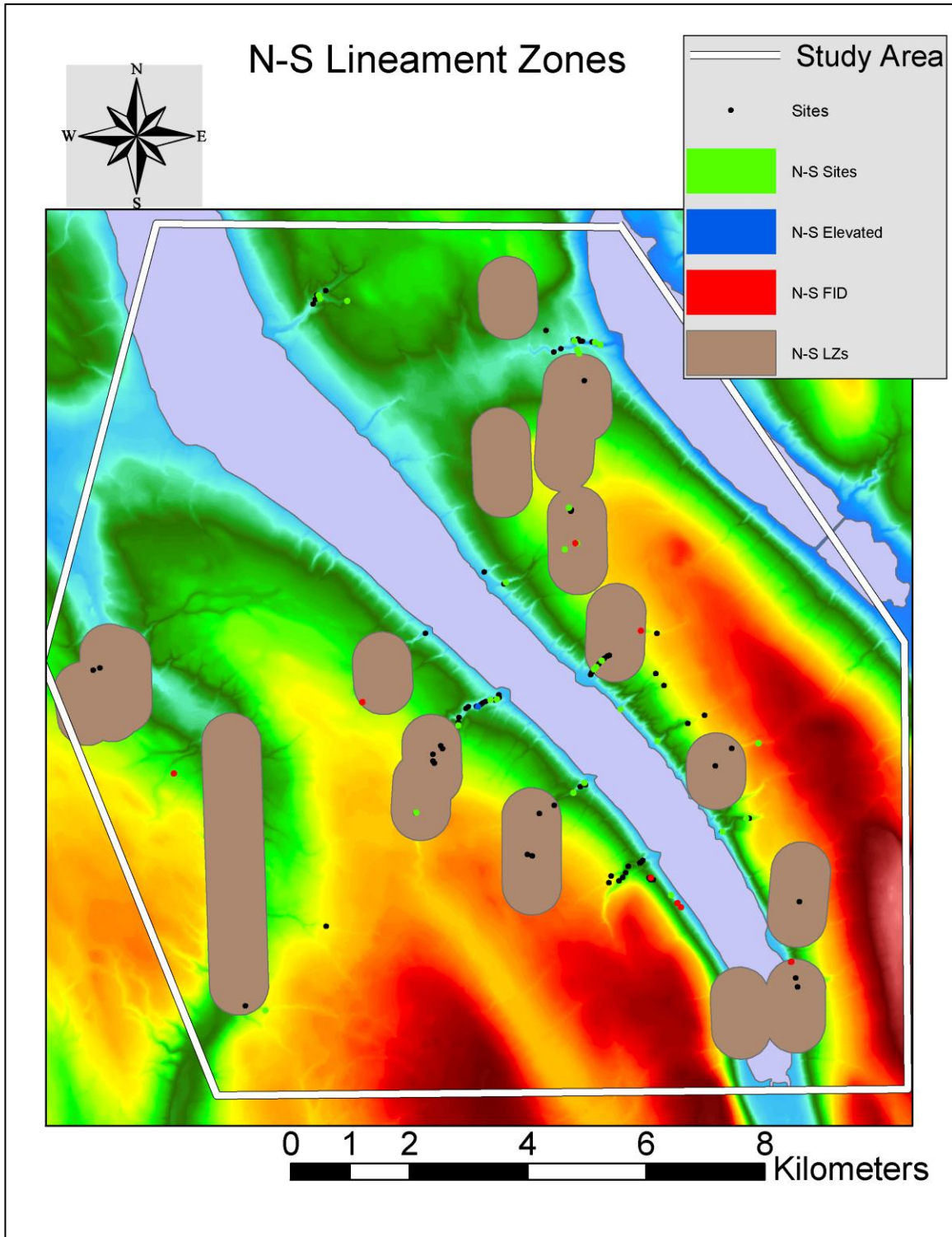


Figure 22. Buffered N-trending topographic lineaments on the DEM base. Buffer is 0.5 km. Colored field sites indicate those that exhibit fractures with strikes collinear with the lineament trend. Sites with elevated fracture frequencies (2-4 fractures/m) shown in blue, and those sites with above 4 fractures/m shown in red. B = Borodino Reef area.

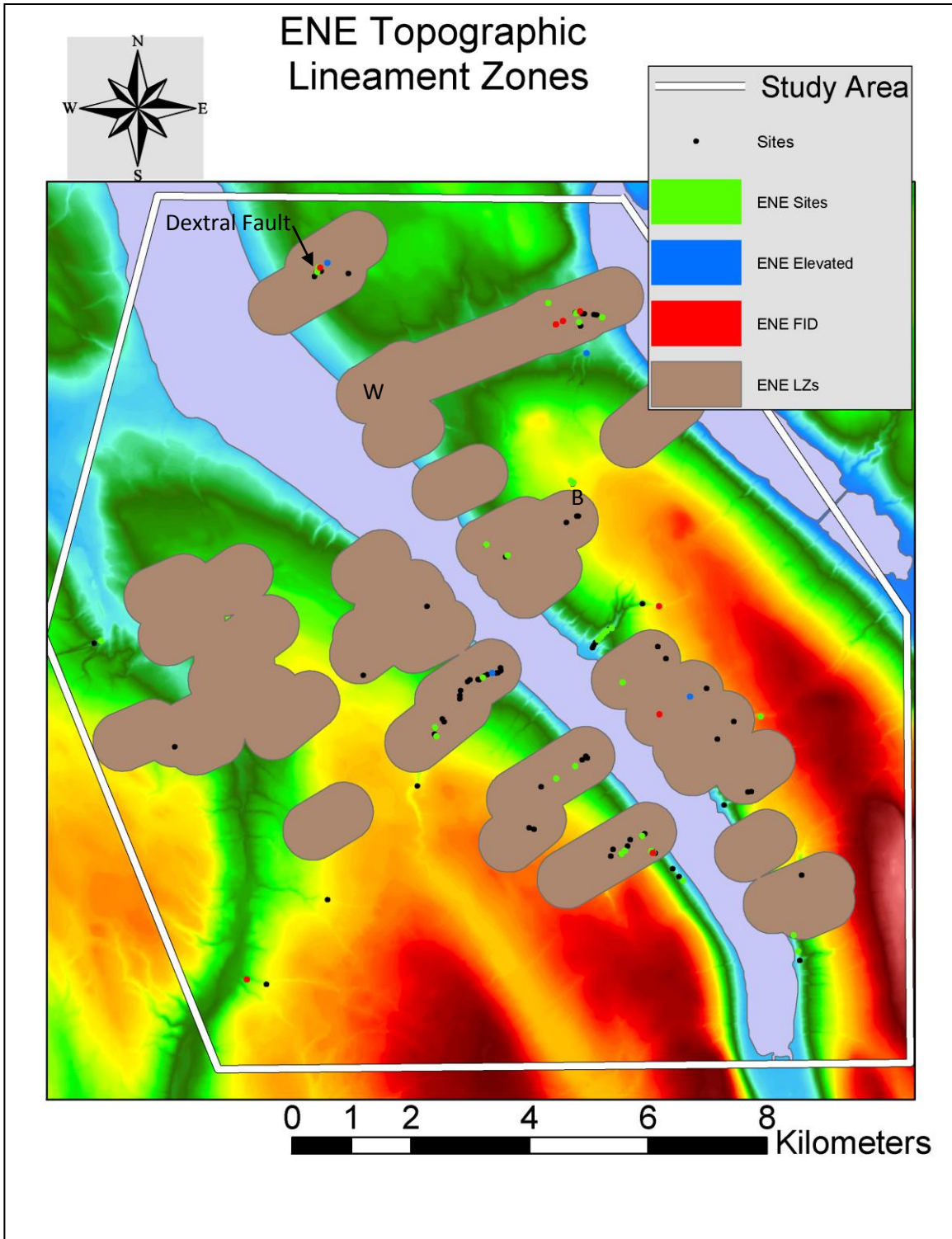


Figure 23. Buffered ENE-trending topographic lineaments on the DEM base. Buffer is 0.5 km. Colored field sites indicate those that exhibit fractures with strikes collinear with the lineament trend. Sites with elevated fracture frequencies (2-4 fractures/m) shown in blue, and those sites with above 4 fractures/m shown in red. “W” indicates the “Woodland” ENE-trending cluster of lineaments in a broad topographic low.

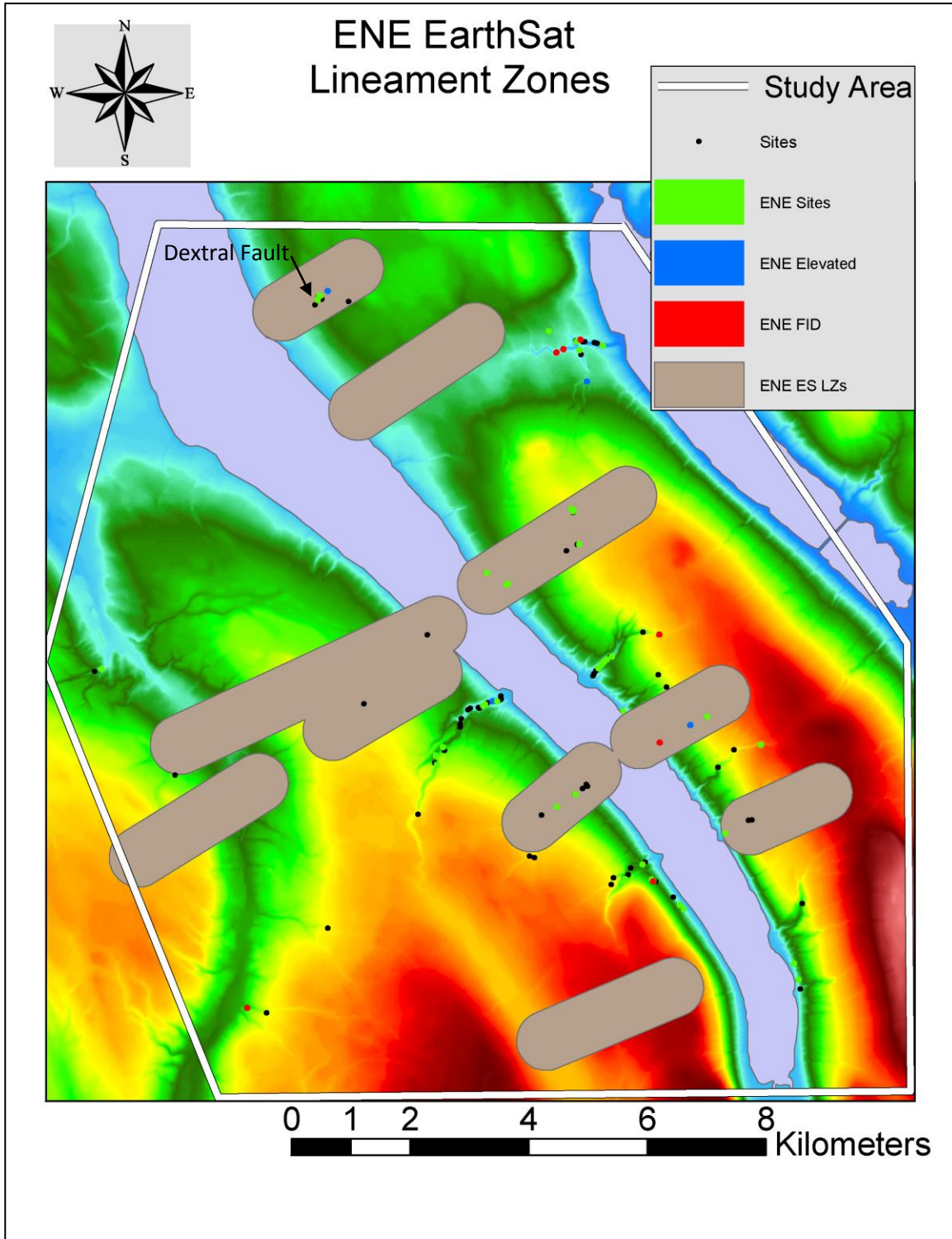


Figure 24. Buffered ENE-trending EarthSat (1997) lineaments on the DEM base. Buffer is 0.5 km. Colored field sites indicate those that exhibit fractures with strikes collinear with the lineament trend. Sites with elevated fracture frequencies (2-4 fractures/m) shown in blue, and those sites with above 4 fractures/m shown in red. The dextral fault strikes ENE.

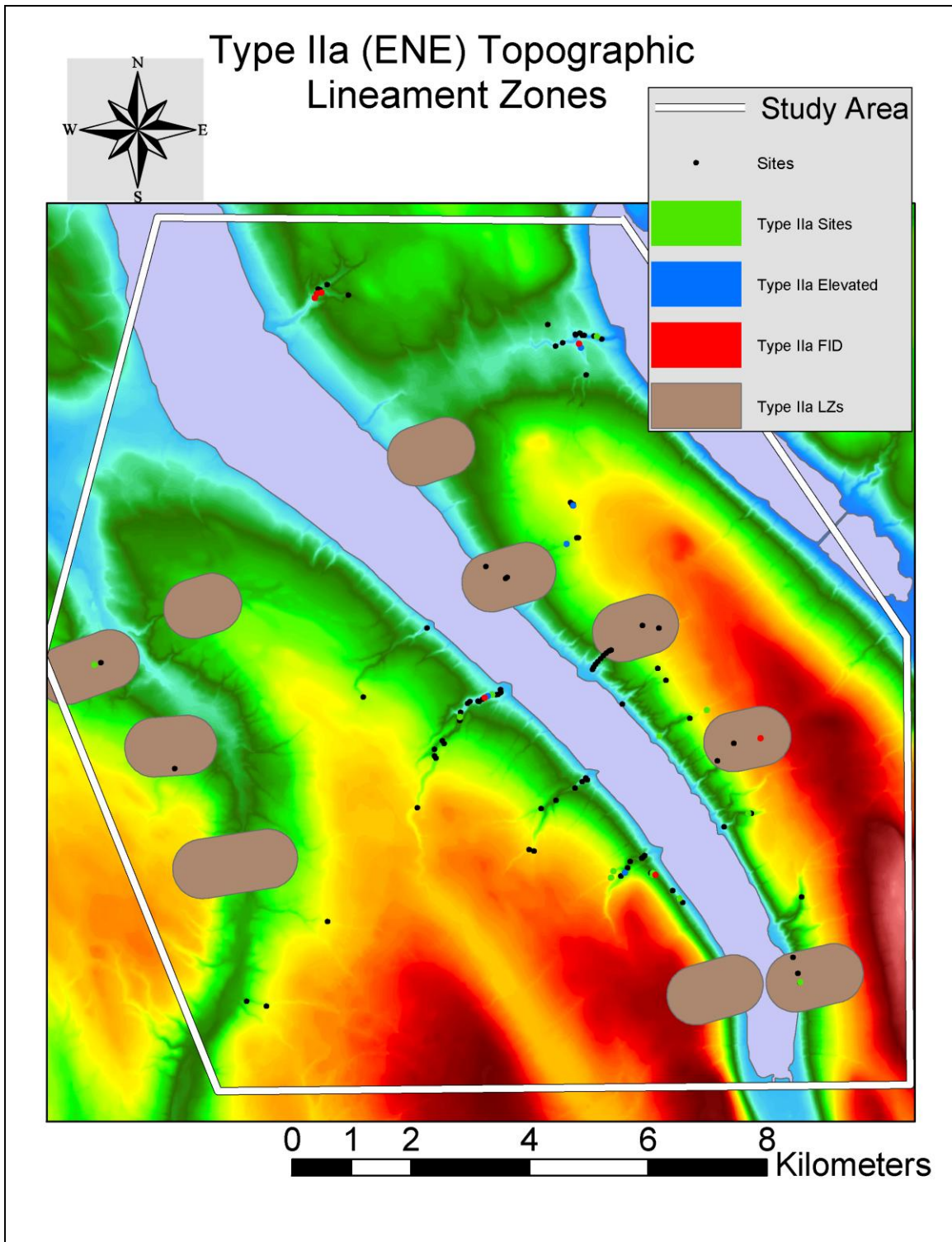


Figure 25. Buffered Type IIa ENE-trending topographic lineaments on the DEM base. Buffer is 0.5 km. Colored field sites indicate those that exhibit fractures with strikes collinear with the lineament trend. Sites with elevated fracture frequencies (2-4 fractures/m) shown in blue, and those sites with above 4 fractures/m shown in red.

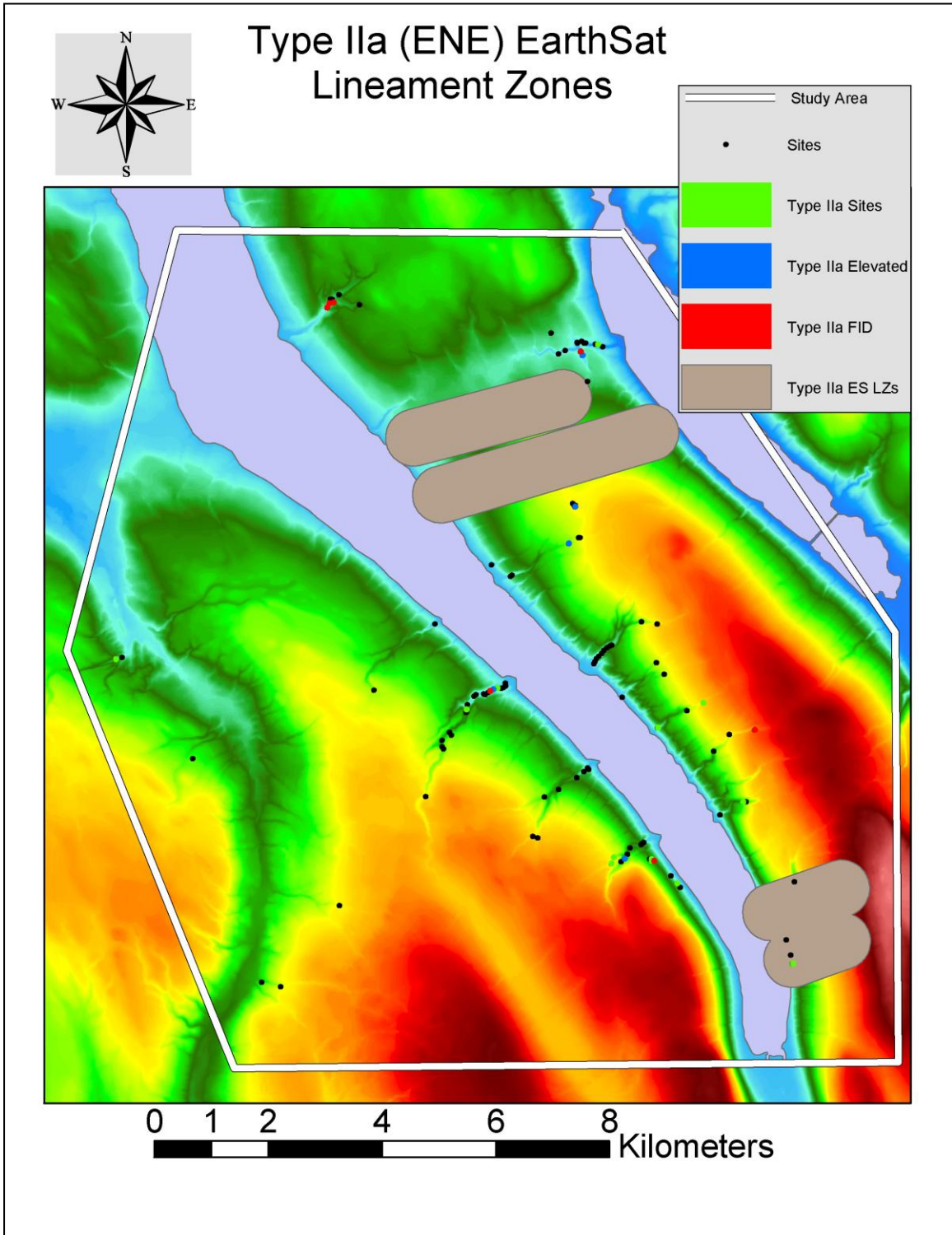


Figure 26. Buffered Type IIa ENE-trending EarthSat (1997) lineaments on the DEM base. Buffer is 0.5 km. Colored field sites indicate those that exhibit fractures with strikes collinear with the lineament trend. Sites with elevated fracture frequencies (2-4 fractures/m) shown in blue, and those sites with above 4 fractures/m shown in red.

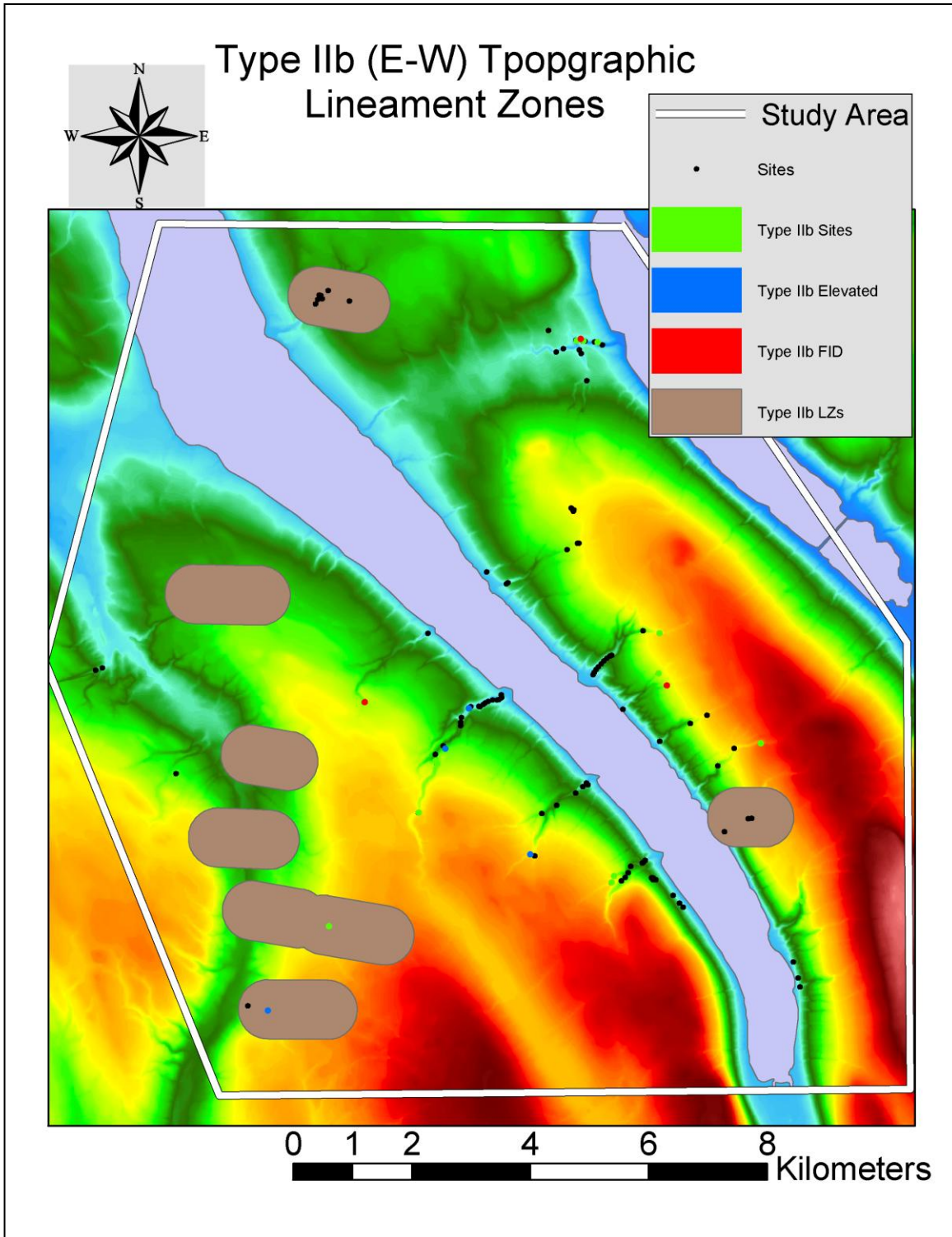


Figure 27. Buffered Type IIb E-trending topographic lineaments on the DEM base. Buffer is 0.5 km. Colored field sites indicate those that exhibit fractures with strikes collinear with the lineament trend. Sites with elevated fracture frequencies (2-4 fractures/m) shown in blue, and those sites with above 4 fractures/m shown in red.

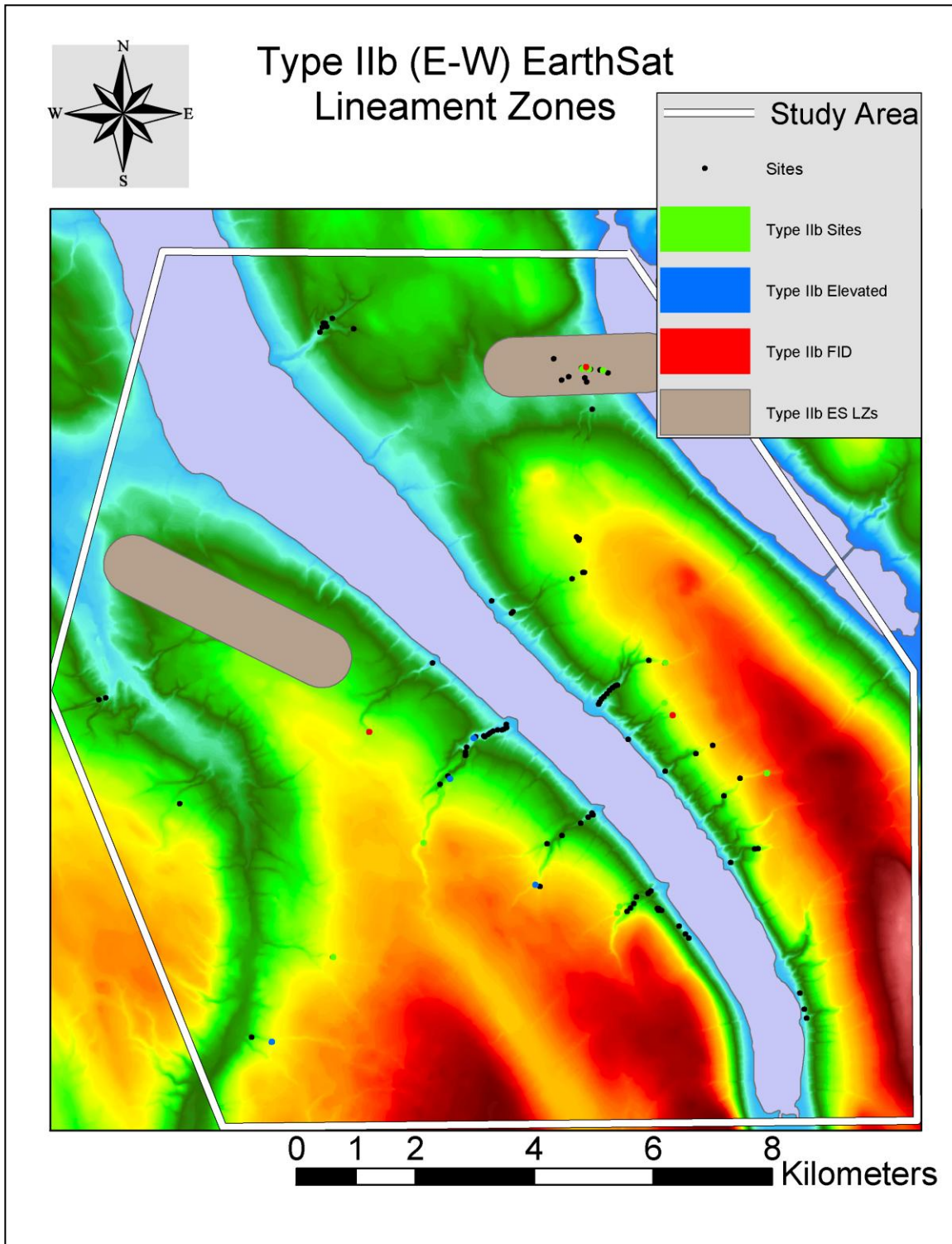


Figure 28. Buffered Type IIb E-trending EarthSat (1997) lineaments on the DEM base. Buffer is 0.5 km. Colored field sites indicate those that exhibit fractures with strikes collinear with the lineament trend. Sites with elevated fracture frequencies (2-4 fractures/m) shown in blue, and those sites with above 4 fractures/m shown in red.

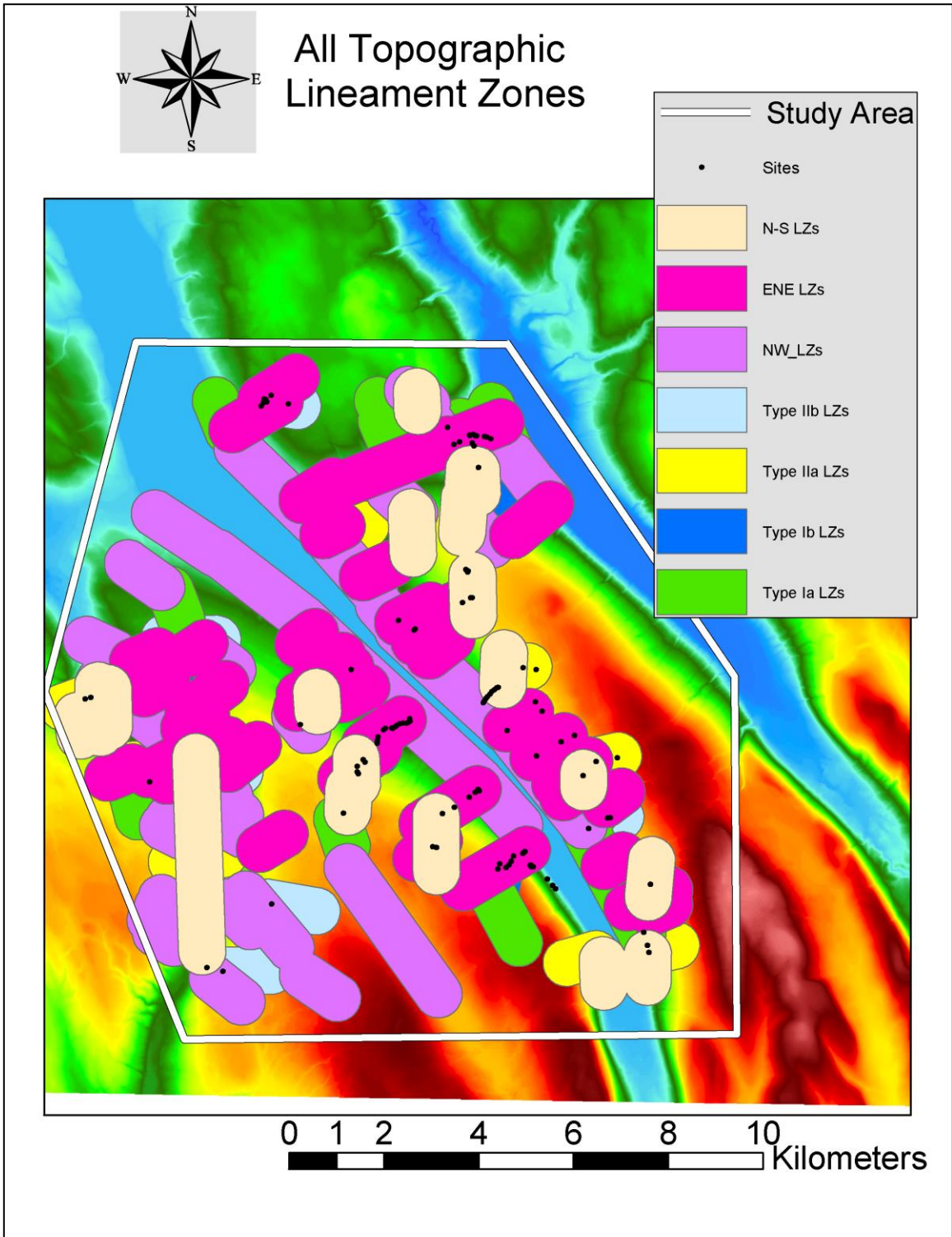


Figure 29. Buffered topographic lineaments of all trends on the DEM base. Buffer is 0.5 km.

TABLES

	NW	NNW	NS	NNE	NE	ENE	EW	WNW	
Figure 4		2				2			
	2	2	1						
			1			2			
		2			3	1			
			2					3	
			2			1			
		2				1			
			c rotation and faulting						
Figure 5				2	1				
				2			1	2	
		1					2		
			1				2		
			1		1			3	
		2	1		cc rotation?				
			2		1			3	
		1					2		
		1		2			2		
				1			2		
			1				2		
		1			1			3	
				1	2				
Figure 6		2	2				1		
		1					2		
	3	2					1		
	2	1	2						
	1	3	2						
		1					2		
			1				2		
		1	1				3		
		1						2	

(Table 1 is continued on the following pages)

Figure 7			2	1			2
					2	1	
		1				2	
	2	1					
		1					1
		1					1
		1					1
		1					1
		2				1	2
	2	1					
	1	1			1		
		1	1				
		2	1	c rotation?			1
		2				1	2
Figure 8		c rotation	1				2
	2	1					
		1				2	
	2	1					
	3	2	1				
		2	1				
				1			2
Figure 9		1				2	3
		2		3		1	
		1				2	
		2				1	
			2			1	
	1					1	
	1		2				
	3	1	2				
		1				2	
		2				1	
					1	2	
	3			2	1	2	
		2					1
		1				2	
		1	3			2	

(Table 1 continued on following page)

OTHER SITES		2	1		CC Rotation?		
		1		2			2
		1	1				3
		3	2				1
		1	1	INTERSECTING			
	2	1				3	
		2				1	
	2	1					
	2	1					
	2	1			3		
	2	1			3		
	3	2				1	
		3	1			2	
		2				1	
	4	3	1			2	
	4	1	4		2		3
	3	1				1	INTERSECTING
		2	1			3	
	2	1					
			1		3	2	
		2	1			2	
	2	1					
			1			2	
		1	2				3
		2	2			1	

TABLE 1. Abutting relationships in the Skaneateles detailed areas (Figures 4-9). 1 = master to 2, and so on. Master fracture is the older fracture. C rotation = clockwise rotation of fractures, based on abutting relationships.

percentage of Stroup's lineaments matching Jacobi's = $100 - ((\text{Sum of Stroup's missing lineaments} / \text{sum of Jacobi's lineaments}) * 100) =$ $100 - ((24 / 110) * 100)$ $100 - (0.17237 * 100)$ $(100 - 17.273) =$	78.18%
percentage of Jacobi's lineaments matching Stroup's = $100 - ((\text{Sum of Jacobi's missing lineaments} / \text{sum of Stroup's lineaments}) * 100) =$ $100 - ((19 / 102) * 100)$ $100 - (0.18627 * 100)$ $(100 - 18.627) =$	81.37%
Total percentage of Stroup's and Jacobi's lineaments matching = $100 - ((\text{Sum of total non-matching lineaments} / \text{total number of lineaments}) * 100) =$ $100 - ((43 / 129) * 100)$ $100 - (0.33333 * 100)$ $(100 - 33.333) =$	66.67%
Average angle difference between lineaments =	4.3°
standard deviation between lineament angle differences =	5.1808
Average difference in length between lineaments =	611 (m)
standard deviation between differences in lineament lengths =	929.25

Table 2. Comparison of lineaments identified by Jacobi and Stroup in the same area of Figure 17 during the same allotted time).

Topographic Lineaments								
Greater than 0.0 Fracture Frequency 50 m								
	wnw	nw	nnw	ns	nne	ne	ene	ew
Area of F points	249981	254311	522486	422396	101983	146909	316569	189528
Area of L	24054922	4226962	25825293	30118084	22374392	33466316	41556971	14848693
Area of L and F points	7424	116886	137742	159331	15690	71321	218469	23535
Area of ROI	129567325.1	129567325.1	129567325.1	129567325.1	129567325.1	129567325.1	129567325.1	129567325.1
Area of L - Area of F points	23804941	3972651	25302807	29695688	22272409	33319407	41240402	14659165
Area of F points - Area of L	242557	137425	384744	263065	86293	75588	98100	165993
# of Lineaments	36	22	23	31	23	45	47	13
Area of F points - Area of L	105262422	125086052	103219546	99026845	107090950	95954100	87693785	114529104
Area of ROI - Area of F points	129317344	129313014	129044839	129144929	129465342	129420416	129250756	129377797
# F points with in the Lineaments	1	19	21	24	2	11	33	3
# F points outside the Lineaments	36	27	64	58	10	11	23	45
# F points	37	46	85	82	12	22	56	48
# F points with in the Lineaments / total number of F points	0.027027027	0.413043478	0.247058824	0.292682927	0.166666667	0.5	0.589285714	0.0625
(Area of L - Area of F points) / (Area of ROI - Area of F points)	0.001875673	0.001062731	0.002981475	0.002036975	0.000666534	0.00058405	0.00075899	0.00128301
# F points outside the Lineaments / total number of F points	0.972972973	0.586956522	0.752941176	0.707317073	0.833333333	0.5	0.410714286	0.9375
(Area of ROI - (Area of L and F points)) / Area of ROI - Area of F points	1.001875673	1.001062731	1.002981475	1.002036975	1.000666534	1.00058405	1.00075899	1.00128301
W _i ⁺	-5.407809607	2.354045587	-0.818331869	-0.387415239	-1.72115591	0.634303591	1.132452202	-2.616427251
W _i ⁻	-3.407854194	-0.933643487	-1.197078958	-1.090387014	-1.58676082	-0.365319615	-0.422637183	-2.718735444
contrast	-1.999955413	3.287689074	0.378747089	0.702971775	-0.134395089	0.999623207	1.555089386	0.102306294
Area is represented in meters								
F = Field Data Point L = Lineament ROI = Region of Interest #NUM! and #DIV/0! Indicate that no contrast value could be calculated								

Table 3a. Weights-of-evidence calculations and contrast values for topographic lineaments and sites with appropriately oriented fractures with frequencies > 0 fractures/m. Contrast values with yellow are significantly positive numbers. (Site buffer is 50m).

Topographic Lineaments								
Greater than 2.0 Fracture Frequency 50 m								
	wnw	nw	nnw	ns	nne	ne	ene	ew
Area of F points	31379	49205	121443	70380	0	23535	149778	39224
Area of L	24054922	4226962	25825293	30118084	22374392	33466316	41556971	14848693
Area of L and F points	0	33516	23943	30172	0	7845	115938	7945
Area of ROI	129567325.1	129567325.1	129567325.1	129567325.1	129567325.1	129567325.1	129567325.1	129567325.1
Area of L - Area of F points	24047498	4193446	25801350	30087912	22374392	33458471	41441033	14840748
Area of F points - Area of L	31379	15689	97500	40208	0	15690	33840	31279
# of Lineaments	36	22	23	31	23	45	47	13
Area of ROI - (Area of L + Area of F points)	105481024	125291158	103260589	99378861	107192933	96077474	87860576	114679408
Area of ROI - Area of F points	129535946	129518120	129445882	129496945	129567325	129543790	129417547	129528101
# F points with in the Lineaments	0	5	4	4	0	1	13	1
# F points outside the Lineaments	8	3	15	6	0	2	9	5
# F points	8	8	19	10	0	3	22	6
# F points with in the Lineaments / total number of F points	0	0.625	0.210526316	0.4	#DIV/0!	0.333333333	0.590909091	0.166666667
(Area of L - Area of F points) / (Area of ROI - Area of F points)	0.000242242	0.000121134	0.000753211	0.000310494	0	0.000121117	0.000261479	0.000241484
# F points outside the Lineaments / total number of F points	1	0.375	0.789473684	0.6	#DIV/0!	0.666666667	0.409090909	0.833333333
(Area of ROI - (Area of L and F points)) / Area of ROI - Area of F points	1.000242242	1.000121134	1.000753211	1.000310494	1	1.000121117	1.000261479	1.000241484
W _i ⁺	#NUM!	3.557151281	-1.332688773	0.207073896	#DIV/0!	-0.438045496	1.250398699	-1.039662703
W _i ⁻	#NUM!	-0.599029289	-1.31882163	-0.700590394	#DIV/0!	-0.799748205	-0.732493102	-1.714022396
contrast	#NUM!	4.15618057	-0.013867142	0.907664291	#DIV/0!	0.361702709	1.982891701	0.674359693
Area is represented in meters								
F = Field Data Point L = Lineament ROI = Region of Interest #NUM! and #DIV/0! Indicate that no contrast value could be calculated								

Table 3b. Weights-of-evidence calculations and contrast values for topographic lineaments and sites with appropriately oriented fractures with frequencies >2 fractures/m. Contrast values with yellow are significantly positive numbers. (Site buffer is 50m).

Topographic Lineaments								
Greater than 4.0 Fracture Frequency 50 m								
	wnw	nw	nnw	ns	nne	ne	ene	ew
Area of F points	23534	27748	78448	62536	0	15690	94481	23535
Area of L	10383182	26217444	7277374	5171926	0	14279815	35869592	3040369
Area of L and F points	0	15690	0	0	0	7845	39225	7845
Area of ROI	129567325.1	129567325.1	129567325.1	129567325.1	129567325.1	129567325.1	129567325.1	129567325.1
Area of L - Area of F points	10383182	26201754	7277374	5171926	0	14271970	35830367	3032524
Area of F points - Area of L	23534	12058	78448	62536	0	7845	55256	15690
# of Lineaments	2	8	4	1	0	7	14	1
Area of ROI - (Area of L + Area of F points)	119160609	103322133	122211503	124332863	129567325	115271820	93603252	126503421
Area of ROI - Area of F points	129543791	129539577	129488877	129504789	129567325	129551635	129472844	129543790
# F points with in the Lineaments	0	2	0	0	0	0	5	1
# F points outside the Lineaments	4	3	13	8	0	2	8	3
# F points	4	5	13	8	0	2	13	4
# F points with in the Lineaments / total number of F points	0	0.4	0	0	#DIV/0!	0	0.384615385	0.25
(Area of L - Area of F points) / (Area of ROI - Area of F points)	0.000181668	9.30835E-05	0.000605828	0.000442886	0	6.0555E-05	0.000426777	0.000121117
# F points outside the Lineaments / total number of F points	1	0.6	1	1	#DIV/0!	1	0.615384615	0.75
(Area of ROI - (Area of L and F points)) / Area of ROI - Area of F points	1.000181668	1.000093084	1.000605828	1.000442886	1	1.000060555	1.000426777	1.000121117
W _i ⁺	#NUM!	0.622554787	#NUM!	#NUM!	#DIV/0!	#NUM!	-0.0644127	1.557399118
W _i ⁻	#NUM!	-1.012765698	#NUM!	#NUM!	#DIV/0!	#NUM!	-0.68201942	-1.480327777
contrast	#NUM!	1.635320485	#NUM!	#NUM!	#DIV/0!	#NUM!	0.61760672	3.037726895
Area is represented in meters								
F = Field Data Point L = Lineament ROI = Region of Interest #NUM! and #DIV/0! Indicate that no contrast value could be calculated								

Table 3c. Weights-of-evidence calculations and contrast values for topographic lineaments and sites with appropriately oriented fractures with frequencies >4 fractures/m. Contrast values with yellow are significantly positive numbers. (Site buffer is 50m)

Topographic Lineaments								
Greater than 0.0 Fracture Frequency 500 m								
	wnw	nw	nnw	ns	nne	ne	ene	ew
Area of F points	14919609	15603306	25633901	24607842	8509979	9205461	18234709	13260186
Area of L	24054922	50723541	25825293	30118084	22374392	33466316	41556971	14848693
Area of L and F points	723930	6143137	6307902	8367109	407	4038342	10402371	2055539
Area of ROI	129567325.1	129567325.1	129567325.1	129567325.1	129567325.1	129567325.1	129567325.1	129567325.1
Area of L - Area of F points	23330992	44580404	19517391	21750975	22373985	29427974	31154600	12793154
Area of F points - Area of L	14195679	9460169	19325999	16240733	8509572	5167119	7832338	11204647
# of Lineaments	36	22	23	31	23	45	47	13
Area of F points - Area of L	91316724	69383615	84416033	83208508	98683361	90933890	80178016	103513985
Area of ROI - Area of F points	114647716	113964019	103933424	104959483	121057346	120361864	111332616	116307139
# F points with in the Lineaments	2	25	31	44	5	17	41	3
# F points outside the Lineaments	35	21	54	38	7	5	15	45
# F points	37	46	85	82	12	22	56	48
# F points with in the Lineaments / total number of F points	0.054054054	0.543478261	0.364705882	0.536585366	0.416666667	0.772727273	0.732142857	0.0625
(Area of L - Area of F points) / (Area of ROI - Area of F points)	0.123819989	0.083010138	0.185945947	0.154733355	0.07293727	0.042929869	0.070350795	0.096336709
# F points outside the Lineaments / total number of F points	0.945945946	0.456521739	0.635294118	0.463414634	0.583333333	0.227272727	0.267857143	0.9375
(Area of ROI - (Area of L and F points)) / Area of ROI - Area of F points	1.123819989	1.083010138	1.185945947	1.154733355	1.070293727	1.042929869	1.070350795	1.096336709
W _i ⁺	-4.295856363	0.180794482	-0.284664815	0.641762542	-8.596043616	1.808369769	1.717789116	-2.364953854
W _i ⁻	-2.684409506	0.170192851	-0.629468095	-0.036714432	-0.132172048	0.926663796	0.488728959	-2.759959892
contrast	-1.611446856	0.010601631	0.34480328	0.678476974	-8.463871569	0.881705973	1.229060157	0.395006039
Area is represented in meters								
F = Field Data Point L = Lineament ROI = Region of Interest								
#NUM! and #DIV/0! Indicate that no contrast value could be calculated								

Table 3d. Weights-of-evidence calculations and contrast values for topographic lineaments and sites with appropriately oriented fractures with frequencies >0 fractures/m. Contrast values with yellow are significantly positive numbers. (Site buffer is 500m).

Topographic Lineaments								
Greater than 2.0 Fracture Frequency 500 m								
	wnw	nw	nnw	ns	nne	ne	ene	ew
Area of F points	4168130	3427183	8820131	6159945	0	2353503	9341225	3911295
Area of L	24054922	4226962	25825293	30118084	22374392	33466316	41556971	14848693
Area of L and F points	0	1742008	2241791	2160371	0	782046	6417779	769037
Area of ROI	129567325.1	129567325.1	129567325.1	129567325.1	129567325.1	129567325.1	129567325.1	129567325.1
Area of L - Area of F points	24054922	2484964	23583502	27957713	22374392	32684270	35199192	14079656
Area of F points - Area of L	4168130	1685175	6578340	3999574	0	1571457	2923446	3142258
# of Lineaments	36	22	23	31	23	45	47	13
Area of ROI - (Area of L + Area of F points)	101344273	121913180	94921901	93289296	107192933	93747506	78669129	110807337
Area of ROI - Area of F points	125399195	126140142	120747194	123407380	129567325	127213822	120226100	125656030
# F points with in the Lineaments	0	6	6	6	0	1	20	1
# F points outside the Lineaments	8	2	13	4	0	2	2	5
# F points	8	8	19	10	0	3	22	6
# F points with in the Lineaments / total number of F points	0	0.75	0.315789474	0.6	#DIV/0!	0.333333333	0.909090909	0.166666667
(Area of L - Area of F points) / (Area of ROI - Area of F points)	0.03323889	0.013359546	0.054480272	0.03240952	0	0.012352879	0.024316234	0.025006822
# F points outside the Lineaments / total number of F points	1	0.25	0.684210526	0.4	#DIV/0!	0.666666667	0.090909091	0.833333333
(Area of ROI - (Area of L and F points)) / Area of ROI - Area of F points	1.03323889	1.013359546	1.054480272	1.03240952	1	1.012352879	1.024316234	1.025006822
W _i ⁺	#NUM!	4.349051498	-0.509799856	0.842475023	#DIV/0!	-0.435918367	3.157276849	-1.047105295
W _i ⁻	#NUM!	0.422827439	-0.825799582	0.253370655	#DIV/0!	-0.791784576	1.56503407	-1.702609521
contrast	#NUM!	3.926224059	0.315999726	0.589104368	#DIV/0!	0.355866209	1.592242779	0.655504227
Area is represented in meters								
F = Field Data Point L = Lineament ROI = Region of Interest								
#NUM! and #DIV/0! Indicate that no contrast value could be calculated								

Table 3e. Weights-of-evidence calculations and contrast values for topographic lineaments and sites with appropriately oriented fractures with frequencies >2 fractures/m. Contrast values with yellow are significantly positive numbers. (Site buffer is 500m).

Topographic Lineaments								
Greater than 4.0 Fracture Frequency 500 m								
	wnw	nw	nnw	ns	nne	ne	ene	ew
Area of F points	2353429	2353436	6674518	5375461	0	0	6182964	2342312
Area of L	10383182	26217444	7277374	5171926	0	14279815	35869592	3040369
Area of L and F points	0	1332916	0	0	0	0	957162	773638.523
Area of ROI	129567325.1	129567325.1	129567325.1	129567325.1	129567325.1	129567325.1	129567325.1	129567325.1
Area of L - Area of F points	10383182	24884528	7277374	5171926	0	14279815	34912430	2266730
Area of F points - Area of L	2353429	1020520	6674518	5375461	0	0	5225802	1568673
# of Lineaments	2	8	4	1	0	7	14	1
Area of ROI - (Area of L + Area of F points)	116830714	102329361	115615433	119019938	129567325	115287510	88471931	124958283
Area of ROI - Area of F points	127213896	127213889	122892807	124191864	129567325	129567325	123384361	127225013
# F points with in the Lineaments	0	2	0	0	0	0	6	1
# F points outside the Lineaments	4	3	13	9	0	2	7	3
# F points	4	5	13	9	0	2	13	4
# F points with in the Lineaments / total number of F points	0	0.4	0	0	#DIV/0!	0	0.461538462	0.25
(Area of L - Area of F points) / (Area of ROI - Area of F points)	0.018499779	0.00802208	0.054311706	0.04328352	0	0	0.042353844	0.012329914
# F points outside the Lineaments / total number of F points	1	0.6	1	1	#DIV/0!	1	0.538461538	0.75
(Area of ROI - (Area of L and F points)) / Area of ROI - Area of F points	1.018499779	1.00802208	1.054311706	1.04328352	1	1	1.042353844	1.012329914
W _i ⁺	#NUM!	0.657651118	#NUM!	#NUM!	#DIV/0!	#DIV/0!	-0.757269627	1.821217497
W _i ⁻	#NUM!	-1.023356	#NUM!	#NUM!	#DIV/0!	#DIV/0!	0.010278862	-1.481543088
contrast	#NUM!	1.681007119	#NUM!	#NUM!	#DIV/0!	#DIV/0!	-0.767548489	3.302760585
Area is represented in meters								
F = Field Data Point L = Lineament ROI = Region of Interest								
#NUM! and #DIV/0! Indicate that no contrast value could be calculated								

Table 3f. Weights-of-evidence calculations and contrast values for topographic lineaments and sites with appropriately oriented fractures with frequencies >4 fractures/m. Contrast values with yellow are significantly positive numbers. (Site buffer is 500m).

EARTH SAT 97 Lineaments								
Greater than 0.0 Fracture Frequency 50 m								
	wnw	nw	nnw	ns	nne	ne	ene	ew
Area of F points	249981	254311	522486	422396	101983	146909	316569	189528
Area of L	10383182	26217444	7277374	5171926	0	14279815	35869592	3040369
Area of L and F points	0	156900	7845	0	0	47070	125520	7845
Area of ROI	129567325.1	129567325.1	129567325.1	129567325.1	129567325.1	129567325.1	129567325.1	129567325.1
Area of L - Area of F points	10133201	25963133	6754888	4749530	-101983	14132906	35553023	2850841
Area of F points - Area of L	249981	97411	514641	422396	101983	99839	191049	181683
# of Lineaments	2	8	4	1	0	7	14	1
Area of F points - Area of L	118934162	103095570	121767465	123973003	129465342	115140601	93381164	126337428
Area of ROI - Area of F points	129317344	129313014	129044839	129144929	129465342	129420416	129250756	129377797
# F points with in the Lineaments	0	20	1	0	0	6	16	5
# F points outside the Lineaments	37	26	84	82	12	16	40	43
# F points	37	46	85	82	12	22	56	48
# F points with in the Lineaments / total number of F points	0	0.434782609	0.011764706	0	0	0.272727273	0.285714286	0.104166667
(Area of L - Area of F points) / (Area of ROI - Area of F points)	0.001933082	0.000753296	0.003988079	0.003270713	0.000787724	0.000771432	0.001478127	0.001404283
# F points outside the Lineaments/ total number of F points	1	0.565217391	0.988235294	1	1	0.727272727	0.714285714	0.895833333
(Area of ROI - (Area of L and F points)) / Area of ROI - Area of F points	1.001933082	1.000753296	1.003988079	1.003270713	1.000787724	1.000771432	1.001478127	1.001404283
W _i ⁺	#NUM!	0.860244828	-5.679645059	#NUM!	#NUM!	0.095535362	-0.550637675	-1.521298443
W _i ⁻	#NUM!	-0.995403543	-4.387898686	#NUM!	#NUM!	-1.250171567	-1.096237312	-2.170255108
contrast	#NUM!	1.855648372	-1.291746373	#NUM!	#NUM!	1.345725129	0.545599636	0.648955286

Area is represented in meters
F = Field Data Point L = Lineament ROI = Region of Interest
#NUM! and #DIV/0! Indicate that no contrast value could be calculated

Table 3g. Weights-of-evidence calculations and contrast values for EarthSat (1997) lineaments and sites with appropriately oriented fractures with frequencies >0 fractures/m. Contrast values with yellow are significantly positive numbers. (Site buffer is 50m).

EARTH SAT 97 Lineaments								
Greater than 2.0 Fracture Frequency 50 m								
	wnw	nw	nnw	ns	nne	ne	ene	ew
Area of F points	31379	49205	121443	70380	0	23535	149778	39224
Area of L	10383182	26217444	7277374	5171926	0	14279815	35869592	3040369
Area of L and F points	0	31380	0	0	0	7845	54915	7845
Area of ROI	129567325.1	129567325.1	129567325.1	129567325.1	129567325.1	129567325.1	129567325.1	129567325.1
Area of L - Area of F points	10383182	26186064	7277374	5171926	0	14271970	35814677	3032524
Area of F points - Area of L	31379	17825	121443	70380	0	15690	94863	31379
# of Lineaments	2	8	4	1	0	7	14	1
Area of ROI - (Area of L + Area of F points)	119152764	103300676	122168508	124325019	129567325	115263975	93547955	126487732
Area of ROI - Area of F points	129535946	129518120	129445882	129496945	129567325	129543790	129417547	129528101
# F points with in the Lineaments	0	4	0	0	0	1	7	1
# F points outside the Lineaments	8	4	19	10	0	2	15	5
# F points	8	8	19	10	0	3	22	6
# F points with in the Lineaments / total number of F points	0	0.5	0	0	#DIV/0!	0.333333333	0.318181818	0.166666667
(Area of L - Area of F points) / (Area of ROI - Area of F points)	0.000242242	0.000137626	0.000938176	0.000543488	0	0.000121117	0.000733	0.000242256
# F points outside the Lineaments/ total number of F points	1	0.5	1	1	#DIV/0!	0.666666667	0.681818182	0.833333333
(Area of ROI - (Area of L and F points)) / Area of ROI - Area of F points	1.000242242	1.000137626	1.000938176	1.000543488	1	1.000121117	1.000733	1.000242256
W _i ⁺	#NUM!	1.148768937	#NUM!	#NUM!	#DIV/0!	0.413962028	-0.48082152	0.535652248
W _i ⁻	#NUM!	-0.789216404	#NUM!	#NUM!	#DIV/0!	-0.981818251	-0.894290721	-1.808835307
contrast	#NUM!	1.937985341	#NUM!	#NUM!	#DIV/0!	1.395780279	0.413469202	2.344487555

Area is represented in meters
F = Field Data Point L = Lineament ROI = Region of Interest
#NUM! and #DIV/0! Indicate that no contrast value could be calculated

Table 3h. Weights-of-evidence calculations and contrast values for EarthSat (1997) lineaments and sites with appropriately oriented fractures with frequencies >2 fractures/m. Contrast values with yellow are significantly positive numbers. (Site buffer is 50m).

EARTH SAT 97 Lineaments								
Greater than 4.0 Fracture Frequency 50 m								
	wnw	nw	nnw	ns	nne	ne	ene	ew
Area of F points	23534	27748	78448	62536	0	15690	94481	23535
Area of L	24054922	4226962	25825293	30118084	22374392	33466316	41556971	14848693
Area of L and F points	0	19904	8254	30172	0	0	86637	0
Area of ROI	129567325.1	129567325.1	129567325.1	129567325.1	129567325.1	129567325.1	129567325.1	129567325.1
Area of L - Area of F points	24054922	4207058	25817039	30087912	22374392	33466316	41470334	14848693
Area of F points - Area of L	23534	7844	70194	32364	0	15690	7844	23535
# of Lineaments	36	22	23	31	23	45	47	13
Area of ROI - (Area of L + Area of F points)	105488869	125312615	103663584	99386705	107192933	96085319	87915873	114695097
Area of ROI - Area of F points	129543791	129539577	129488877	129504789	129567325	129551635	129472844	129543790
# F points with in the Lineaments	0	3	2	4	0	0	9	0
# F points outside the Lineaments	4	2	11	4	0	2	4	4
# F points	4	5	13	8	0	2	13	4
# F points with in the Lineaments / total number of F points	0	0.6	0.153846154	0.5	#DIV/0!	0	0.692307692	0
(Area of L - Area of F points) / (Area of ROI - Area of F points)	0.000181668	6.05529E-05	0.000542085	0.000249906	0	0.000121117	6.05841E-05	0.000181676
# F points outside the Lineaments/ total number of F points	1	0.4	0.846153846	0.5	#DIV/0!	1	0.307692308	1
(Area of ROI - (Area of L and F points)) / Area of ROI - Area of F points	1.000181668	1.000060553	1.000542085	1.000249906	1	1.000121117	1.000060584	1.000181676
W _i ⁺	#NUM!	3.500444917	-2.34392586	0.730766316	#DIV/0!	#NUM!	1.862751269	#NUM!
W _i ⁻	#NUM!	-0.824774836	-1.593477141	-0.393996188	#DIV/0!	#NUM!	-1.29062884	#NUM!
contrast	#NUM!	4.325219753	-0.750448719	1.124762505	#DIV/0!	#NUM!	3.153380109	#NUM!

Area is represented in meters
F = Field Data Point L = Lineament ROI = Region of Interest
#NUM! and #DIV/0! Indicate that no contrast value could be calculated

Table 3i. Weights-of-evidence calculations and contrast values for EarthSat (1997) lineaments and sites with appropriately oriented fractures with frequencies >4 fractures/m. Contrast values with yellow are significantly positive numbers. (Site buffer is 50m).

EARTHSAT 97 Lineaments								
Greater than 0.0 Fracture Frequency 500 m								
	wnw	nw	nnw	ns	nne	ne	ene	ew
Area of F points	14919609	15603306	25633901	24607842	8509979	9205461	18234709	13260186
Area of L	10383182	26217444	7277374	5171926	0	14279815	35869592	3040369
Area of L and F points	0	5603720	937322	209034	0	2658957	5785480	1244831
Area of ROI	129567325.1	129567325.1	129567325.1	129567325.1	129567325.1	129567325.1	129567325.1	129567325.1
Area of L - Area of F points	10383182	20613724	6340052	4962892	0	11620858	30084112	1795538
Area of F points - Area of L	14919609	9999586	24696579	24398808	8509979	6546504	12449229	12015355
# of Lineaments	2	8	4	1	0	7	14	1
Area of F points - Area of L	104264534	93360295	97593372	99996591	121057346	108741006	81248504	114511601
Area of ROI - Area of F points	114647716	113964019	103933424	104959483	121057346	120361864	111332616	116307139
# F points with in the Lineaments	0	28	3	1	0	7	20	5
# F points outside the Lineaments	37	18	82	81	12	15	36	43
# F points	37	46	85	82	12	22	56	48
# F points with in the Lineaments / total number of F points	0	0.608695652	0.035294118	0.012195122	0	0.318181818	0.357142857	0.104166667
(Area of L - Area of F points) / (Area of ROI - Area of F points)	0.130134376	0.08774336	0.237619218	0.2324593	0.070297089	0.054390185	0.111820143	0.103307117
# F points outside the Lineaments/ total number of F points	1	0.391304348	0.964705882	0.987804878	1	0.681818182	0.642857143	0.895833333
(Area of ROI - (Area of L and F points)) / Area of ROI - Area of F points	1.130134376	1.08774336	1.237619218	1.2324593	1.070297089	1.054390185	1.111820143	1.103307117
W _i ⁺	#NUM!	1.127706309	-3.819887527	-6.111186923	#DIV/0!	0.333698146	-0.42723713	-0.346599044
W _i ⁻	#NUM!	0.196417375	-3.282417001	-4.354541745	#NUM!	-1.001472005	-0.654444985	-2.234784471
contrast	#NUM!	0.931288934	-0.537470526	-1.756645179	#DIV/0!	1.335170151	0.227207855	1.888185427
Area is represented in meters								
F = Field Data Point L = Lineament ROI = Region of Interest								
#NUM! and #DIV/0! Indicate that no contrast value could be calculated								

Table 3j. Weights-of-evidence calculations and contrast values for EarthSat (1997) lineaments and sites with appropriately oriented fractures with frequencies >0 fractures/m. Contrast values with yellow are significantly positive numbers. (Site buffer is 500m).

EARTHSAT 97 Lineaments								
Greater than 2.0 Fracture Frequency 500 m								
	wnw	nw	nnw	ns	nne	ne	ene	ew
Area of F points	4168130	3427183	8820131	6159945	0	2353503	9341225	3911295
Area of L	10383182	26217444	7277374	5171926	0	14279815	35869592	3040369
Area of L and F points	0	2264044	0	0	0	1121292	2700991	773639
Area of ROI	129567325.1	129567325.1	129567325.1	129567325.1	129567325.1	129567325.1	129567325.1	129567325.1
Area of L - Area of F points	10383182	23953400	7277374	5171926	0	13158523	33168601	2268730
Area of F points - Area of L	4168130	1163139	8820131	6159945	0	1232211	6640234	3137656
# of Lineaments	2	8	4	1	0	7	14	1
Area of ROI - (Area of L + Area of F points)	115016013	99922698	113469820	118235454	129567325	112934007	84356508	122615661
Area of ROI - Area of F points	125399195	126140142	120747194	123407380	129567325	127213822	120226100	125656030
# F points with in the Lineaments	0	4	0	0	0	1	9	1
# F points outside the Lineaments	8	4	19	10	0	2	13	5
# F points	8	8	19	10	0	3	22	6
# F points with in the Lineaments / total number of F points	0	0.5	0	0	#DIV/0!	0.333333333	0.409090909	0.166666667
(Area of L - Area of F points) / (Area of ROI - Area of F points)	0.03323889	0.009221006	0.073046261	0.049915532	0	0.009866141	0.055231218	0.024970202
# F points outside the Lineaments/ total number of F points	1	0.5	1	1	#DIV/0!	0.666666667	0.590909091	0.833333333
(Area of ROI - (Area of L and F points)) / Area of ROI - Area of F points	1.03323889	1.009221006	1.073046261	1.049915532	1	1.009866141	1.055231218	1.024970202
W _i ⁺	#NUM!	1.246697205	#NUM!	#NUM!	#NUM!	#DIV/0!	0.834229178	-0.320772976
W _i ⁻	#NUM!	-0.847619596	#NUM!	#NUM!	#DIV/0!	-1.221176251	-0.354692801	-1.80533676
contrast	#NUM!	2.094316801	#NUM!	#NUM!	#DIV/0!	2.05540543	0.033919825	2.590589566
Area is represented in meters								
F = Field Data Point L = Lineament ROI = Region of Interest								
#NUM! and #DIV/0! Indicate that no contrast value could be calculated								

Table 3k. Weights-of-evidence calculations and contrast values for EarthSat (1997) lineaments and sites with appropriately oriented fractures with frequencies >2 fractures/m. Contrast values with yellow are significantly positive numbers. (Site buffer is 500m).

EARTHSAT 97 Lineaments								
Greater than 4.0 Fracture Frequency 500 m								
	wnw	nw	nnw	ns	nne	ne	ene	ew
Area of F points	2353429	2353436	6674518	5375461	0	0	6182964	2342312
Area of L	24054922	4226962	25825293	30118084	22374392	33466316	41556971	14848693
Area of L and F points	0	1376820	1432858	2160371	0	0	4874711	0
Area of ROI	129567325.1	129567325.1	129567325.1	129567325.1	129567325.1	129567325.1	129567325.1	129567325.1
Area of L - Area of F points	24054922	2850142	24392435	27957713	22374392	33466316	36682260	14848693
Area of F points - Area of L	2353429	976616	5241660	3215090	0	0	1308253	2342312
# of Lineaments	36	22	23	31	23	45	47	13
Area of ROI - (Area of L + Area of F points)	103158974	124363747	98500372	96234151	107192933	96101009	86702101	112376320
Area of ROI - Area of F points	127213896	127213889	122892807	124191864	129567325	129567325	123384361	127225013
# F points with in the Lineaments	0	3	3	6	0	0	12	0
# F points outside the Lineaments	4	2	10	3	0	2	1	4
# F points	4	5	13	9	0	2	13	4
# F points with in the Lineaments / total number of F points	0	0.6	0.230769231	0.666666667	#DIV/0!	0	0.923076923	0
(Area of L - Area of F points) / (Area of ROI - Area of F points)	0.018499779	0.00767696	0.042652293	0.025888089	0	0	0.01060307	0.018410782
# F points outside the Lineaments/ total number of F points	1	0.4	0.769230769	0.333333333	#DIV/0!	1	0.076923077	1
(Area of ROI - (Area of L and F points)) / Area of ROI - Area of F points	1.018499779	1.00767696	1.042652293	1.025888089	1	1	1.01060307	1.018410782
W _i ⁺	#NUM!	3.667866231	-1.1255593	1.272717351	#DIV/0!	#DIV/0!	3.460180813	#NUM!
W _i ⁻	#NUM!	-0.451413904	-1.224379392	0.434201559	#DIV/0!	#DIV/0!	1.284627794	#NUM!
contrast	#NUM!	4.119280134	0.098820091	0.838515792	#DIV/0!	#DIV/0!	2.175553019	#NUM!
Area is represented in meters								
F = Field Data Point L = Lineament ROI = Region of Interest								
#NUM! and #DIV/0! Indicate that no contrast value could be calculated								

Table 3l. Weights-of-evidence calculations and contrast values for EarthSat (1997) lineaments and sites with appropriately oriented fractures with frequencies >4 fractures/m. Contrast values with yellow are significantly positive numbers. (Site buffer is 500m).

Topographic Lineaments	wnw	nw	nnw	ns	nne	ne	ene	ew
Greater than 0.0 Fracture Frequency 50 m		3.287689				0.999623	1.555089	
Greater than 2.0 Fracture Frequency 50 m		4.156181				0.361703	1.982892	
Greater than 4.0 Fracture Frequency 50 m		1.63532					0.617607	3.037727
Greater than 0.0 Fracture Frequency 500 m			0.344803	0.678477		0.881706	1.22906	0.395006
Greater than 2.0 Fracture Frequency 500 m		3.926224	0.316	0.589104		0.355866	1.592243	0.655504
Greater than 4.0 Fracture Frequency 500 m		1.681007						3.302761
EARTHSAT 97 Lineaments								
Greater than 0.0 Fracture Frequency 50 m		1.855648				1.345725	0.5456	0.648955
Greater than 2.0 Fracture Frequency 50 m		1.937985				1.39578	0.413469	2.344488
Greater than 4.0 Fracture Frequency 50 m		4.32522					3.15338	
Greater than 0.0 Fracture Frequency 500 m		0.931289				1.33517	0.227208	1.888185
Greater than 2.0 Fracture Frequency 500 m		2.094317				2.055405		2.59059
Greater than 4.0 Fracture Frequency 500 m		4.11928					2.175553	

Table 3M. Summary chart displaying significant positive contrast values for topographic and EarthSat (1997) lineaments and sites with appropriately oriented fractures with frequencies (Site buffers are as indicated, 50 and 500m).